The Use of Experimental Petrology to Generate an Impact Model for Formation of the Unique CB_b Chondrules

by

Claire Condie

A Dissertation submitted to the

Graduate School-New Brunswick

Rutgers, The State University of New Jersey

in partial fulfillment of the requirements

for the degree of

Doctor of Philosophy

Graduate Program in Geological Sciences

written under the direction of

Dr. Roger Hewins

and approved by

_____

_____

_____

_____

New Brunswick, New Jersey

October 2012

ABSTRACT OF THE DISSERTATION

The Use of Experimental Petrology to Generate an Impact Model for Formation of the Unique CB_b Chondrules

By Claire Condie

Dissertation Director:
Dr. Roger Hewins

In this research, an impact between the protoplanet Pallas, which hosts a large crater and has a surface composition very similar to the CR carbonaceous chondrites and an iron-nickel impactor, is suggested to be the formation mechanism for the CBb chondrules. The CB_b chondrules may have formed by melting, evaporation and condensation, possibly in the vapor cloud generated by the impact between Pallas and the iron-nickel impactor.

Through experimental petrology, the skeletal olivine (SO) texture of the CB_b chondrules has been replicated using cooling-reheating cycles. By combining my new cooling-reheating temperature data for the formation of the CB_b chondrules with previous research a unified impact model has been developed for the CB_b chondrites and their genetically related partners, CBa, CH, and CR.

List of tables

List of illustrations

Chapter 1: Chondrules: Nebular or Planetary Origin

1.1 Introduction

Chondrules are silicate melt droplets that accreted to asteroidal bodies. The observed abundances of chondrules indicate a major astrophysical or planetary heating process in parts of or throughout the early solar system or alternatively that they formed in planetary environments during a period of heavy bombardment. Chondrites are rocks composed of chondrules and CAIs embedded in a fine grained matrix and account for 86% of falls. The chondrites are classified as ordinary or carbonaceous. The carbonaceous chondrites (CI, CM, CO, CV, CK, CR, CH, and CB) have a higher content of CAIs, are enriched in refractory lithophile elements, and plot below the terrestrial fractionation line on an oxygen isotope plot relative to the ordinary chondrites. Only the CM, CR, and CI groups are actually enriched in carbon and water relative to the ordinary chondrites. The compositions and textures of chondrules in most chondrites suggest they were once balls of dust floating in the solar nebula that were strongly heated and cooled over the space of a few hours (Jones et al., 2000; Desch and Connolly, 2002). Models in which dust is melted by shock waves in the nebula are currently popular (Desch and Connolly 2002, Weidenschilling et al., 1998).

CB_b chondrites are metal-rich (~70%) and are members of the CR chondrite clan, which is composed of CR, CH, CB_a, CB_b, and LEW 85332 chondrites (Krot et al., 2001; Weisberg et al., 1995; Weisberg et al., 1993). The members of the CR chondrite clan have characteristics discussed below that suggest that they formed differently than other

chondrite groups. The concentrations of the platinum group elements in the metal in CB_a chondrites are up to 30% higher than values expected from condensation from the solar nebula (Campbell et al., 2002) suggesting that they did not form in the solar nebula. CB_b and CH chondrites are unusual in having zoned metal formed by condensation and being composed of chondrules unique in texture and composition. The characteristics of the CR chondrite clan suggest that different processes were involved in the formation of the CB_a, CB_b and CH chondrules. The purpose of my research is to clarify the origin of these unusual meteoritic chondrules in CB_b chondrites, using experimental petrology.

"Normal" chondrules in other carbonaceous chondrites are igneous and have dominantly porphyritic textures, with phenocrysts of olivine and low-Ca pyroxene set in glassy mesostasis. These textures are explained by (partial) melting and crystallization. These chondrules' textures are consistent with crystal growth from a rapidly cooling (100 or slower -1000 K/hour) silicate melt (Krot et al., 2005; Desch and Connolly, 2002) The chondrules often contain relic fragments of earlier generations of chondrules indicating that the formation process was repetitive, and chondrules in most chondrites are surrounded by fine grained igneous rims or accretionary rims in CM chondrules (Krot et al., 2002; Krot et al 2001; Wasson et al., 1995).

The CB_b chondrules have cryptocrystalline and unique skeletal barred olivine (SO) textures (Krot et al., 2001) and a different formation origin seems required to explain the SO textures of CB_b chondrules versus normal chondrules found in other carbonaceous chondrite groups. The CB_b chondrules may have formed by melting of an impacted parent body, followed by evaporation and condensation, possibly in a cloud generated by

an impact between asteroids or planetary embryos (Krot et al., 2005). If so, the heating and cooling conditions needed to produce their textures may be different from those for normal chondrules, which can be tested with experimental petrology.

Here I first review the possible settings for CB_b chondrule formation, evaluate the plausibility of the formation of some chondrules during large scale impacts, and compare chondrules from CB_b to those in other chondrites. Though normal chondrules have been simulated in high temperature furnaces, there has been no systematic experimental work on the unusual CB_b chondrules. In the following chapters I discuss the range of textures in CB_b chondrules and those I have formed by crystallization of synthetic analogs. As some CB_b chondrules are intermediate between Type IAB and Al-rich chondrules in composition, my research extends the range of chondrule compositions studied experimentally. In particular, I provide experimental constraints on the thermal characteristics of the environment of formation of CB_b chondrules, complementing theoretical modeling (Krot et al., 2007; Krot et al., 2006; Krot et al., 2005; Campbell et al., 2005; Petaev et al., 2003; Campbell et al., 2002; Krot et al., 2002; Campbell et al., 2001; Krot et al., 2001; Meibom et al., 2001; Petaev et al., 2001; Meibom et al., 2000; Weisberg et al., 1990) and reexamine theories for their formation.

1.2 The Solar Nebula

Stars and protostellar nebulae formed from cold gas and dust in interstellar clouds (Wood 2000; Shu et al., 1987). The self-gravitational collapse of a particular volume of gas gave rise to the Sun and solar nebula. In its initial, extended state this material possessed a

large amount of gravitational potential energy; as it collapsed most of this was converted into kinetic energy and then into internal energy. Also, in its initial state, the protosolar material would have had some net angular momentum because it was part of a galaxy that rotates. Even if only a fraction of this angular momentum were retained as the interstellar material collapsed to solar system proportions, it guarantees that the condensed structure that was formed would have been rotating and would have spun out as a viscous accretion disk (Cassen 1994; Nakamoto and Nakagawa 1994; Wood 1984).

Since Cameron's (1973) seminal work, all models have been in the framework of the viscous accretion disk. The continuing accretion of infalling material that has too much angular momentum to fall directly onto the prestellar central object creates a disk that forms around the star in a plane perpendicular to the rotation axis of the system. The infalling large dust aggregates are decelerated and heated by gas drag. The drag occurs when a large dust aggregate continues to move by inertia through gas decelerated in the shock fronts that bound the top and bottom surfaces of the disk (Wood and Morfill, 1988; Wood 1988). This protoplanetary disk is also called the solar nebula.

1.3 Chondrules, Asteroids and Impacts

"Aristocrats Edward Charles Howard and Jacques Louis Compte de Bournon published arguably the first scientific investigations of meteorites including the curious globules found in them in varying amounts in 1802" (Sears 2004). After over 200 years of research the origin of chondrules, the curious globules, is still not resolved. The two

main scenarios involve formation in the solar nebula or formation by impact. Numerous specific heating mechanisms have been proposed for melting chondrules in the nebula, and the gas shock wave model predicts conditions which match those required to reproduce the properties of typical chondrules (Desch and Connolly, 2002). Many researches support chondrule formation in the solar nebula (Richter et al., 2005; Chambers and Cassen 2002; Desch and Connolly, 2002; Jones et al., 2000; Shu et al., 1996; Grossman 1988; Taylor et al., 1983) but current research (Dwyer et al., 2012; Krot et al., 2005; Krot et al., 2001) questions the solar nebula being the origin for all chondrule types and requires that the model dismissed earlier, chondrule formation via impact be reevaluated. Although the geochemistry and isotopic compositions of chondrules and other components are consistent with solar nebula formation models these explanations are not proof and have gaps. The degree to which chondrules reflect nebula conditions and processes is still an open question.

Discussed below are some of the most compelling reasons to readdress an impact model as a formation model for *some* chondrules. I consider first the reasons to reexamine impact as a formation mechanism to explain the CB_b unique SO chondrules. The unique textures, chemical compositions, and age of the CB_b chondrules make them an ideal candidate to suggest that these chondrules may have formed through a different process, impact. Impact as a formation mechanism for chondrules has been pushed aside in the mainstream as a likely scenario for the majority of chondrules. I reevaluate the most aggressive arguments against impact to determine if these arguments are still justified. Second, I examine large body collisions which result in disruption to determine

if this mechanism is even probable in the formation of these chondrules. The impact must allow for disruption of the chemically similar parent body, a melt fraction, a mechanism to allow for size sorting, and the growth of both the SO and CC chondrules. Third if large bodies greater that 1000km existed in the solar nebula during the chondrule formation process. If large bodies existed at this time than this would indicate that collisions between bodies is also likely and could be the key to the unique characteristics of the CB_b chondrules.

1.3.1 Chondrule Occurrence and Abundance

Chemically, the most primitive meteorites are the CI chondrites. Their elemental abundances agree very well with spectroscopic observations of the solar photosphere. The CI chondrites contain no chondrules and the class that comes next to CI in composition, the CM chondrites, contains 10% volume chondrules (Sears 2004; Jones et al., 2000; Kallemeyn and Wasson, 1981**).** Lunar chondrules, spherical objects resembling meteoritic chondrules found in samples returned from the Moon by the Apollo 14 and 15 missions, are present in Apollo 14 breccias collected from the Moon's surface in about the same fraction (King et al., 1972) as in the CM chondrites. Since the meteorite classes that represent the primitive solar system material are relatively chondrule poor, the mechanism for producing them need not be on the scale of solar system wide. The mechanism may be highly efficient, localized, and happen rarely (Sears and Akridge, 1998).

1.3.2 Impact Melt Production

The asteroid belt was a violent place with major impacts making craters and fragmenting the asteroids, and, if the principle of uniformitarianism applied, then every impact of sufficient scale must have produced impact melt (O'Keefe and Ahrens, 1994). Many researchers have suggested that chondrules are crystallized impact-melt spherules (Sears et al., 1996b; Sanders 1996; Zook 1981; Zook 1980; Dodd 1974; Dodd 1971; Urey and Craig, 1953). However, Taylor et al. (1983) published a detailed review concluding that the properties of most chondrules are inconsistent with an impact origin. As outline below, he based his argument largely on a comparison of the petrography of meteorites with that of samples from the lunar regolith

The fraction of 'chondrules' present on the Moon constitutes a minor component of the regolith. The authors argue that if chondrules are created by impact then the volume or mass fraction of lunar chondrules should be more abundant than observed. The Moon's regolith is composed primarily of agglutinates (Heiken 1975), broken rocks, minerals, and glass fragments, and not chondrules. This relationship caused the authors to conclude that chondrites should contain a larger percentage of agglutinates which is contrary to what is found in the majority of chondrites. In addition, the composition of lunar agglutinates shows that impact breaks more rock than it melts. Micro-craters (hypervelocity impact pits) blanket the surface of the regolith grains on the moon and are not found on the surface of chondrules. Chondrules do have craters, but their characteristics are not similar to those of the hypervelocity impact craters seen in grains

from the lunar regolith. The characteristics found on chondrules are interpreted to be a function of low velocity collisions and not of high speed impact (Taylor et al., 1983).

Chondrules have rims around them and their formation model must account for the presence and composition of these rims. Taylor et al. (1983) argue that the only way rims would form on chondrules by impact is if the chondrules rolled in the regolith dust. The composition of the rims also varies from chondrule to chondrule; if the chondrules were rolling around in the regolith dust than the composition should be more homogenous. Not only do the compositions of the rims around chondrules vary but chondrule compositions in a single meteorite vary (Gooding et al., 1980, Gooding and Keil, 1981). Taylor concluded that if chondrules formed by impact than the composition of the parent rock would control the chemistry of both the chondrule and its rim and they should not vary significantly (Taylor et al., 1983).

Since Taylor's article was published in 1983 Hubble images of asteroids and dwarf planets, Pallas, Ceres, Vesta, and the impact of two asteroids (http://hubblesite.org/newscenter/) continues to support the occurrence of collisions and craters. The Galileo spacecraft took images of the asteroids Gaspra and Ida and NEAR Shoemaker took images of Mathilde on its way to Eros. All of the asteroids have cratered surfaces (Sears 2004). These images also demonstrate that impacts did occur and that they did not completely destroy the larger protoplanets. Combining these images with terrestrial impact crater studies (Gibson and Reimold, 2010; Ivanov et al., 2010; Reimold 2007, Ivanov 2005; Jones 2005; Grieve 1996; O'Keefe and Ahrens, 1994;

Melosh 1985; Melosh 1980) reopens a door to reexamine impacts involving early bodies as a formation mechanism for some chondrule groups.

Over twenty years ago it was argued that impact velocities on asteroids were too low for significant amounts of melt production (Scott et al., 1985; Pohl et al., 1977; O'Keefe and Ahrens, 1975) but (Giacomuzzo et al., 2007; Podosek and Cassen, 1994; Russell et al., 1996; Durda and Flynn, 1999) later research suggests this might not be true. Following an impact, melt would form droplets that would cool, solidify and crystallize as they cycled around the parent body in the atmosphere which was temporarily produced by the impact (Scheeres et al., 2002; Sears 2004). These droplets would crystallize as chondrules. The main obstacle would be to generate a sufficient volume of melt and to separate the melt droplets from the unmelted debris

In the past it was assumed that chondrules formed when a smaller projectile hit a target with radii between 10 and 100km (Sanders 1996). In cratering on a planet you have a melt fraction mixed with fragmental material which lands in proximity to the crater that is produced (Grieve and Pesonen1996). In an impact with equal bodies, smaller than planets, colliding or grazing past each other you can have aerodynamic sorting in an expanding plume (Blander 1983). The sorting would separate fragments and small droplets in convection cells that are produced by the energy of the impact.

Early research did not focus on the porosity of the target or the impactor and the outcome it would have on the amount of melt produced in the impact. The rate of deposition of

energy in a porous target is much higher than in a dense target and the amount of melt produced is much higher in the former (Horz and Schaal, 1981). A pressure of 60GPa (600kbar) can produce as much as 50% volume melt in a porous target (Sears 2004). In fact, metallic (iron-meteorite like) or even porous basalt impactors (from achondritic parent bodies) into a porous surface will produce a significant volume of melt; a dense projectile impacting at 5km/s, a typical impact velocity for the asteroid belt a few 10^5 years after solar system formation, gives a peak pressure as a function of impact velocity of 60GPa and ~50 volume % melt production (Fig. 1.1) (Horz and Schaal, 1981).

Impacts produce melt, but to be responsible for chondrules there must be a way of producing abundant droplets, separating them from solid debris and accreting them. The target materials that receive the most energy tend to be heated and transported the most, as in tektites and microtektites (O'Keefe and Ahrens, 1993). Planetary scale impacts produce wholesale melting (Cameron and Benz, 1991). Collisions between partly melted bodies produce sprays of melt droplets than can be accreted into new bodies down range (Asphaug et al., 2011). Fragmental debris can also re-accrete to form new asteroids (Michel et al., 2001). There may be many combinations of target temperature and projectile mass that permit large melt fractions to be separated from other debris and accreted either by late fall back on the target body or by formation of a new body down range. In Chapter 4 I develop a model for the accretion of CB_b material derived from a CR target.

1.3.3 Chondrule Ages

Chondrule ages have played a focal point in the development of their formation models in respect to the evolution of the protoplanetary disk and the earliest solids, (Calcium Aluminum Inclusions, CAIs). Radiometric observations indicate that the CAIs formed 4567.2 +/- 0.6 Ma ago and normal chondrules formed 4564.7 +/- 0.6 million years ago. This gives an interval of 2.5 +/- 1.2 million years between the formation of the CAIs and the chondrules (Amelin et al., 2007). Recent radiometric dating using lead isotopes from CB_a (Gujba) and CB_b (Hammadah al Hamra 237) chondrules identify their ages as 4562.7 ±0.5 MA and 4,562.8 ±0.9 MA respectively (Krot et al., 2005). These dates indicate that these chondrules formation occurred up to ~4 million years after the formation of the first solids and ~2 million years after normal chondrules (Amelin et al, 2007; Krot et al., 2005; Connelly et al., 2008) if post accretionary shock events did not reset their Pb-Pb ages (Weisberg et al., 2010).

The ages of the CB_a and CB_b chondrules correlate to when some asteroids had become large bodies (several hundred kilometers) (Fig 1.2) which may have had an active igneous geology (Morbidelli et al., 2009, Johansen et al., 2007, Cuzzi et al., 2008, Hewins and Newsom, 1998). In this time frame, the asteroid belt was violent with proto Jupiter and proto Saturn stirring up the belt and increasing relative velocities of asteroids to about 6 km/s, more than enough to make impact melts (Podosek and Cassen, 1994; Russell et al., 1996). Since Jupiter formed very quickly, within ~10^5 years of the onset of accretion (Cameron, 1995), the Asteroid Belt was stirred up by resonances with proto Jupiter or the jovian core (Davis et al., 1979), and encounter velocities were ~ 5km/s

prior to the formation of the chondrules and thus sufficient to produce impact melts (Sears 2004).

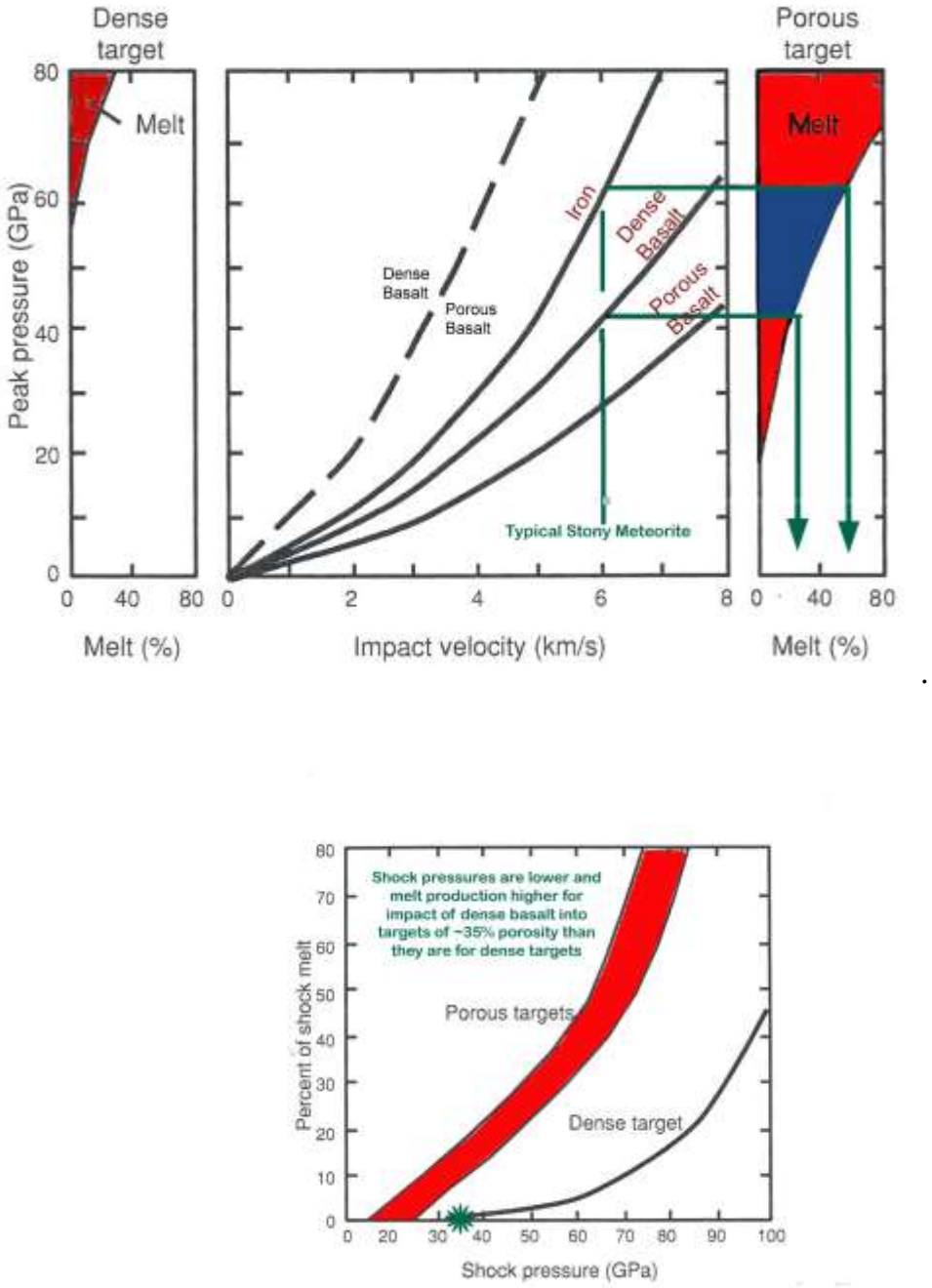

Figure 1.1: Variation of impact on a dense vs porous target. Shock pressures are lower and melt production higher for impact of dense basalt. Peak pressures as a function of impact velocity for various impactors (iron, dense basalt, and porous basalt) into dense basalt and porous basalt. Little or no melt is produced by impact into dense targets as porosity increases percent melt increases (Horz and Schaal, 1981).

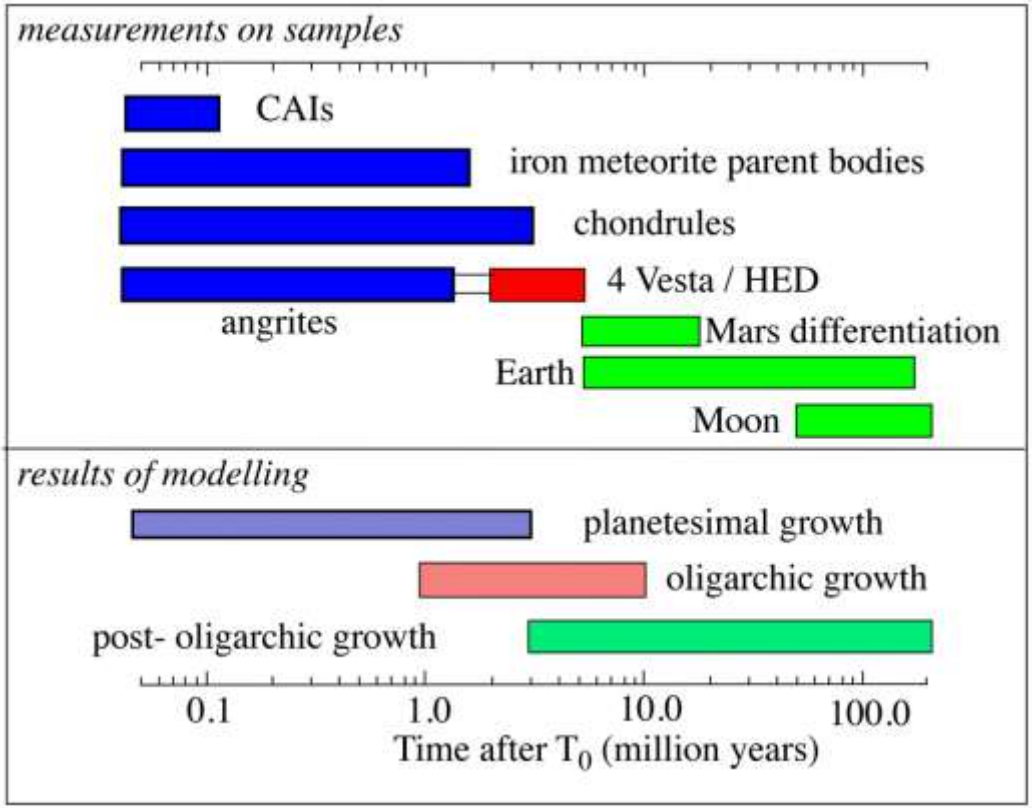

Figure 1.2 Summary of the time scale of formation of various solar system objects from small scale CAIs and chondrules to differentiated planetesimals and embryos. The bottom half of the diagram shows the three stages of planet formation and the colors are keyed to measurements made on the real objects in the top of the diagram. The summary supports that larger protoplanets existed at the same time as chondrules and could be involved in an impact to produce some of the chondrules (Righter and O'Brien, 2010)

1.3.4 Compound Chondrules

Some chondrules were still plastic when they collided into each other or into a rock fragment in space or agglomerated into rock so they stuck together (Sears 2004; Wasson 1993). This behavior indicates that at the place of chondrule formation densities were sufficiently high that the short time spent in free flight did not always allow solidification before collision or accumulation. Usually the compound chondrules are of similar texture suggesting similar maximum temperatures, nucleation site density, and cooling rates.

1.3.5 Chondrule Cooling Rates

Chondrule cooling rates have been estimated from crystallization experiments and olivine zoning to be between 10 – 1000 °C /hr (Hewins and Radomsky, 1990). A chondrule sized object in free space with an effective temperature of 2000Kwill cool within a matter of seconds (Morris and Desch, 2010; Grossman 1988) which strongly contradicts findings of chondrule petrology. The strong implication is that chondrules were located in surroundings of gas and dust with a much higher effective temperature while they cooled. Chambers and Cassen (2002) calculated that in order to obtain chondrule cooling rates, 10-100km sized clouds of nebular dust are required. A 10-100km cloud of dust moving through the early solar system had previously been hypothesized to be the size constraint for an asteroid in the making (Whipple 1972a; Whipple 1972b). More recently it has been estimated that the chondrule forming regions were at least 150 to 6000km in radius (Alexander et al., 2008).

1.3.6 Protoplanetary Collisions.

Morbidelli et al. (2009) summarize the classic model for terrestrial planet formation in three steps and I use his model to determine if bodies large enough to produce the necessary amount of melt for chondrule formation existed at the time the CB_a and CB_b chondrules formed. In the first step, the planetesimals, primordial bodies that accreted into asteroids or planets form. Second, the planetary embryos form, and third, the terrestrial planets form. The best understood phase is step 3, the formation of the terrestrial planets. The least understood is step 1, planetesimal formation, because a

complete understanding is lacking of how material grows from dust particles to meter size. The process which overcomes the meter-size barrier and allows planetesimals to grow to 1 – 10km in size (Morbidelli et al., 2009) is also poorly understood.

New models show that large planetesimals can form directly from the concentration of small solid particles in the turbulent structures of the gaseous component of the protoplanetary disk overcoming the meter barrier. Johansen et al. (2007) showed that the turbulence in the disk may help the solid particle population to develop gravitational instabilities which would limit the time the concentration of solid particles in their vicinity would exist. The numerical simulations of Johansen (2007) show that the density maxima are sufficiently long lived to be able to concentrate a large quantity of meter sized objects. These models indicate that the local density of the solids may become large enough to allow the formation of massive planetesimals by gravitational instability (Morbidelli et al., 2009). This is further supported by simulations in Johansen et al. (2007) which display the formation of planetesimals with 3.5 times the mass of Ceres within a few local orbital periods (Morbidelli et al., 2009; Pollack et al, 1996).

Gravitational accretion of planetesimals in computer simulations shows that a few bodies experience run-away growth at the expense of their neighbors and become planetary embryos (Chambers and Cassen, 2002). This inevitably leads to very large scale collisions such that Moon to Mars size bodies became incorporated into the growing Earth and Venus (Morbidelli et al., 2009; O'Brien et al., 2006). The most famous of these

collisions is the last major collision affecting the Earth, which led to the formation of the Moon (Canup et al., 2004; Cameron and Benz 1991; Wetherill 1986).

1.3.7 Evidence for Large Impacts: Iron Meteorites

Evidence for early large impacts in the asteroid belt has steadily accumulated from cosmochemical studies of meteorites over the past 20 years (Yang et al., 2007). Current understanding is that iron meteorites are fragments from the cores of small differentiated asteroids (20-200 kilometers in diameter) that were broken by impacts long after they had slowly cooled very early in Solar System history. New research questions the size and formation region of iron meteorites (Yang et al., 2007; Bottke et al., 2006). The cooling rates for one group of iron meteorites (IVA group) and other irons require a much more complex history and much larger parent bodies.

Iron meteorites are commonly assumed to have originated in the same region as most stony meteorite parent bodies, the main asteroid belt located between Mars and Jupiter (Yang et al., 2007). The presence of iron core fragments indicates that there were powerful collisions that repeatedly shattered their parent bodies during the early history of our Solar System. Irons represent over two thirds of the unique parent bodies sampled among all meteorites in our meteorite collections today (Bottke et al., 2006).

The origin of the IVA group is recognized to be from a body at least 600km in diameter or larger that was shattered by an impact leaving a molten metal body 300km in diameter.

The molten metal body solidified and cooled slowly with scarcely any enveloping silicate mantle. This history supports several recent theoretical studies that indicate that differentiated asteroids and meteorites are debris from protoplanetary collisions, protoplanets were abundant in the asteroid belt, and that parent bodies of iron-rich meteorites were broken up early (Yang et al., 2007).

A new origin for the iron meteorites indicates that many iron meteorite parent bodies formed and fragmented in the same regions where Mercury, Venus, Earth, and Mars are found today. Short accretion times of planetesimals in this zone allowed heat produced by radioactive decay of ^{26}Al to melt and differentiate many of these objects into core, mantle, and crust. At the same time, gravitational interactions with planetary embryos increased impact velocities and caused the planetesimals to break apart when they hit each other.

In addition, the Hf-W isotope ages for iron meteorites (Hevey and Sanders 2006; Bizzarro et al., 2005) indicates the core formation in iron meteorite parent bodies was nearly contemporaneous with the formation of the calcium aluminum rich inclusions, CAIs, some of the first solids to form in the Solar System. These data indicate that the iron cores formed prior to the formation of chondrules by one to several million years (Yang et al., 2007; Hevey and Sanders 2006).

Results from over 40 years of research display a consistency between cosmochemical studies of iron meteorites and dynamical modeling of protoplanet formation which has validated the methods used by meteoriticists to improve the understanding of the cooling rates of metal-bearing meteorites (Scott et al., 2007). These continued efforts of

numerous cosmochemists and dynamicists has created an advancement in our understanding of the sizes of meteorite parent bodies, the mass of the primordial asteroid population, and its early impact history (Yang et al., 2007). These advancements must also be incorporated into our chondrule forming models.

1.3.8 Protoplanetary Collisions: Impact Mechanism

The impacts that formed iron meteorites have always been thought to have smashed the meteorites into fragments striping mantles from cores over billions of years. This process has been reevaluated because a projectile capable of removing the mantle from a 600km asteroid would possibly destroy the core, unless the shock wave from the impact reflects off the core-mantle boundary. A new mechanism that indicates that iron meteorites formed in hit and run collisions between protoplanets has been suggested (Asphaug et al., 2006). A glancing collision between a Moon-sized and a Mars-sized protoplanet could have broken the smaller body and converted its core into a string of metal-rich bodies. If protoplanets were once abundant in the asteroid belt, as many dynamicists conclude, the IVA irons could have been derived from part of a molten protoplanetary core (Asphaug et al., 2006).

1.3.9 Evidence for Large Impacts: Formation of Pallasites

Most pallasites are composed of angular fragments of olivine embedded in iron-nickel and their structure and composition of the metal is similar to iron meteorites. Current understanding is that impacts mix olivine fragments from the mantle with molten metal

from the core. The chemical compositions of the metal in pallasites and IIIAB iron meteorites are similar except that most main-group pallasites are strongly depleted in iridium (Ir) and other elements that prefer solid metal to liquid metal. This depletion suggests that their metal was derived from the core of an asteroid after ~80% had solidified (Scott et al., 2010). The metal in main-group pallasites is a good compositional match for the iron meteorites at the low-Ir end of group IIIAB and their oxygen isotopic compositions appear indistinguishable: these similarities suggest that they originated from the same asteroid (Scott et al., 2010).

Recent studies (Yang et al., 2010) on the thermal histories of 28 members of the largest group of pallasites show that they cooled at diverse rates (2.5 -20 K/Myr). These rates are much slower than the cooling rates of another group, IIIAB irons (50-350K/Myr), proving that the IIIAB irons did not cool in the core of the main-group pallasite body contrary to widespread belief. If the pallasites cooled at the core-mantle boundary of a single body they would have similar cooling rates. The main group pallasites and several groups of iron meteorites appear to have cooled in bodies that were formed after the original differentiated bodies were split open by glancing collisions with larger bodies. Pallasites, the iron meteorites, and their parent asteroids are differentiated bodies with a violent early impact history (Scott et al., 2010).

1.4 Asteroids as Meteorite Parent Bodies

Earth-crossing asteroids originate in the Main Asteroid Belt, which is located between Mars and Jupiter, and they are considered the parent bodies for the chondritic meteorites based on the mineralogical characteristics of their visible/ near infrared spectra (Nesvorný et al., 2009; Gaffey et al., 2002; Sears 2004; Pieters and McFadden, 1994). More recently it has been suggested that CI carbonaceous chondrites might be cometary meteorites from the outer solar system (Gounelle 2011). Of course, there are difficulties linking asteroids to meteorites that arrive on Earth. Photometric and spectroscopic techniques only allow the surface of asteroids to be identified and this may be the reason why there is this disparity; the commonest types of meteorites have spectra that match very few asteroids, while the majority of asteroids have spectra that match very few meteorites (Sears 2004).

There are over sixteen classes of asteroids that are *now* recognized by asteroid astronomers and this number varies depending upon the classification scheme that is being utilized (Sears 2004; Sato et al., 1997; Gaffey et al., 1993). The three main classes are referred to as the C class asteroids (75%), the S class (17%) asteroids, the M class asteroids. Asteroids that resemble the carbonaceous chondrites are the C asteroids. The C asteroids have low albedo, flat spectra, and they predominate in the outer regions of the main asteroid belt. A 3μm absorption band has been used to detect water on 1/3 to 1/2 of them. The mean density of C asteroids is ~1.8g/cm^3 indicating that they are very porous or water is present. Type S asteroids are moderately bright asteroids composed of

metallic nickel-iron and iron and magnesium silicates and make up 17% of all asteroids. Most of the other asteroids are type M, and are bright asteroids, composed of pure nickel-iron. There are a few other rare types of asteroids (Table 1.1).

Many carbonaceous chondrites (CI or CM2) show strong absorption bands near 3μm (Miyamoto and Zolensky, 1992) due to secondary hydrous minerals that are considered to be produced by aqueous activity on parent asteroids (Sato 1997). This allows absorption features near 3μm to be sensitive indicators of the presence and quantity of hydrous minerals on planetary surfaces such as C-type asteroids (including G-B- and F types), which have been thought to be compositionally similar to carbonaceous chondrites. The C-type asteroids that predominate in the belt, especially in the outer main belt (Chapman et al., 1975; Gradie and Tedesco, 1982), are distinct from other asteroids because of their low albedos and neutral colors in the visible-near infrared wavelength region.

The most intensely studied C-type asteroids in the belt are Ceres, Pallas, and Vesta (Schmidt et al., 2009, Gaffey et al., 1993). These asteroids are considered dwarf planets or surviving protoplanets due to their intermediate size, up to1000km (McCord et al., 2006). Their estimated densities are Ceres 2077 kg/m^3, Pallas 2762 kg/ m^3, and Vesta 3478 kg/ m^3 (Schmidt et al., 2008) but the density of Pallas was recently revised to 3400±900kg/m^3 (Carry et al., 2010). Model protoplanets are moon-sized or larger planetary embryos within the protoplanetary disk that may have undergone internal melting to produce differentiated interiors. Vesta is thought to have an iron-nickel core.

Protoplanets may have formed from the accretion of kilometer-sized planetesimals or, as discussed above, directly from the concentration of small solid particles in the turbulent structures of the gaseous component of the protoplanetary disk, thus overcoming the meter barrier (Johansen et al.,2007, Cuzzi et al., 2008). According to dynamical modeling, protoplanets perturb each other's orbits slightly and thus collide in giant impacts to gradually form the dominant planets (McBride et al., 2004). These few surviving asteroidal protoplanets, Ceres, Pallas, and Vesta, serve as a fossil record for an important time in the solar system development (Schmidt et al., 2009).

Pallas is an intermediate object between Ceres and Vesta. It is about the same size as Vesta, but spectroscopy shows its surface composition to be more similar to that of Ceres which is chondritic (Schmidt et al., 2008, 2009). Pallas's size and earlier mass estimate suggested that it has undergone at least some degree of thermal alteration and partial differentiation, e.g. hydration of silicates and perhaps formation of an ice crust (Schmidt et al., 2008). It is denser than Ceres, however, indicating it had less water when it was formed or at least retained less water during evolution. The newer density estimate is more consistent with a metal-silicate mixture and is the same as that of CR chondrites (3100) within error.

It is plausible that the protoplanets stayed almost completely intact from the early days of the solar system (Schmidt et al., 2009). Pallas has most likely remained unchanged since the rocky region between Mars and Jupiter first formed and in its early history it was smashed by a massive impact that broke off a number of smaller asteroids that share its orbit (Schmidt et al., 2009). More than 10 members of the Pallas family have been

identified by comparing their spectra (Foglia and Masi, 1999; Lemaitre and Morbidelli, 1994) which would have formed by this impact.

The spectra of Ceres and Pallas are classified as G- and B- type respectively. The classification is based on the Tholen taxonomy (Tholen 1989; Barucci et al., 1987). Reflectance spectra of Ceres and Pallas show broad absorption bands near the 3μm hydration feature. Although the spectra of Ceres and Pallas resemble those of CI or CM2 chondrites in the wavelength region near 3 μm, the intensity of the 3 μm bands is weaker than those of CI and CM2 chondrites, indicating less hydrated silicate (Miyamoto and Zolensky, 1994; Sato et al., 1997). The surface composition of Pallas is very similar to the Renazzo (CR) carbonaceous chondrite (Sato et al., 1997) with a type B spectrum.

A possible genetic relationship between the members of the CR clan, including CB_b chondrites, has been suggested (Weisberg et al., 1995, Krot et al., 2002) which is supported by a unique CR-mixing line of these chondrites' whole rock oxygen isotopic ratios (Fig 1.3 a, b, and c) (Clayton and Mayeda, 1999, Krot et al., 2006). Given the existence of the Hirayama family asteroids accompanying Pallas (Foglia and Masi, 1999; Lemaitre and Morbidelli, 1994), we consider in chapter 4 how the CR clan chondrites might be distributed among these bodies

Type	Major Mineral Phases	Possible meteorite analogy [b]
V	Pyroxene +/- Feldspar	Eucrites, howardites, diogenites
A	Olivine +/- FeNi metal	Olivine achondrites pallasites, *Olivine-metal partial residue melts*
E	Enstatite (<Fsl)	Enstatite achondrites (aubrites), iron-bearing enstatite (Fs2-4) *Fe-bearing aubrites (Fs2-4)*
R	Olivine + orthopyroxene	Olivine-pyroxene cumulates, *Olivine-pyroxene partial melt residues*
M	Metal +/- enstatite hydrated silicates + organics?	Iron meteorites, enstatite chondrites
S (I)	Olivine>>pyroxene (+/- FeNi metal)[d]	Pallasites, pyroxene-poor ureilites, Pyroxene- poor brachinites, *Olivine-metal partial melt residues*
S (II)	Olivine>>clinopyroxene (+/- FeNi metal)[c], (0.05 <cpx/(ol+cpx) < .20)[d]	Cpx-bearing ureilites, Cpx-bearing brachinites, *olivine-Cpx cumulate, Cpx-bearing pallasites, highly metamorphosed, C-type assemblages*
S (III)	Olivine > clinopyroxene + orthopyroxene (+/- FeNi metal)[d]	Cpx- and opx-bearing ureilites
S (IV)	Olivine – orthopyroxene (+/- FeNi metal)[d], (.20< opx/(ol+opx) < 0.50)	Opx-bearing ureilites, lodranites, winonites & IAB iron, H, L, LL chondrites
S (V)	Olivine - clinopyroxene (+/- FeNi metal)[d]	Lodranites, *Cpx-basalt intrusions into H-chondrite matrix*
S (VI)	Olivine – orthopyroxene (+/- FeNi metal)[d]	Siderophyres (Steinbach), lodranites, winonites & IAB irons, *subsolidus-reduced chondrites, anorthosites*
S (VII)	Pyroxene > olivine (+/- FeNi metal) (orthopyroxene > clinopyroxene)	Mesosiderites siderophyres (Steinbach), lodranites, winonites & IAB irons, *Cpx-poor mesosiderites, subsolidus-reduced chondrites, anorthosites*
Q	Olivine + pyroxene + melt	Ordinary chondrites
C	Iron-bearing hydrated silicates	CI1& CM2 chondrites, *dehydrated CI1 & CM2 assemblages*
B	Iron-poor hydrated silicates	*Partially dehydrated highly leached CI1-type assemblages*
G	Iron-poor hydrated silicates	*Highly leached CI1-type assemblages*
F	Hydrated silicates + organics	Organic-rich CI1 & CM2 assemblages
P	Anhydrous silicates + organics	Olivine-organic cosmic dust particles
D	Organics + anhydrous silicates	Organic-olivine cosmic dust particles
T	Troilite (FeS) (+FeNi metal)	Troilite-rich iron meteorites
K	Olivine + opaques	CV3/CO3 chondrites
Z	Organics (+anhydrous silicates	Organic- rich cosmic dust particles

Table 1.1
(Gaffey et al., 1993a) [a] Mineral species or assemblages in italic font are inferred from spectral properties which are not specifically diagnostic
[b] Analogs in italic font have not been found or presented in meteorite collections
[c] Characterized from Gaffey et al (1993b)

1.5 Clues from CAIs and Isotopes

Calcium-aluminum-rich (CAIs) or refractory inclusions *(RI = CAI + AOA)* are a major component of some chondrites and provide clues for temperature, formation mechanisms, and temporal relationships. Although the formation conditions of CAIs found in these chondrites were not determined experimentally in my research, their presence and unique oxygen isotope signature are clues about the environment of formation (Paque and Toppani, 2007; Teng et al., 2007; Weisberg et al., 2007; Amelin et al., 2002). CAIs are common in some chondrite groups and are most abundant in the CV Chondrites. Initially, when CAIs were first studied they were thought to be residues of evaporation processes (Marvin et al., 1970). Some inclusions were later interpreted as the products of condensation of solids from the primordial solar nebula gases (Grossman 1972). Currently, Type B CAI are partly evaporated melted condensates (Richter et al., 2005), fluffy and some fine-grained CAI are condensates (MacPherson et al., 2005). From this the idea emerged that the refractory CAI inclusions were the first solids to form in the solar system and dating these objects showed they are the oldest solar system materials (Sears 2004, Amelin et al., 2002).

Based on melilite crystals a maximum heating temperature of 1400° C was determined for Type B CAIs (Stolper and Paque, 1986) with cooling rates of 2-50 C°/hr. McSween (1977) found a compositional continuum between refractory inclusions, Type I chondrules, and aluminum rich chondrules and suggested that they all formed by condensation. However, isotopic data indicates that most CAIs formed several million

years prior to the formation of most chondrules, consistent with the difference in maximum heating temperatures and cooling rates and with formation in different reservoirs by different processes.

1.5.1 Oxygen Isotopes

The most primitive condensate-related material (CAI, AOA) is usually very ^{16}O-rich (Fig. 1.3a). Oxygen isotope data (Krot et al., 2010; Krot et al., 2009; Krot et al., 2008; Krot et al., 2006; Krot et al., 2001) indicate that CAIs found in the CB_b chondrites and in some CH chondrites are depleted in ^{16}O compared to those in other chondrite groups. The CAIs found in the CB_b chondrites are unique because they are depleted in ^{16}O ($\Delta^{17}O$ = -6‰ to -10‰) compared to CAIs in other chondrites groups (Fig 1.3a, b, c). This behavior has previously been explained by these CAIs forming from a unique parcel of nebula gas that was depleted in ^{16}O or by a parcel of nebula gas that was more evolved.

1.5.2 Lead Isotopes

The Pb-Pb ages (Krot et al. 2005a) of chondrules in the CB_a chondrite Gujba (4562.7±0.5 Ma) and in the CB_b chondrite Hammadah al Hamra 237 (4562.8±0.9 Ma) indicate that these chondrules formed later than many normal chondrules and more than 4myr **after** the formation of CAIs. They are the youngest precise absolute ages of chondrules determined from unequilibrated chondrites and are distinctly younger than the ages of chondrules in CR and CV chondrites (Amelin et al. 2004; 2007). The chondrule Pb-Pb

dates (4.9 ± 2.5 Myr after formation of CAIs) are similar to the ages of the metal grains using Hf-W ages of the metal silicate fraction recorded by the CB condensates (Kleine et al., 2005). This is consistent with CC chondrules inside zoned metal. The similar ages of the chondrules and the metal grains suggest that a single stage highly energetic event formed these young chondrules; the event which would allow these characteristics to be produced in a giant impact between two large planetesimals (Krot et al., 2005)

1.5.3 Iron Isotopes

Iron isotopes were analyzed to determine if the unique CB_b chondrules formed in the solar nebula (with a range of pressures, T and G/D ratios) or later in the vapor cloud of a giant impact (Zipfel and Weyer, 2007; Zipfel and Weyer, 2006). The Fe isotopic composition of HaH 237 and Isheyevo metal is much lighter than typical of bulk carbonaceous and ordinary chondrites (Zipfel and Weyer, 2007; Zipfel and Weyer, 2006; (Weyer et al., 2005) and combined with previous findings of light δ^{65}Cu in HaH 237 (Russell S.S. et al., 2003) imply that the metal formed in a reservoir with increasingly heavier Fe from Gujba through HaH 237 to Isheyevo (Zipfel and Weyer, 2006).

In addition, the lightest Fe isotopic compositions were found in the Ni-rich cores of chemically zoned metal grains in HaH 237 confirming previous findings that Ni-rich grains are enriched in light Fe (Alexander and Hewins, 2004). There is zonation in both Fe and Ni isotopes in the metal, δ^{62}Ni and δ^{57}Fe, increasing by 8‰ into the Ni-rich rims, the opposite to evaporation (Alexander and Hewins, 2004).The light Fe cores support a

condensation origin for some of the metal grains. This might be the result of condensation from a gas derived by partial evaporation of metal. This requires rapid (non-equilibrium) condensation, i.e. an event on a smaller scale than nebular condensation such as a vapor cloud produced after an impact.

Some of the CC chondrules found in CB chondrites are included in these zoned iron nickel grains, the cores of which have lower isotopic values than carbonaceous and ordinary chondrites. The CC chondrules must have formed prior to the Fe-Ni grains to be enclosed inside them, i.e. condensed at higher temperature during the same formation process.

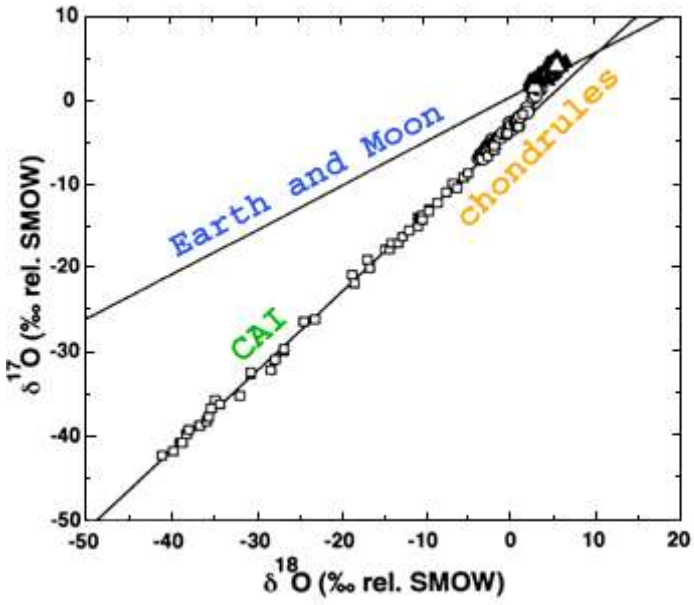

Figure 1.3a Oxygen Isotopes in Meteorite (Clayton 1993)

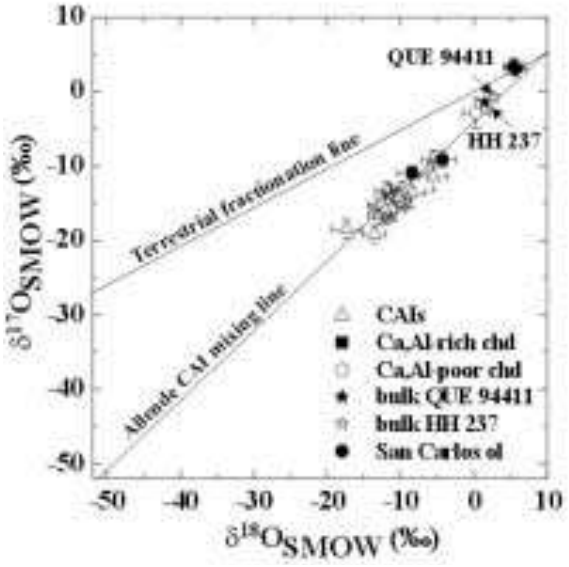

Figure 1.3b CB_b chondrules are depleted in ^{16}O compared to other chondrule types (Krot et al., 2002 data from Clayton and Mayeda).

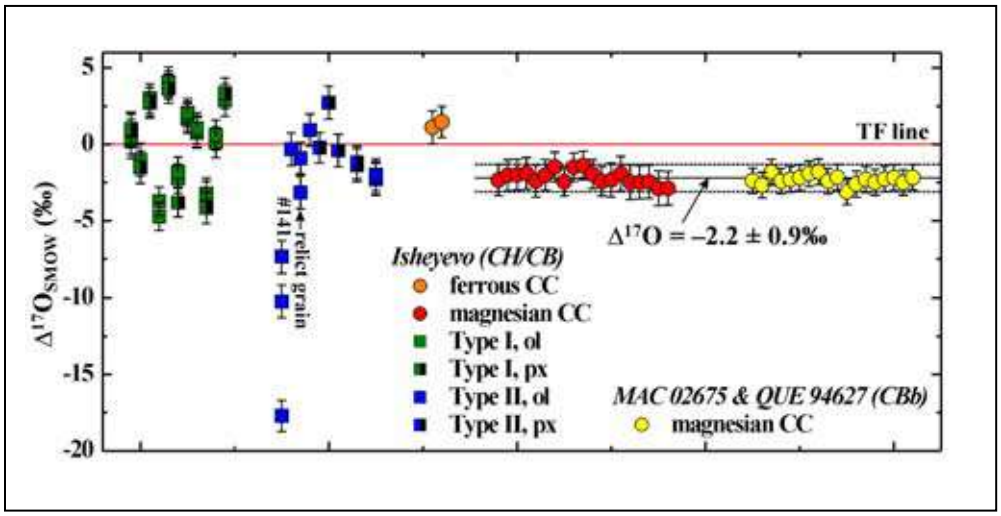

Figure 1.3c Oxygen isotope data of CH and CB_b chondrules (Krot et al., 2010).

1.6 Chondrules: Clues to an Impact Origin

Chondrite spectra match asteroidal sources and the Kirkwood Gaps document high relative velocities in the asteroid belt. Energetic collisions then are expected, and the largest may generate a significant melt fraction. Thus not all chondrules need necessarily be formed in the nebula. CB_b chondrules are a good candidate for formation in an impact plume, because of the unique textures, composition patterns, ages, relationship to condensate metal, and may well have a different thermal history from normal chondrules.

Considering that after numerous years of research the mechanism for chondrule formation has not been resolved and, as discussed in this chapter, new insight into the formation of planetesimals, protoplanets, and impact have been gained, the previous hypothesis that some chondrules formed via impact needs to be reexamined. This chapter has outlined the main reasons why this hypothesis has been disregarded and highlights the reasons why it should be re-scrutinized as a formation mechanism for these enigmatic silicate droplets.

In the chapters which follow, my research has focused on the most plausible group of chondrules which may have formed via an impact between two bodies. Through repeated experiments of synthetic chondrule material the unique chondrules which are found in the CB_b chondrules have been reproduced and a model has been developed which supports their formation through impact and the development of a vapor plume. In chapter 4, I relate the required thermal history of these chondrules to the aerodynamic sorting and

convection currents that would be produced following impact, and a scenario for the generation of these chondrules, their chondritic hosts, and their possible genetically related chondritic groups is proposed.

Chapter 2: The CR Chondrite Clan

2.1 CR Chondrite Clan Characteristics

The discovery that chondrites have the composition of condensable matter of the Sun was the turning point for chondrite studies and in turn chondrule research. Bulk chemical information was used to divide chondrites into three main classes, Ordinary, Carbonaceous, and Enstatite, which are essentially solar in composition with differences in the amount of total iron and in the proportion of iron in the metal state to iron in the minerals (Sears 2004). The carbonaceous chondrites are divided into 8 groups, CI, CM, CO, CV, CK, CR, CH, and CB.

The CR (Renazzo) chondrite clan is considered carbonaceous because their whole rock elemental abundances and oxygen isotopic compositions are similar to other members of the Carbonaceous chondrites (Krot et al., 2002; Weisberg et al., 1995, 1993). Their refractory lithophile/Mg abundances relative to CI (Ivuna-type) chondrites, which are thought to most closely represent the composition of the solar system, contain no chondrules, no metal phases, and consist of only a highly altered matrix like material (Zanda 2004), are ≥ 1.0 (Fig 2.1). Although hydrously altered, the CR chondrites are considered to be among the most pristine early solar system materials because their refractory lithophile/Mg abundance ratios relative to CI chondrites are ~1.0 (Krot et al., 2002; Krot et al., 2001; Weisberg et al., 1993; Kallemeyn and Wasson, 1981). In addition, their bulk oxygen-isotopic compositions plot below the terrestrial fractionation

line (Fig 2.2) (Krot et al., 2002; Krot et al., 2001). The CR chondrites clan is made up of the following members (Ivanova et al., 2006; Weisberg et al., 1995):

1. Renazzo like group CR
2. High metal group CH
3. Bencubbin-like subgroup CBa meteorites (i.e. Bencubbin, Gujba, and Weatherford)
4. Bencubbin-like subgroup CBb meteorites (i.e. HaH 237 and QUE 94111 paired w/ QUE4627, MAC 02675)

CH/CBb Isheyevo

5. Lewis Cliff (LEW) 85332

The CR *clan* is characterized by a high content of FeNi metal (up to ~70% volume) abundant chondrules (~30% volume), rare refractory inclusions, and very rare clasts of fine grained, heavily hydrated CI chondrite like material (Krot et al., 2001; Weisberg et al., 1993). With the exception of the CR chondrules that have glassy or phyllosilicate mesostasis (Krot et al., 2002), the Type I chondrules and rare refractory inclusions found in the rest of the clan show no evidence of aqueous alteration (Krot et al., 2002). Their bulk compositions show large depletions in moderately volatile lithophile and siderophile elements, increasing as a function of volatility (Krot et al., 2001; 2002). It was proposed by Meibom et al. (2000) that the CB_b escaped thermal metamorphism above ~500K because of the presence of metastable FeNi metal grains. Meibom et al., (2000) concluded that the volatility-related abundance patterns were established in the nebula before formation of these meteorites' parent bodies and more recently an impact

formation model has been proposed in which chondrules and metal grains formed from a vapor-melt plume after the protoplanetary disk had mostly dissipated (Krot et al., 2005, 2006). Their primitive nature makes these chondrites important for understanding high-temperature processes that resulted in the formation of their components (Krot 2001).

The CB chondrites consist of six meteorites, Bencubbin, Gujba, Weatherford (BGW), Mac Alpine Hills 02675 (MAC), Hammadah al Hamra 237 (HH237) and Queen Alexandra Range (QUE) 94411 which are characterized by similar oxygen isotopic compositions, high (60-70 vol %) abundance of Fe, Ni metal +/- sulfide, and depletion in moderately volatile elements (Krot et al., 2001; Weisberg et al., 1995; Weisberg et al., 1993).These meteorites are subdivided into CB_a (BGW) and CB_b (MAC, HH237 and QUE 94411) types. CB_b are finer grained than BGW, contain rare uniformly ^{16}O poor refractory inclusions and abundant chemically zoned Fe, Ni metal grains that are not present in BGW. The CB chondrules are metal free, but small cryptocrystalline chondrules are commonly observed in thin section inside chemically zoned metal condensates in CB_b (Krot et al., 2005).

2.2 CB_b Chondrules

The textures of the chondrules in the CB_b chondrites are different from those in normal chondrites and these differences may be the result of the formation environments or evolving formation conditions. Normal chondrules show igneous, porphyritic textures, with phenocrysts of olivine and low-Ca pyroxene set in glassy mesostasis. These textures

are consistent with crystal growth from a rapidly cooling (100 or slower -1000 K/hour) silicate melt (Krot et al., 2005; Desch and Connolly, 2002) The chondrules often contain relic fragments of earlier generations of chondrules indicating that the formation process was repetitive, and chondrules in most chondrites are surrounded by fine grained igneous rims or accretionary rims in CM chondrules (Krot et al., 2002; Krot et al 2001; Wasson et al., 1995).

Chondrules found in the CB_b chondrites have no phenocrysts or the igneous rims found in some chondrules in other groups, contain no FeNi metal or sulfide, and can be divided into two textural types: (skeletal) barred olivine (SO) and cryptocrystalline (CC) (Fig 2.3a-e). These chondrules are magnesium rich (type I) and their bulk compositions normalized to Si and CI chondrites show a continuum in refractory elements between SO and CC (Krot et al., 2001; Krot et al., 2005) though there are slightly different trends for SO and CC for some element pairs. SO and CC chondrules show large depletions in Mn, Na, and K. The SO are enriched in refractory lithophile elements (Ca, Al, Ti) over CI levels, spanning the range from ~1.2 to 10X that of CI. Calcium, Al, and Ti abundance patterns are flat. The CC chondrules are depleted and complementary in these refractory elements to SO chondrules and span the range from ~1 to <.03 X CI.

A review of all available data displays an overlap of SO and CC chondrule compositions, at about 52%SiO2, 4%Al2O3, (Fig. 2.4a) 2.8%CaO (Fig. 2.4b), and 2 to 4%FeO (Fig. 2.4c). The overlap may indicate the transition between condensation and evaporation in the formation of these chondrules. The overlap corresponds to bulk CR chondrite if we

remove components lost by liquid immiscibility and evaporation, i.e. metal, sulfide, Na and all except 3% of the FeO. Typical CV Type I chondrules CC are included in the review of the data to emphasis that the CBb chondrules have a unique trend.
Skeletal olivine chondrules (25 – 250μm) are typically larger than CC chondrules (20-100um) (Krot et al., 2002). There is a correlation between bulk chemical compositions of chondrules and their sizes: CaO and Al_2O_3 increase, and MgO and SiO_2 decrease with increasing chondrule size. Simply stated, the refractory-enriched SO chondrules are larger than the refractory-depleted, fine grained CC chondrules (Krot et al., 2006).

The absence of fine grained rims and chondrules with porphyritic or granular textures suggests that these chondrules crystallized in a dust free environment from melts completely free of nuclei (Krot et al., 2001). A review of the bulk compositions of all available data for CB_b SO and CC chondrules' complementary behavior of refractory lithophile and volatile elements (Fig 2.5.a, b c) suggests that they formed in a chemically closed system by fractional condensation (Krot et al., 2001; Krot et al., 2002) or evaporation and condensation (Krot et al., 2001, 2002). The observed depletion of chondrules and metal (Krot et al., 2005) in moderately volatile elements requires formation of both at high ambient temperature above the highest condensation temperature (~1200 K) of these elements (Mn, Na, K, S, Cu, Zn, and Ga).

2.3 Relationship between CH and CB Chondrites

The CH chondrites are a group of primitive carbonaceous chondrites (Bischoff et al. 1993). Typical members include Allan Hills 85085, Acfer 182, and Northwest Africa (NWA) 739 and 770 and Isheyevo which has properties of both CH and CB chondrites (Krot et al., 2005) (Figure 1.9). They are characterized by 1) abundant FeNi (~20% vol) grains; 2) small chondrules and CAIs; 3) very abundant cryptocrystalline chondrules; 4) lack of matrix (<5 vol %) and presence of heavily hydrated clasts; 5) large depletions in bulk volatile and moderately volatile element abundances (Krot et al. 2002; Scott and Krot, 2007).

The CH chondrites contain up to 15% nickel iron and belong to petrologic types 2 or 3, and isotopically and chemically they are very close to the CR chondrites and the CB chondrites. Most of the chondrules and CAIs are very small and contain certain amounts of phyllosillicates and other traces of aqueous alteration that took place during their formation. There is a close relationship between CH and CB chondrites (Fig 2.6).

2.4 Impact Model

I have compiled all available data for the CB chondrules and have shown that the CB_b chondrule analyses are coherent and they can be derived from an impact into a CR- like parent. The bulk FeO composition of the CR (Renazzo) chondrite is 19%. An impact would cause most of the Na and Fe to be lost from evaporation. By developing a model

for Fe loss to 3% supports that a CR parent body can be a suitable candidate for the formation of these unique chondrules (Fig 2.6a and b).

I have shown above that the chondrules can be derived from a CR-like material, though CB_b chondrites contain more metal than CR chondrites, so that an external source is required such as an iron impactor. Both the SO and the CC chondrules may have formed when a FeNi core fragment collided with a grandparent body, their host chondrites accreting either back on this target or as a new parent body down range from the collision. The most suitable grandparent body to fit this model is Pallas, which has been suggested to be the parent material for CR chondrites by IR spectrum analysis (Sato 1997).

A genetic relation has previously been *suggested for* all members of the CR clan. The recent discovery of the Isheyevo meteorite may provide the genetic link between these two carbonaceous chondrite groups (Ivanova et al., 2006); this meteorite contains metal-rich material similar to the CB_b chondrites and metal-poor material similar to CH chondrites in sharp contact. The metal rich material is dominated by zoned metal grains and non-porphyritic chondrules and the metal poor lithology contains much less (zoned) metal and some porphyritic chondrules. The presence of metal rich and metal poor lithologies and similar mineralogies that are clearly defined by a contact boundary in this meteorite provides strong evidence for its formation in time and proximity to each other (Figure 2.7).

The relationship between the CR, CH, CB_a, and CB_b chondrites can be explained by an impact model. An impact between a dense iron rich impactor and a large target would create a melt and a vapor plume composed of residues and condensates. A temporary atmosphere or an ejected cloud would be generated with convection cells resulting in aerodynamic sorting and an unusual cooling history of the impact material.

In the next chapter I constrain the model further through experimental petrology. I investigate simple and complex cooling histories and show that the SO chondrules of CB_b chondrites have textures that cannot be duplicated for linear cooling, as is the case for normal porphyritic chondrules, but require a complex heating and cooling which is consistent with convection cycles in this vapor plume.

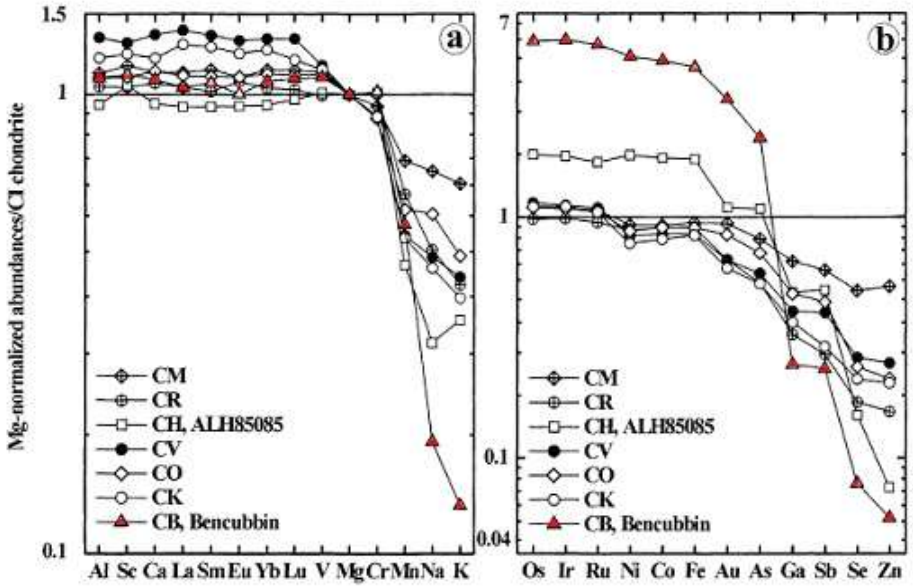

Figure 2.1: Magnesium and CI normalized bulk lithophile (a) and siderophile (b) element abundances of the carbonaceous chondrites groups. The CR, CH (ALH 85085), and CB (Bencubbin) have CI-like abundances of refractory and normal lithophile elements and are highly depleted in moderately volatile lithophile elements such as Mn, Na, and K. The CH and CB chondrites are highly enriched in refractory and normal siderophile elements and depleted in moderately volatile siderophile elements (Krot et al., 2002) (data from Kallemeyn and Wasson , 1981, 1982, 1985, Kallemeyn et al., 1978, 1991, 1994, and Weisberg et al, 2001).

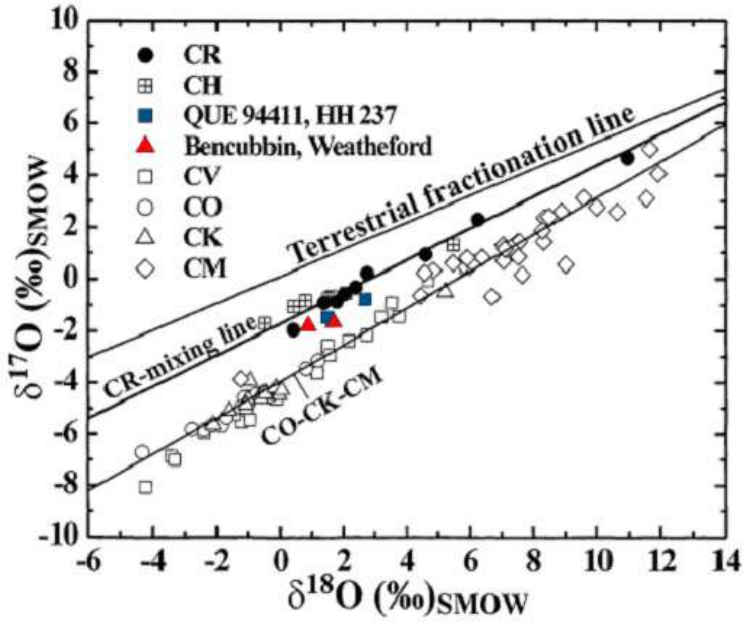

Figure. 2.2: Bulk oxygen-isotopic compositions of the major carbonaceous chondrites groups. The Bencubbin, Weatherford, Hammadah al Hamra 237, QUE 94411, CR and CH chondrites define a unique CR-mixing line (Krot et al., 2002) (data from Clayton and Mayeda, 1999).

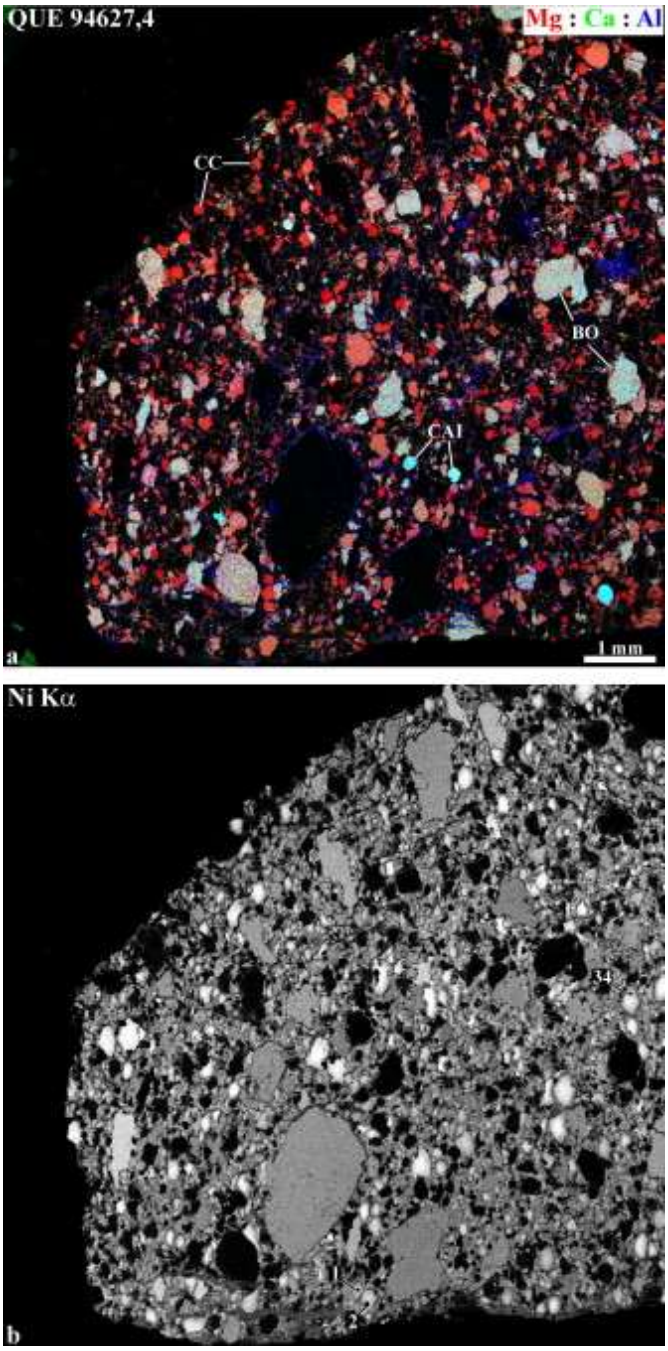

Fig. 2.3: (a) Combined elemental map in Mg (red), Ca (green) and Al Kα X-rays (blue) and (b) elemental map in Ni Kα of the CB_b carbonaceous chondrite QUE 94627, *4*. Two types of chondrules can be recognized: magnesium-rich cryptocrystalline (CC, reddish in color) and aluminum-rich barred (SO, bluish in color). The cryptocrystalline chondrules are systematically smaller than the skeletal chondrules. Cryptocrystalline silicate inclusions are found inside chemically-zoned metal grains (Krot et al., 2009)

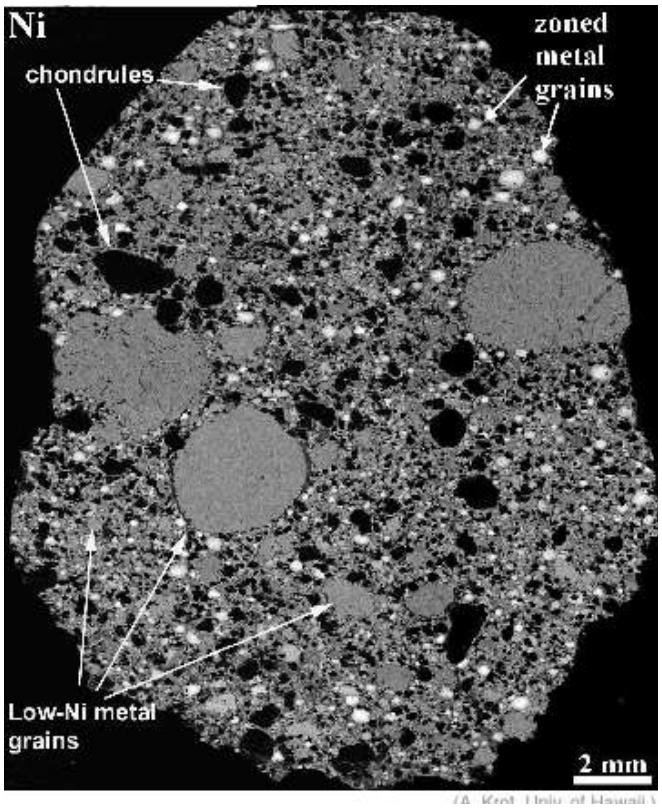

Figure 2.3c: Skeletal olivine (SO) chondrules, cryptocrystalline chondrules (CC), and Fe Ni grains found in the CB_b chondrites HaH 237 (Krot et al., 2009).

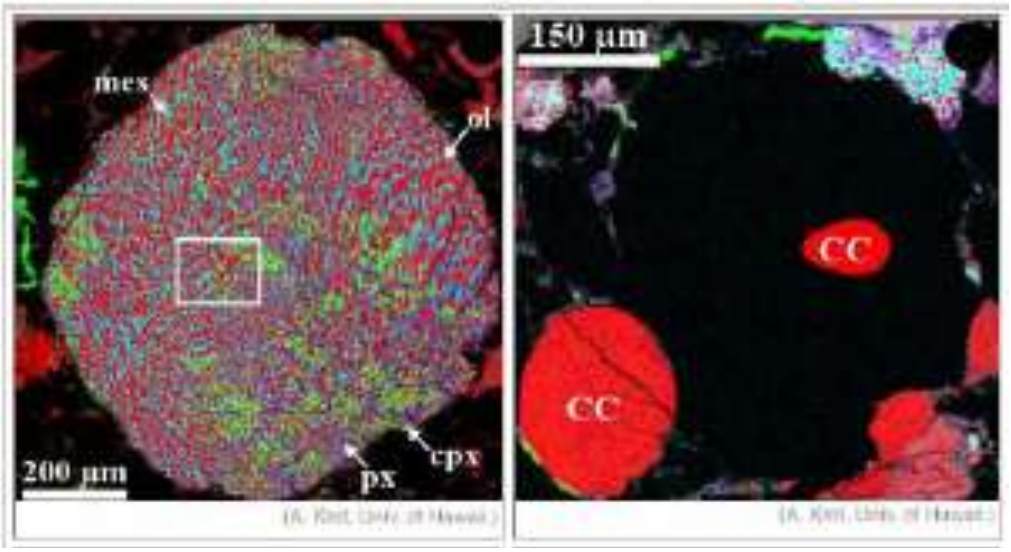

Figure 2.3d: The image is of the CB_b chondrite HH237 was created by combining x-ray intensities due to magnesium (red), calcium (green), and aluminum (blue). The reddest grains are olivine, greenish is pyroxene and the bluest is glassy material. (Krot et al., 2001) The red blebby material is the olivine.

Figure 2.3e: The uniform red color in this image of CB_b chondrite HH237 indicates that they are Mg-rich and homogeneous. The black area is a zone metal grained (Krot et al., 2001) condensates cooled rapidly and there was no time for additional solid condensates to form around the edges of the spheres (Morfill et al., 1998). In contrast to typical chondrules, these chondrules appear to have escaped remelting. If remelted, porphyritic textures, relic grains, and enrichment of chondrules in moderately volatile elements would have been created (Krot et al., 2001).

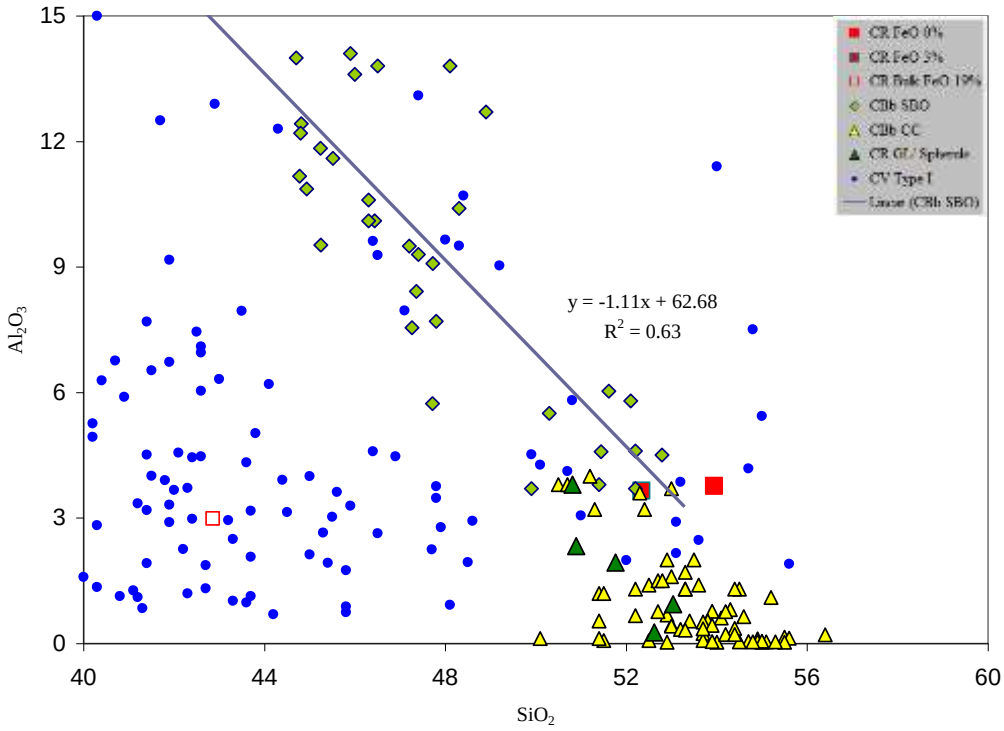

Figure 2.4a: There is overlap of SO and CC chondrule compositions, at about 52% SiO_2 and 4% Al_2O_3. This overlap corresponds to bulk CR chondrite if we remove components lost by liquid immiscibility and evaporation, i.e. metal, sulfide, Na and all except 3% of the FeO (data from Krot et al., 2002, 2007, 2010and McSween, 1977a, 1977b).

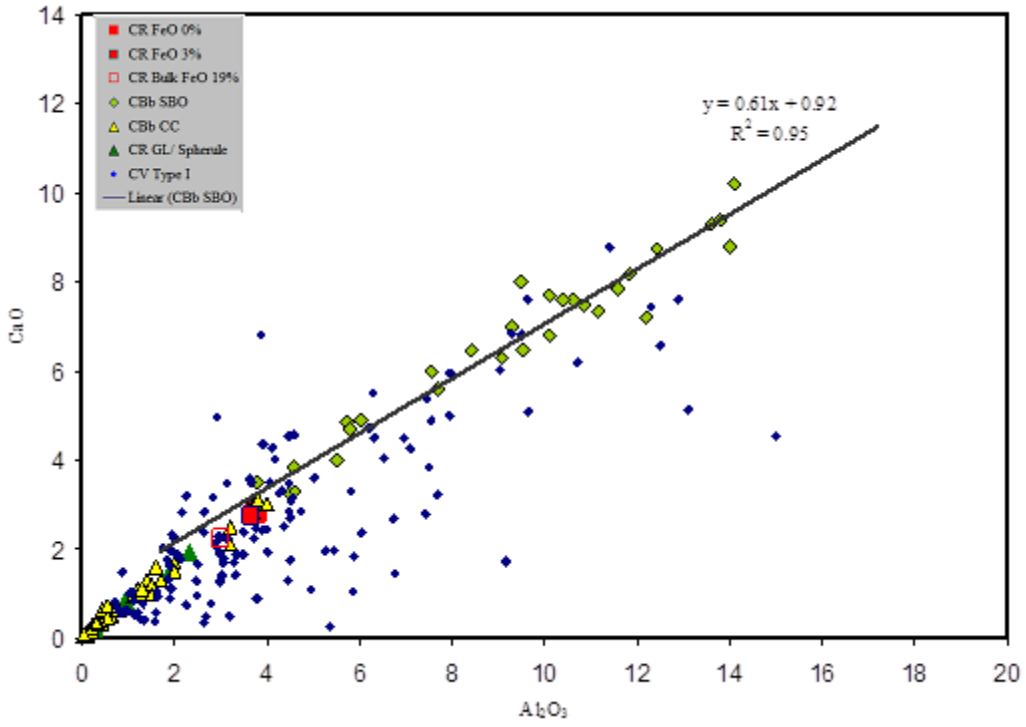

Figure 2.4b: There is overlap of SO and CC chondrule compositions, at about 4% Al_2O_3 and 2.8% CaO. This overlap corresponds to bulk CR chondrite if we remove components lost by liquid immiscibility and evaporation, i.e. metal, sulfide, Na and all except 3% of the FeO (data from Krot et al., 2002, 2007, 2010and McSween, 1977a, 1977b).

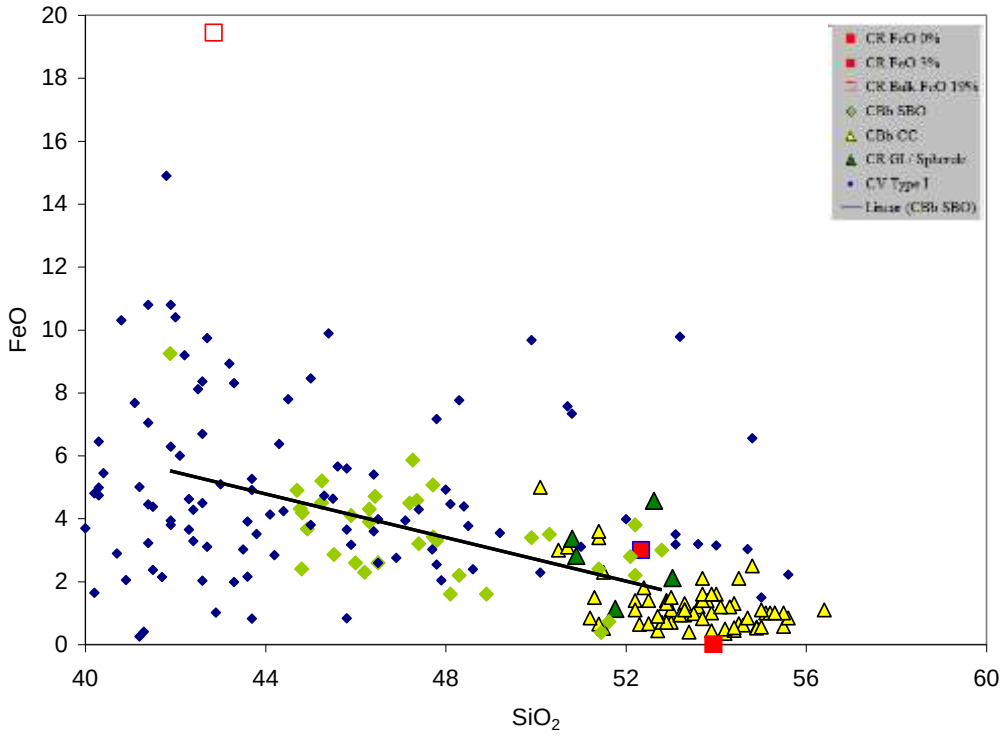

Figure 2.4c: There is overlap of SO and CC chondrule compositions, at about 52%SiO_2 and 2 to 4%FeO. This overlap corresponds to bulk CR chondrite if we remove components lost by liquid immiscibility and evaporation, i.e. metal, sulfide, Na and all except 3% of the FeO (data from Krot et al., 2002, 2007, 2010and McSween, 1977a, 1977b).

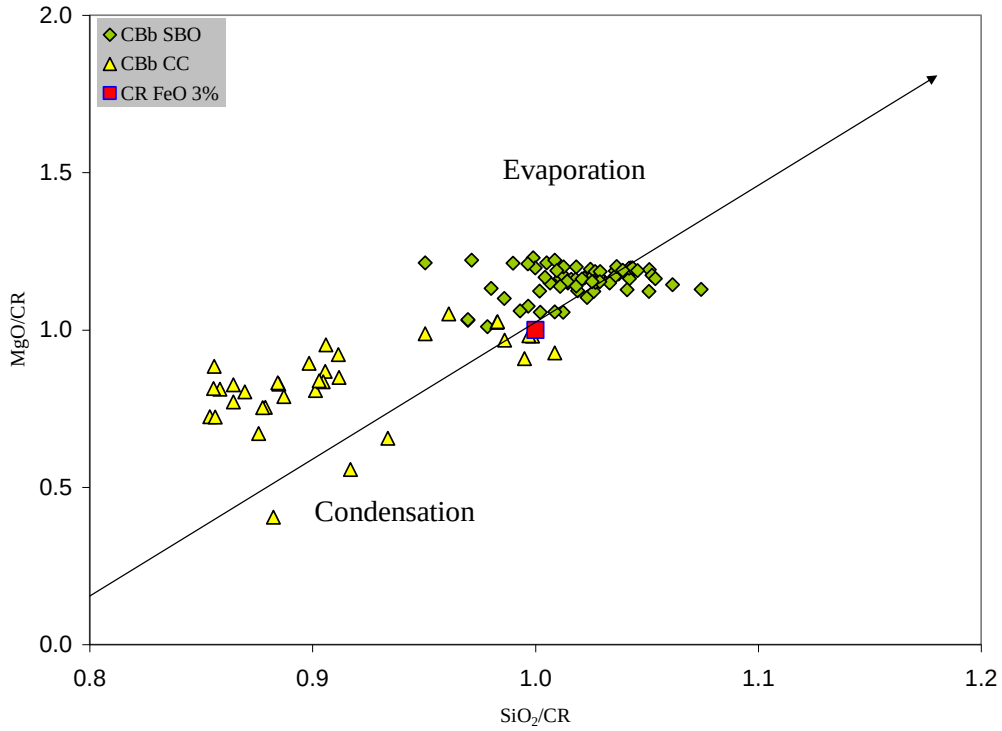

Figure 2.5a: A review of the SiO_2 and MgO bulk compositions of all available data for CBb SO and CC chondrules' complementary behavior of refractory lithophile and volatile elements (data from Krot et al., 2002, 2007, 2010).

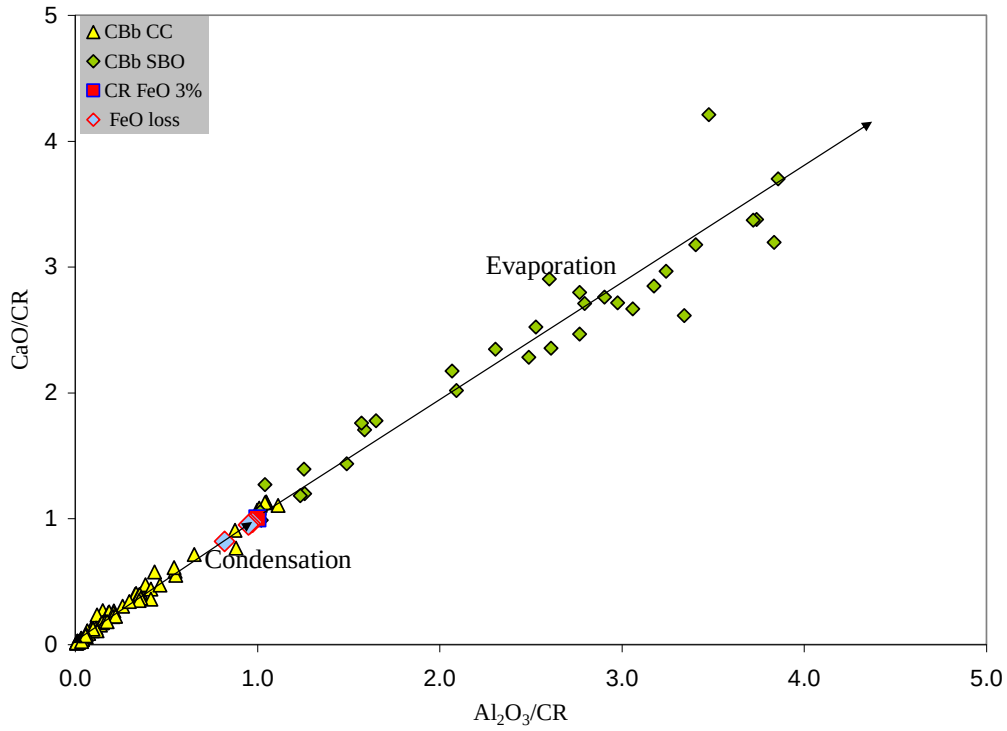

Figure 2.5b: A review of the Al_2O_3 and CaO bulk compositions of all available data for CB_b SO and CC chondrules' complementary behavior of refractory lithophile and volatile elements (data from Krot et al., 2002, 2007, 2010).

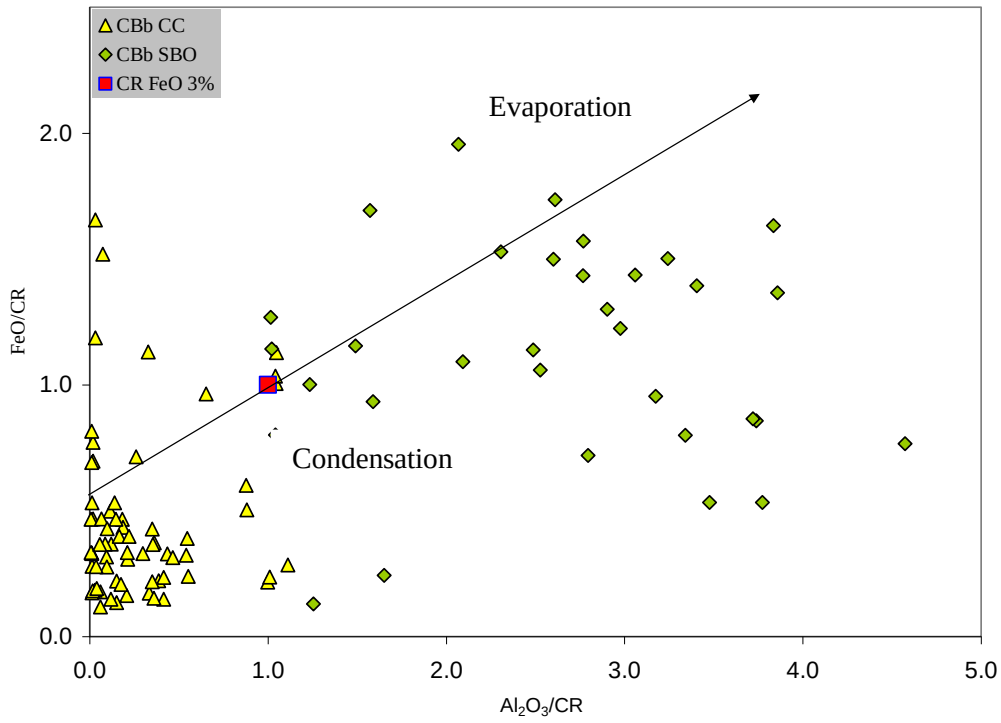

.

Figure 2.5c: A review of the Al_2O_3 and FeO bulk compositions of all available data for CB_b SO and CC chondrules' complementary behavior of refractory lithophile and volatile elements (data from Krot et al., 2002, 2007, 2010).

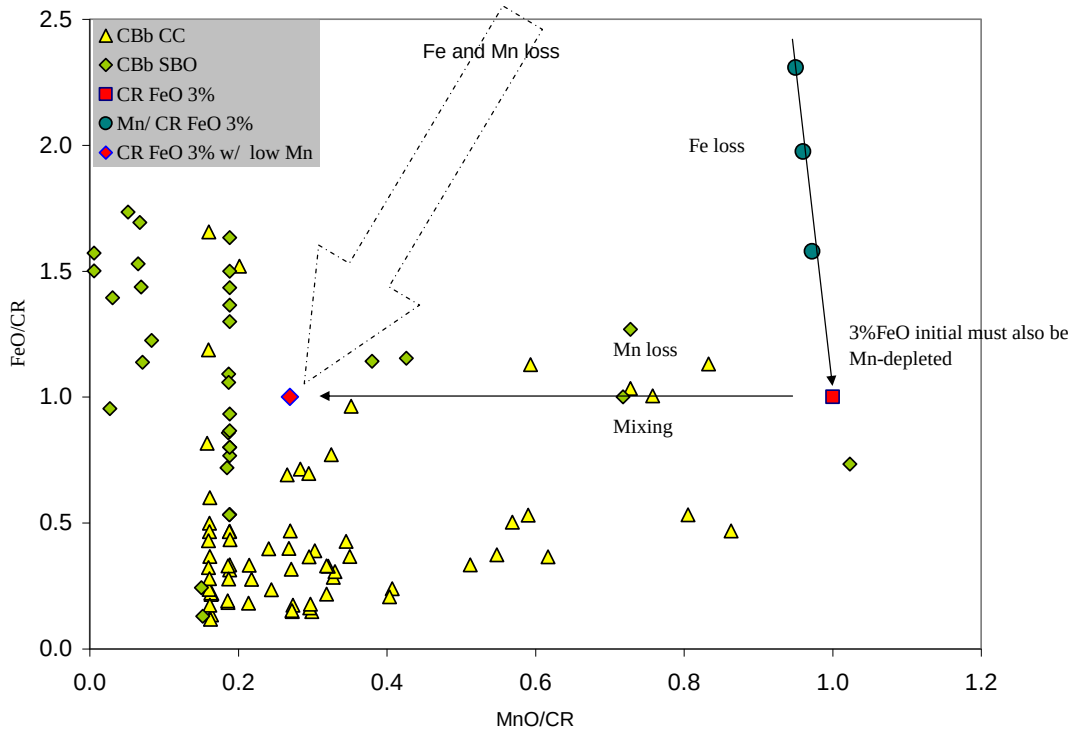

Figure 2.6a: The bulk FeO composition of the CR (Renazzo) chondrite is 19%. An impact would cause most of the Na and Fe to be lost from evaporation. By developing a model for Fe loss to 3% supports that a CR parent body can be a suitable candidate for the formation of these unique chondrules (data from Krot et al., 2002, 2007, 2010).

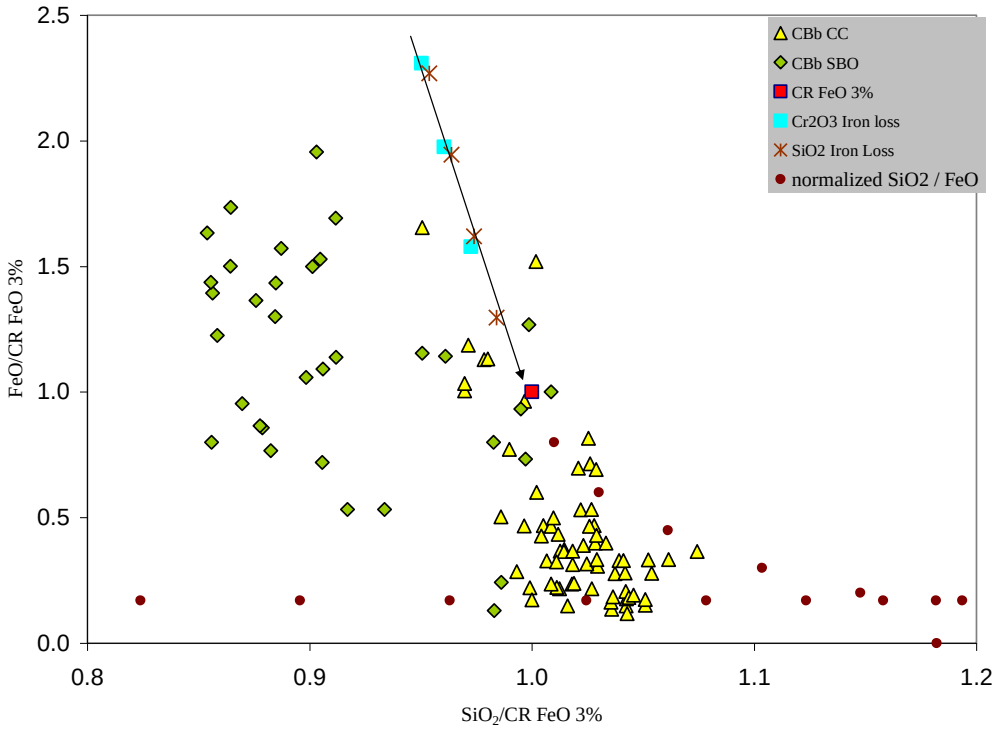

Figure 2.6b: The bulk FeO composition of the CR (Renazzo) chondrite is 19%. An impact would cause most of the Na and Fe to be lost from evaporation. By developing a model for Fe loss to 3% supports that a CR parent body can be a suitable candidate for the formation of these unique chondrules (data from Krot et al., 2002, 2007, 2010).

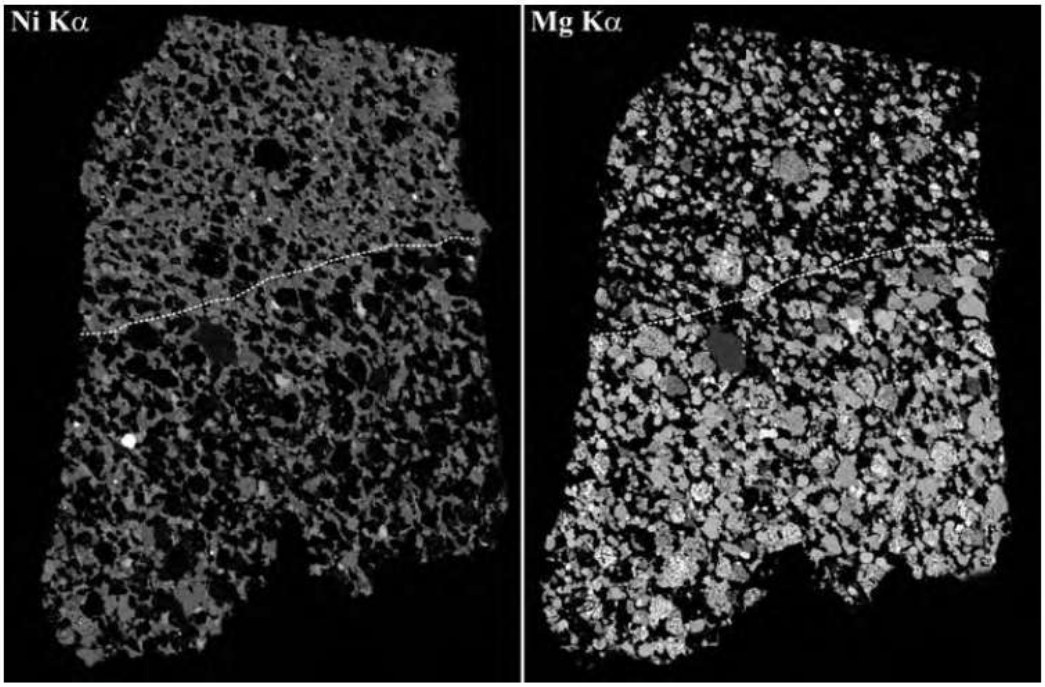

Figure 2.7: Elemental maps in Ni Kα and Mg Kα X-rays of Isheyevo displaying a gradual contact between metal-rich (top) and metal poor lithologies. The metal rich lithology is texturally similar to the CB_b chondrites HaH 237 and QUE 94411. It is dominated by zoned Fe, Ni metal grains and non-porphyritic (cryptocrystalline and skeletal olivine) chondrules. The metal poor lithology is mineralogically similar to CH chondrites. It contains much less metal and higher abundance of chondrules compared to the metal rich lithology; most metal grains are chemically zoned; large proportion of chondrules has porphyritic texture although non-porphyritic chondrules are also common (Ivanovo et al., 2006).

Chapter 3: Experimental Methods and Results

3.1 Introduction

Porphyritic textures are produced from (partial) melting at temperatures below the liquidus. The textures progress from porphyritic to barred to glass and the variation in texture is a function of greater melting temperatures which correlates to an increase in the degree of melting experienced by the experimental charges (Connolly et al., 1988). Elongate hopper porphyritic olivine is a transitional texture dominated by hopper olivine crystals with an aspect ratio of at least 3 to 1 set in a glassy mesostasis (Connolly et al., 1988). The olivine crystals found in chondrules are actually plates embedded in glass or mesostasis; the crystallographic orientations of olivine in a parallel platelet domain are, by definition (of parallel) identical (Tsuchiyama et al., 2004). A barred olivine chondrule usually has an olivine crystal that covers the chondrule surface; this rim has the same crystallographic orientation as inner olivine platelets, which connect to the rim. The rim of the olivine crystal is different from accretionary or igneous rims composed of fine grained or coarse grained material that also surround chondrules (Tsuchiyama et al., 2004). Barred olivine chondrules are regarded as rapid crystallization products (Miura et al., 2010) which are a function of nucleation delay of olivine from supercooled melts (Tsuchiyama et al., 2004; Lofgren and Lanier 1990; Hewins and Newsom, 1988).

A chondrule with a single set of parallel platelets with an olivine rim is described as a classic BO chondrule while ones with multiple sets of parallel olivine platelets described as multiple BO chondrules (Weisberg 1987). Numerous experiments have been

conducted to determine thermal histories of chondrules to gain insight into their region of formation (Tsuchiyama et al., 2004, Faure et al., 2003, Hewins and Fox 2003; Connolly and Hewins 1995, Connelly et al., 1998; Nagahara et al., 1994; Radomsky and Hewins 1990; Lofgren and Lanier 1990; Lofgren and Russell 1985; Donaldson 1976; Blander et al., 1976; Nelson et at., 1972). However, single classic BO textures have rarely been produced except for a seeded experiment by Radomsky and Hewins (1990). Connolly et al. (1988) reported an 'almost' classic texture and textures close to classic BO were created in small samples (<10mg) by Tsuchiyama et al., (2004). I emphasize that there is a hierarchical sequence from porphyritic to barred to glassy chondrules, whose formation conditions are well understood. However, skeletal barred olivine chondrules do not have a simple place in this sequence and have not been produced in previous experiments with conditions thought more, or even less, appropriate for chondrules.

This chapter reports the results from an extensive suite of dynamic crystallization cooling rate experiments on the CB_b chondrule compositions. In several of the dynamic crystallization experiments a unique blebby skeletal olivine texture was created. The unique skeletal barred olivine (SO) and cryptocrystalline (CC) textures present in aluminum and magnesium rich CB_b chondrules add additional constraints to the formation environment of the components in CB_b chondrites. By combining the thermal histories of these chondrules with metal condensation conditions, a formation model may be created.

In addition, the experiments conducted on the synthetic magnesium and aluminum rich chondrules resulted in near classic barred, multiple barred, elongate hopper porphyritic and dendritic olivine textures as well as glass, which are of interest for the understanding of normal chondrules. The role of pressure at the time of formation and its influence on evaporation and condensation temperatures will be addressed in the later modeling chapter where I reconstruct the sequence of conditions that generated these unique CB_b chondrules and the possible relationship between them and other members of the CR chondrite clan.

As previously stated, CB_b chondrules have a skeletal/ barred olivine texture or are cryptocrystalline; chondrules with porphyritic textures are absent (Krot et al., 2001, 2002). Barred olivine chondrules are rare (Gooding and Keil, 1981) and their textures represent a borderline between complete and incomplete melting. Thus their liquidus temperatures are interpreted as an indicator of the maximum melting temperatures experienced by the chondrule (Connolly et al., 1998). Skeletal (barred) olivine chondrules differ from typical barred olivine chondrules by not having an outermost olivine shell (Krot et al., 2006) and having short blebby rather than elongated "bars". They are thought to represent crystallization from initially superheated melts. Crystals in general become progressively more skeletal with increasing cooling rate and degree of supercooling (Donaldson 1976). Cryptocrystalline chondrules are also reported as the product of crystallization of supercooled droplets (Gooding and Keil, 1981). In order to replicate these textures the liquid~~us~~ temperatures were exceeded and the cooling rate for

these compositions was varied. Some of the experiments described below were successful in replicating the natural SO textures.

The chondrules in CB_b meteorites range from refractory depleted and volatile depleted (CC) to refractory-enriched and volatile depleted (SO). The chondrules in QUE 94411 (Krot et al., 2002) are arranged (Table 3.1) in a compositional sequence from refractory-poor to refractory-rich (Al_2O_3 ~0-14%). This is in the order of decreasing Mg (in these compositions more volatile than Si) and decreasing calculated liquidus temperatures with cryptocrystalline textures at the high end (1675°C) and skeletal olivine textures at the low end (1509°C). Since cryptocrystalline glasses are commonplace, in the experimental work I emphasized the unique SO chondrules.

3.2 Starting Compositions

The compositions used were limited by the capability of the Deltech furnaces with a maximum temperature of approximately 1600°C (Table 3.1). The charges must be able to be heated above their calculated liquidus temperatures, so all nuclei are destroyed and skeletal crystals begin to form after supercooling (Lofgren, 1996). Of the six chondrules with SO texture listed in Krot's paper (Krot et al., 2002), four have compositions that fit this criterion. The two chondrules found in the CB_b chondrite named QUE94411 with the lowest calculated liquidus temperature were selected, the fifth (BO5 -1570) and the sixth (BO6 - 1509), because higher temperature above the liquidus could be reached. A starting material of minerals and oxides with bulk compositions as given by Krot et al.

(2002) was mixed together to create these synthetic chondrule compositions. The chemical compositions of the starting material were verified by analyzing an experimental charge heated at a temperature above the calculated liquidus for five minutes and then quenched in a room temperature water bath.

None of the five analyses listed in Krot's paper of the chondrules with CC texture (Krot et al., 2002) are compatible with the limitations set by the furnace. In order to duplicate these textures, the compositions (Table 3.2) were adjusted from magnesium rich to iron rich by adding a 50% powered mixture of fayalite composition using iron oxide and quartz in the proper proportions. By adjusting the Fe/Mg ratio of the mixture, the liquidus temperature of the composition was decreased so that an equivalent olivine-pyroxene-normative composition could be melted (Table 3.2). This lowered the calculated melting temperature from 1680ºC to 1580ºC, a temperature accessible in the Deltech. It is recognized that adjusting the composition of the magnesium rich synthetic chondrules changes the normative olivine/pyroxene ratio a little, but in order to achieve total melting this adjustment was necessary.

3.3 Methodology

Eighty-seven dynamic crystallization experiments were conducted in the Deltech Dt-31-VT-OS muffle tube furnace housed in the Department of Earth and Planetary Sciences, Rutgers University to reproduce the SO texture and CC textures. Of the 87 experiments

that were run, 52 were successful. The experimental conditions are summarized in table 3.3 and 3.4 and images were taken of the successful runs (Appendix a, b, and c).

A stainless-steel press was used to compress the starting material powder into 5.2 – 7.3 mg cylindrical pellets that were placed into a funnel shaped 15mm long rhenium wire to inhibit iron transfer. The rhenium wire was fastened to platinum wire connected to a type S thermocouple (Pt100-Pt90:Rh10). The type S thermocouple was calibrated against the melting point of Au (1064 C) and Pd (1554 C) to monitor the temperature in the muffle tube furnace. After every ten experiments the thermocouple was re-calibrated against the melting points to ensure accuracy. The oxygen fugacity was established and controlled by mixing gasses of CO-CO_2 (Nafziger et al., 1971) using high precision flow meters, which created an atmosphere with an oxygen fugacity of IW-1, or one log unit below iron-wustite buffer conditions. All charges of the isothermal and cyclic cooling runs were water-quenched within 5 seconds of removal from the furnace.

The samples were observed under a binocular microscope and then were mounted in epoxy and polished sections were made. The samples were observed and images collected from the JEOL JXA 8200 electron microprobe at Rutgers University Laboratory, FEI XL30 SEM at Lehigh University, and the Cameca SX100 electron probe at the Université de Paris.

Chondrule	CC1	CC2	CC3	CC4	CC5	BO1	BO2	BO3	BO4	BO5	BO6
SiO_2	55.1	54.9	55.5	55.2	54.5	49.9	50.3	47.8	47.4	48.3	46.5
TiO_2	<.04	<.04	<.04	0.05	0.07	0.17	0.24	0.3	0.36	0.42	0.46
Al_2O_3	<.04	0.11	0.15	1.1	1.3	3.7	5.5	7.7	9.3	10.4	13.8
Cr_2O_3	0.77	0.76	0.65	0.85	0.8	0.78	0.75	0.62	0.44	0.48	0.35
FeO	1	0.56	0.58	1	0.66	3.4	3.5	3.3	3.2	2.2	2.6
MnO	0.07	0.07	<.07	0.12	0.12	0.14	0.16	<.07	<.07	<.07	<.07
MgO	44.3	44.7	44.3	42	42.9	38.3	36.7	35.3	33.1	32.5	28
CaO	<.04	0.08	0.11	0.95	0.98	2.7	4	5.6	7	7.6	9.4
Na_2O	<.05	<.05	<.05	<.05	<.05	0.07	<.05	0.06	<.05	<.05	<.05
K_2O	<.04	<.04	<.04	<.04	<.04	<.04	<.04	<.04	<.04	<.04	<.04
Total	**101.3**	**101.2**	**101.4**	**101.3**	**101.4**	**99.2**	**101.1**	**100.8**	**100.8**	**101.9**	**101.1**
Calculated Liquidus Temperature °C	1675°	1684°	1656°	1646°	1659°	**1602°**	**1573°**	**1617°**	**1586°**	**1570°**	**1509°**

Table 3.1: The chondrules in QUE 94411 (Krot et al., 2002) are arranged in a compositional sequence from refractory-poor to refractory-rich (Al_2O_3 ~0-14%). This is in the order of decreasing Mg (in these compositions more volatile than Si) and decreasing calculated liquidus temperatures with cryptocrystalline textures at the high end (1675°C) and skeletal olivine textures at the low end (1509°C).

Starting Compositions				
	CC2	CC2*	SBO5	SBO6
Si	54.4	47	47.1	46.5
Ti	0.0	0.04	0.4	0.5
Al	0.1	0.11	9.3	13.6
Cr	0.7	0.76	0.5	0.4
Fe	0.5	33	2.8	2.5
Mn	0.0	0.07	0.0	0.0
Mg	44.1	20	32.4	27.3
Ca	0.1	0.08	7.4	9.1
Na	0.0	0.05	0.1	0.2
K	0.0	0.04	0	0.0
	100	101.15	100	100

Table 3.2: Starting compositions for synthetic chondrules; compositions where selected by the heating capable of the Deltech Furnace.
* denotes modified synthetic compositions to lower liquidus temperature

BO5 & BO6 charges	Duration at liquidus (mins) Δt max	Cooling Rate C°/hr	Quench C°
BO5-1 BO6-1 BO6-7A	30	500	1000
BO5-2 BO6-2 BO6-7B	15	1000	1000
BO5-3 BO6-3 BO6-7C	15	1000	600
BO5-4b BO6-4 BO6-7D	60	1000	1000
BO5-5 BO6-5 BO6-7E	30	100	1000
BO5-6 BO6-6 BO6-7F	30	500	600
BO5-8 BO6-8 BO6-7H	30	1000	1000
BO5-9 BO6-9 BO6-7I	60	500	1000
BO5-10 BO6-10 BO6-7J	120	1000	1000
BO5-11 BO6-11	60	50	1000
BO5-12 BO6-12	180	1000	1000
BO5-13 BO6-7M	60	10	900
BO6-7N	45	isothermal	LIQUIDUS
BO5-15 BO6-15	1860(31hrs)	1000	1000
BO5-19	5	1000°C/hr to 1300°C remain at 1300°C for 96hrs 1000°C/hr to 1040°C	1040
BO5-20	5	1000°C /hr to 1300°C- 2 hrs at 1300°C increased 180°C/hr to 1450°C 1000°C/hr to 1300° C 24 hrs at 1300° C increased at 180°C/hr to 1486°C 1000°C/hr to 1300°C 24 hrs at 1300°C increased 180°C/hr to 1515°C 1000°C/hr to 1300°C	1300
BO5-21 BO6-21	12	BO5-21 inserted into Deltech 1433°C BO6-21 inserted into Deltech 1470°C increased 180°C/hr to 1660°C Remain above liquidus for 12 mins 1000°C/hr to 1330° 24hrs at 1330°C increased 180°C/hr to 1420°C 1000°C/hr to 1340°C 24 hrs at 1340° increased 180°C/hr to 1515°C 1000°C /hr to 1340°C 24hrs at 1340°C increased 180°C/hr to1493°C 1000°/h to 1340° for 72hrs	1340

Table 3.3 Experimental conditions for BO5 and BO6 charges

CC2* Samples	duration at liquidus (mins) Δt max	Cooling Rate C°/hr	Quench C°
CC2*-1	30	500	1000
CC2*-2	15	1000	1000
CC2*-3	15	1000	600
CC2*-4	60	1000	1000
CC2*-5	30	100	1000
CC2*-6	30	500	600
CC2*-8	30	1000	1000
CC2*-9	60	500	1000
CC2*-13	60	1000	1000
CC2*-15	240	1000°C/hr to1400°C and 500°C/hr to 1000°C	1000
CC2*-16	60	Rapid **cooling to 1000°C	1000
CC2*-17	120	1000°C/hr to1400°C and 100°C/hr to 1000°C	1000
CC2*-18	60	Rapid ** to 1400°C and 100°C/hr to 1000°C	1000
CC2*-19	4320 (72hrs)	Rapid ** to 1400°C and 100°C/hr to 1000°C	1000

Table 3.4 Experimental conditions for CC2* charges

* denotes modified synthetic compositions to lower liquidus temperature

** A rapid cooling rate indicates that power to the Deltech furnace was shut off and the charge experienced the fasted cooling rate thermally possibly in the furnace. The rapid rates were recorded on the thermocouple as ranging between 1100°C/h - 1200°C/h.

3.4 Results: Textures Reproduced

Most experiments used superliquidus temperatures and relatively high cooling rates (100-1000°C/hr) conducive to form skeletal crystals, dendrites and glass. Elongate hopper porphyritic olivine textures were produced in samples with short durations at near-liquidus temperatures which did not allow for a significant degree of melting in the charges. Barred olivine textures were produced in a wide range of experimental conditions where the degree of melting was high enough to destroy nuclei in the melt. In quench experiments glass was produced and in experiments with cyclic conditions skeletal blebby barred olivine textures were created.

The maximum temperature ($T_{max)}$ was varied for a subset of experiments; all parameters were kept the same on the samples except T_{max}. Increasing T_{max} allowed the sample texture to progress from ELHPO to BO in most cases (Fig. 3.1a-f). If Tmax was slightly higher than the liquidus temperature, T_{liq} (1509ºC) or the degree of superheating, $+\Delta T$ ($=T_{max} - T_{liq}$) was low the charge was composed of many sets of olivine bars with different directions and widths. If T_{max} was sufficiently higher than T_{liq} the number of olivine bar sets was reduced, appeared finer and were oriented in the same direction. Mirroring the work of Lofgren and Lanier (1990) the width of the olivine bars is thicker for samples with slower cooling rates (Fig. 3.1).

A subset of samples was analyzed to determine if reducing the quench temperature from 1000 to 600°C would affect the textures that were produce. There was no variation in textures (Fig. 3.2). For these moderately fast cooling rates, there is little additional

crystallization when the cooling interval is increased, suggesting that the glass transition temperature is high.

A near classic barred texture was generated in one sample following the classification described by Tsuchiyama et al., (2004) (Fig. 3.3). This near classic texture was produced in samples with an intermediate to large delta T, and with lower cooling rate (100°C/hr). The majority of textures produced were those with multiple bars (Table 3.5) (appendix a & b). The cryptocrystalline textures (CC) were achieved in charges made from the adjusted composition (CC2*) that exceeded the liquidus temperature for four hours and then were cooled at 1000°C/hr to 1400ºC and then 500ºC /hr to 1000ºC (Fig. 3.4) (appendix c).

I conducted numerous systematic conventional heating-cooling experiments during this research which simply varied the time spent above the liquidus and then linearly cooled the samples by varying the cooling rate by temperature and rate. Other experiments conducted varied the time spent above the liquidus, cooled the synthetic chondrules rapidly to a given temperature and then slowed the cooling rates until the charge was quenched at 1000°C. All these experiments produced broadly similar textures.

Because the SO texture is different, with blebby interrupted bars (Fig 3.5), as a last resort I tried many unusual heating-cooling cycles, to see if this texture was replicated by annealing (Figure 3.6, 3.7, 3.8, 3.9). Simple isothermal annealing at 270°C below the liquidus for 96 hours before continued cooling (Fig. 3.6) did not modify the typical

elongate hopper textures. Skeletal barred olivine textures (SO) were produced in charges with thermal histories that were cyclic. The temperatures were fluctuated to replicate the behavior of a chondrule which may have been entrained in turbulent gas convection currents. Two experimental runs (BO5-20 and BO5-21) were heated above their calculated liquidus temperature of 1570°C, annealed at 1300°C but then repeatedly subjected to temperature spikes of 100-200°C (Fig. 3.7 – Fig. 3.9). The synthetic chondrules produced the unique blebbly SO texture without the typical outside shell found in normal barred olivine textures (Fig. 3.10 and Fig. 3.11).

The unique texture was only replicated in the synthetic chondrule composition identified as BO5. The same methodology was utilized on synthetic chondrules identified as BO6 but only the typical barred olivine texture was produced. A different liquidus temperature due to a different bulk composition is thought to be the controlling factor. The calculated liquidus temperature of the synthetic BO5 chondrules is 1570°C and the calculated liquidus temperature for the synthetic BO6 chondrules in 1509°C. The BO6 chondrules were heated approximately 150° above their calculated temperature and the BO5 chondrules were heated approximately 70°C above their calculated temperature. When cyclically heated and cooled, the crystals in the BO6 chondrules were completely melted and during each cooling cycle new nuclei were formed and linearly cooled producing typical barred olivine textures. (Further experimentation is required to verify this hypothesis.)

Samples	Textures produced	Barred texture
BO5-1 BO6-1 BO6-7A	ELHPO, ELHPO, BO	Multiple
BO5-2 BO6-2 BO6-7B	ELHPO, ELHPO, BO	Multiple
BO5-3 BO6-3 BO6-7C	ELHPO, ELHPO, BO	Multiple
BO5-4b BO6-4 BO6-7D	ELHPO, ELHPO, ELHPO	
BO5-5 BO6-5 BO6-7E	ELHPO, ELHPO, BO	Near classic
BO5-6 BO6-6	ELHPO, ELHPO	
BO5-8 BO6-8	ELHPO, BO	Multiple
BO5-9 BO6-9 BO6-7I	ELHPO, ELHPO, BO	Multiple
BO5-10 BO6-10 BO6-7J	ELHPO, ELHPO, ELHPO	
BO5-11 BO6-11	DENDRITIC, ELHPO	
BO5-12 BO6-12	ELHPO, ELHPO	
BO5-13 BO6-7M	BO, ELHPO	BO
BO6-7N	GLASS	
BO5-15 BO6-15	ELHPO, ELHPO	
BO5-19	ELHPO	
BO5-20	SBO	
BO5-21 BO6-21*	SBO	

Table 3.5 Samples and textures reproduced from dynamic crystallization experiments

BO6 1 Tmax 1520ºC

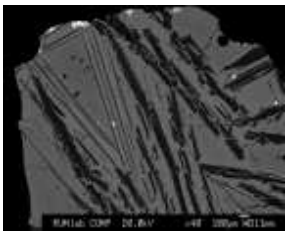

Cooling Rate 500ºC/hr

+ΔT = 11°

BO6 7a Tmax 1590ºC

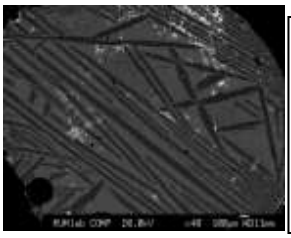

Cooling Rate 500ºC/hr

+ΔT = 81°

Quench 1000ºC
Time above liquidus 30 mins

BO6 5 Tmax 1534ºC

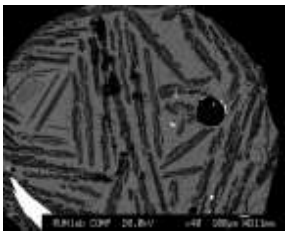

Cooling Rate 100ºC/hr

+ΔT = 25°

BO6 7e Tmax 1587ºC

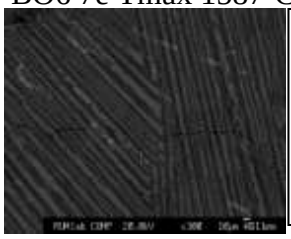

Cooling Rate 100ºC/hr

+ΔT = 78°

Quench 1000ºC
Time above liquidus 30 mins

BO6 2 Tmax 1520ºC

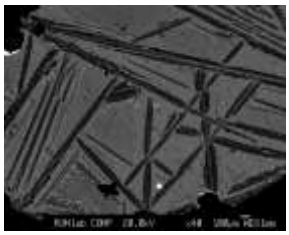

Cooling Rate 1000ºC/hr

+ΔT = 11°

BO6 7b Tmax 1588ºC

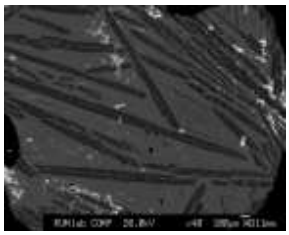

Cooling Rate 1000ºC/hr

+ΔT = 79°

Quench 1000ºC
Time above liquidus 15 mins

Figure 3.1 a-f: Increasing Tmax progressing texture from ELHPO to BO listed in cooling rate order. More melting equates to finer dendrites.

BO5 2 Tmax 1580ºC

Cooling Rate 1000ºC/hr

+ΔT = 10°

Quench 1000ºC

BO5 3 Tmax 1586ºC

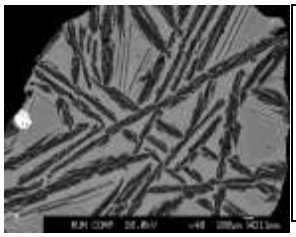

Cooling Rate 1000ºC/hr

+ΔT = 16°

Quench 600ºC

Time above liquidus 15 mins

BO6 2 Tmax 1520ºC

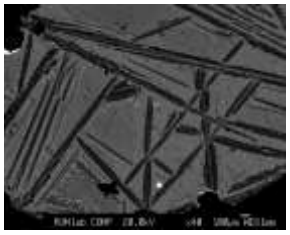

Cooling Rate 1000ºC/hr

+ΔT = 11°

Quench 1000ºC

BO6 3 Tmax 1525ºC

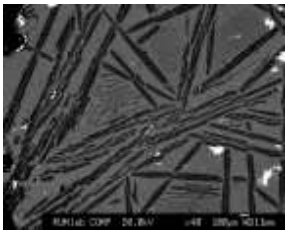

Cooling Rate 1000ºC/hr

+ΔT = 16°

Quench 600ºC

Time above liquidus 15 mins

BO6 1 Tmax 1520ºC

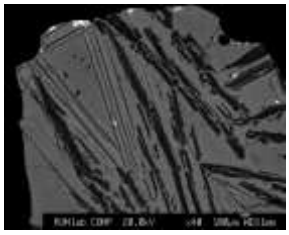

Cooling Rate 500ºC/hr

+ΔT = 11°

Quench 1000ºC

BO6 6 Tmax 1532ºC

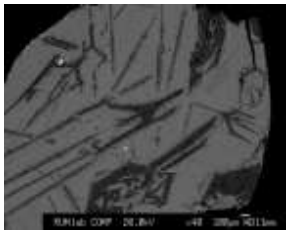

Cooling Rate 500ºC/hr

+ΔT = 23°

Quench 600ºC

Time above liquidus 30 mins

BO5 1 Tmax 1575ºC

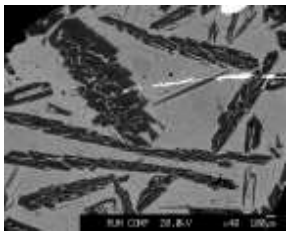

Cooling Rate 500ºC/hr

+ΔT = 2°

Quench 1000ºC

BO5 6 Tmax 1589ºC

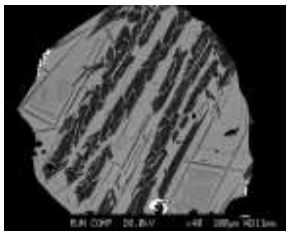

Cooling Rate 500ºC/hr

+ΔT = 19°

Quench 600ºC

Time above liquidus 30 mins

Figure 3.2 a-h: Reducing quench temperatures from 1000°C to 600°C does not change the texture that is created

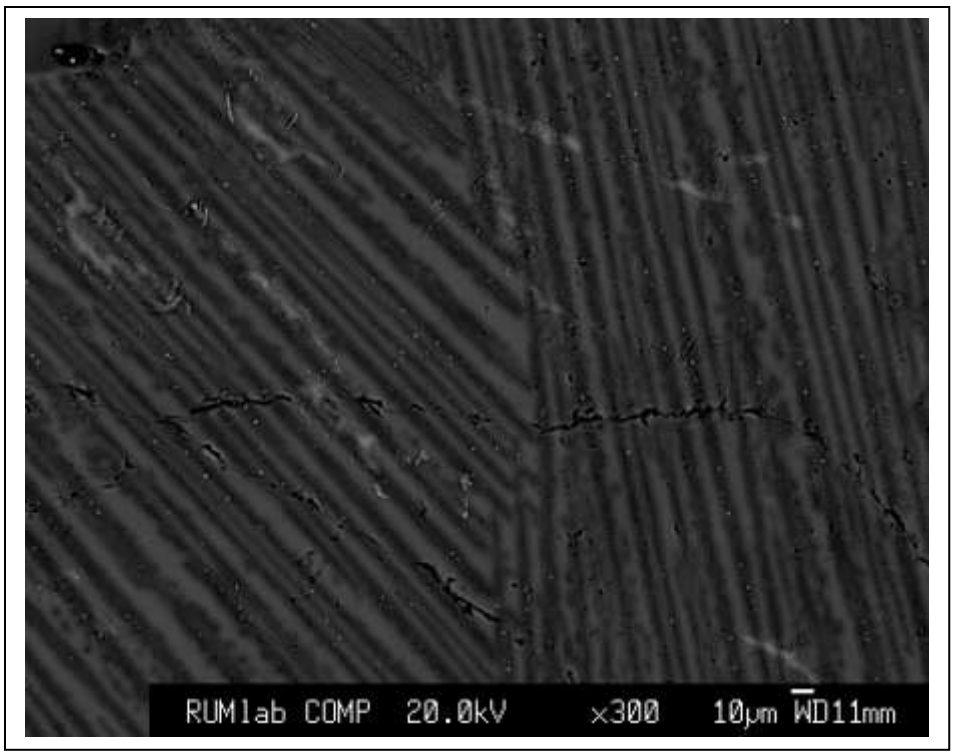

Figure 3.3: Near classic barred olivine (BO) texture in charge BO6-7e Tmax 1587ºC Δtmax 30 Quench 1000ºC Cooling rate 100°C/hr

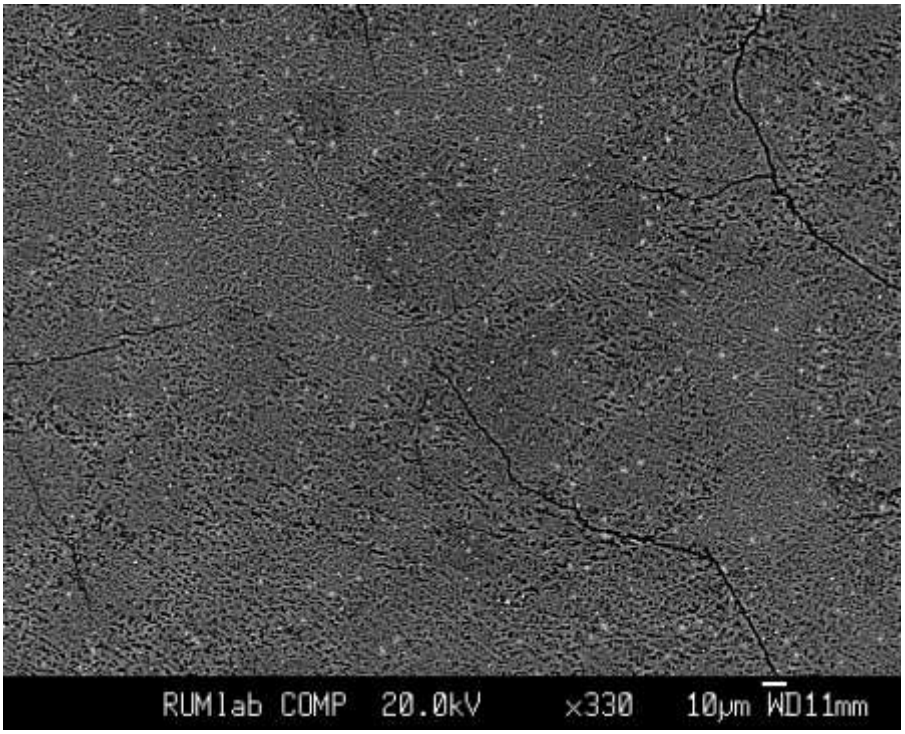

Figure 3-4: Cryptocrystalline (CC) texture replicated in sample charge CC2-15 Tmax 1610ºC Δtmax 240 Quench 1000ºC Cooling rate 1000°C/hr to1400°C and 500°C/hr to 1000°C

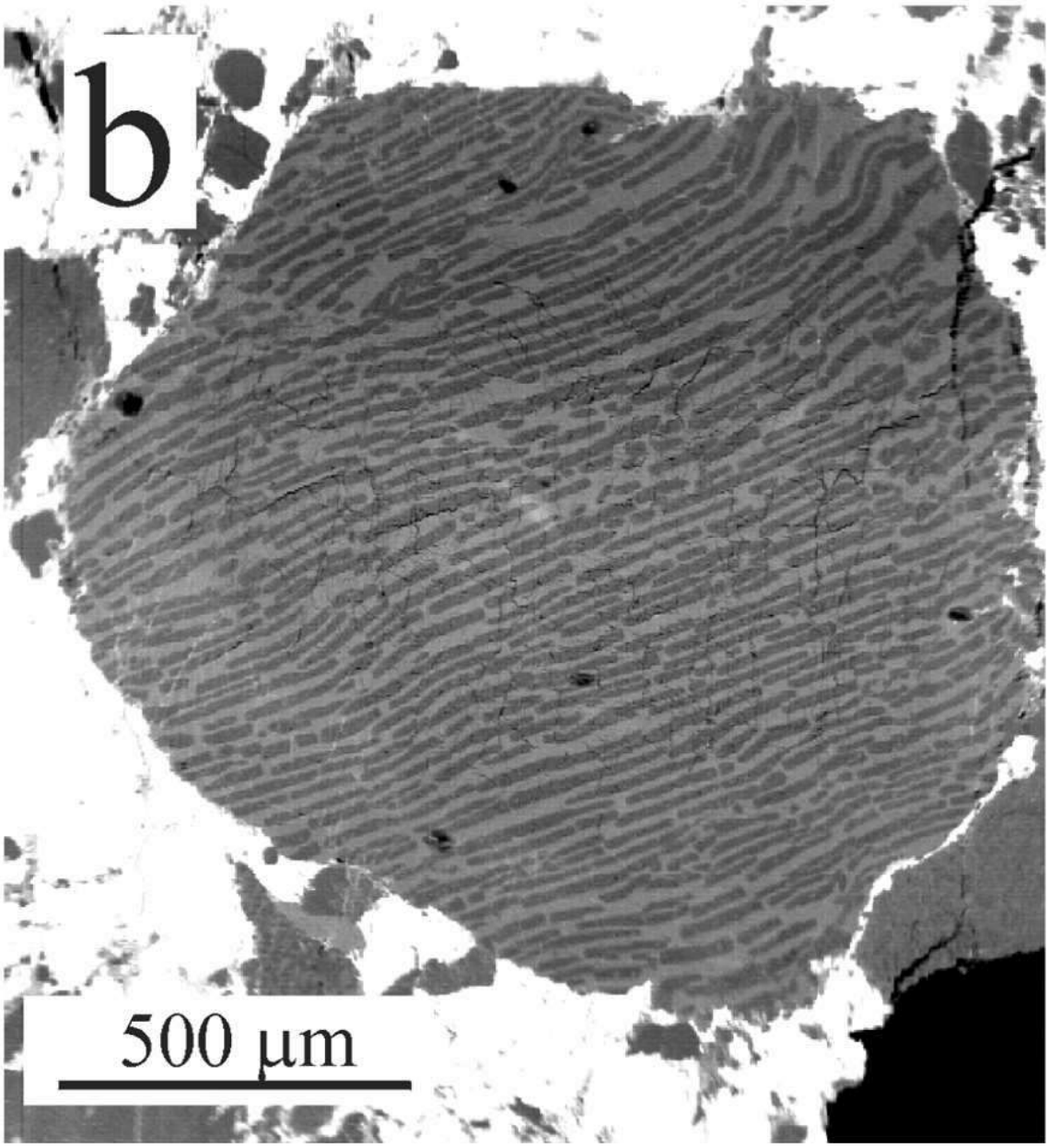

Figure 3.5 Natural skeletal olivine (SO) texture (Krot et al., 2001).

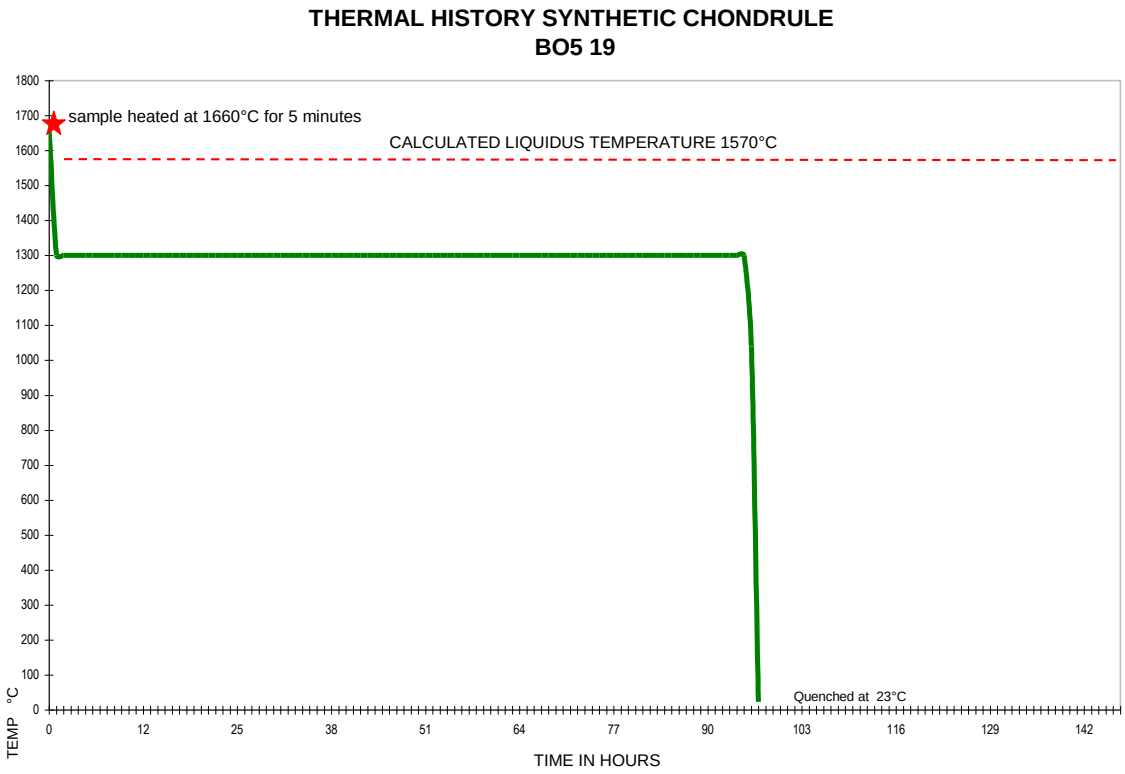

Figure 3-6: Annealing run temperature conditions of charge BO5 19 which did not result in replication of natural skeletal olivine (SO) texture.

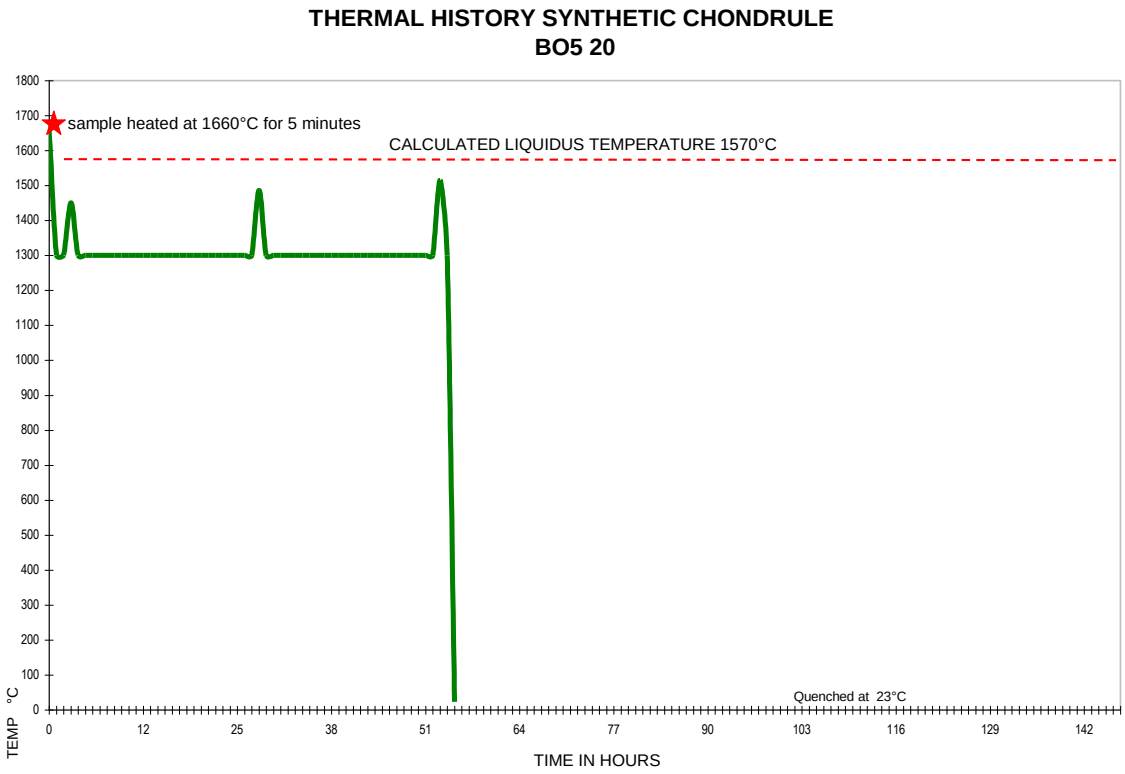

Figure 3-7: Cyclic run temperature conditions of charge BO5 20 replicating a natural skeletal olivine (SO) texture

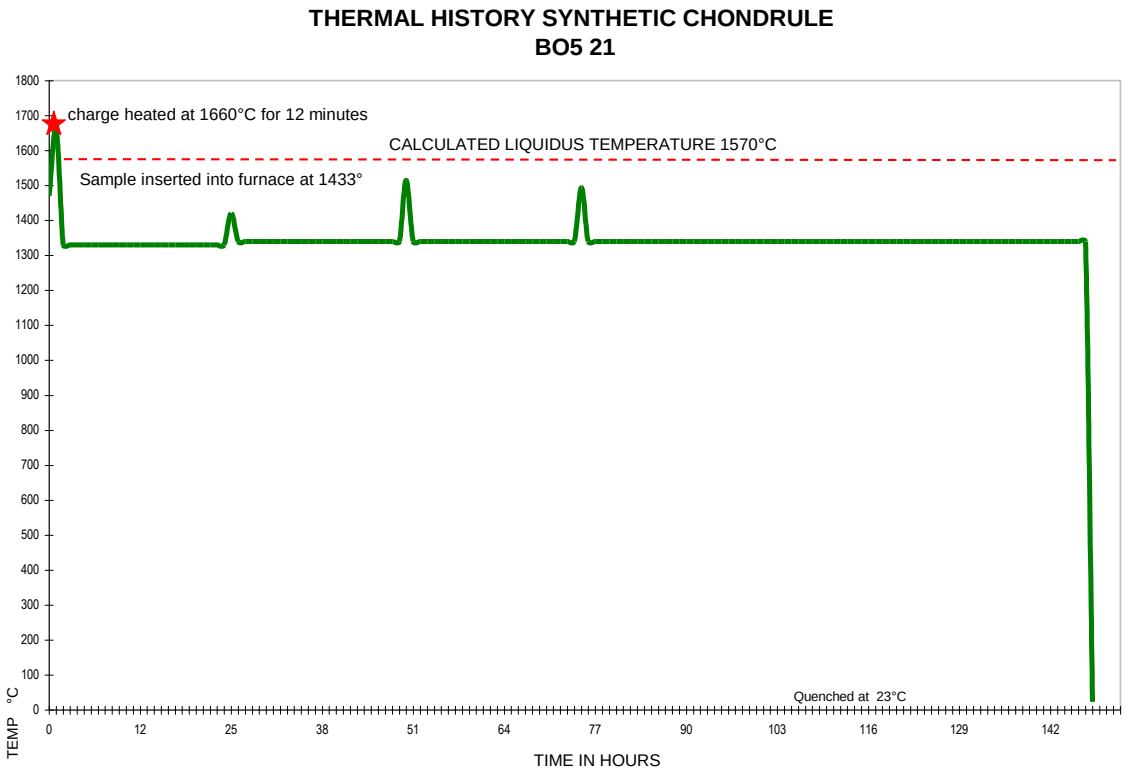

Figure 3-8: Cyclic run temperature conditions of charge BO5 21 replicating a natural skeletal olivine (SO) texture

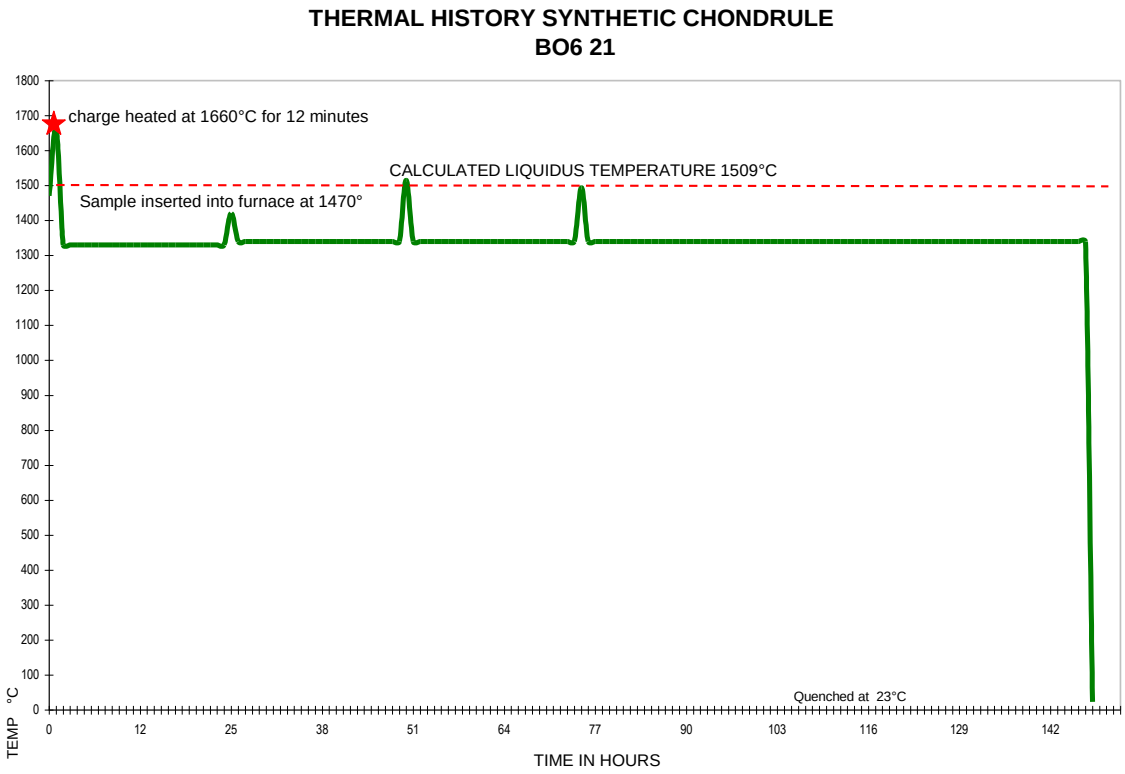

Figure 3-9: Cyclic run temperature conditions of charge BO6 21 which did not replicate a natural skeletal olivine (SO) texture

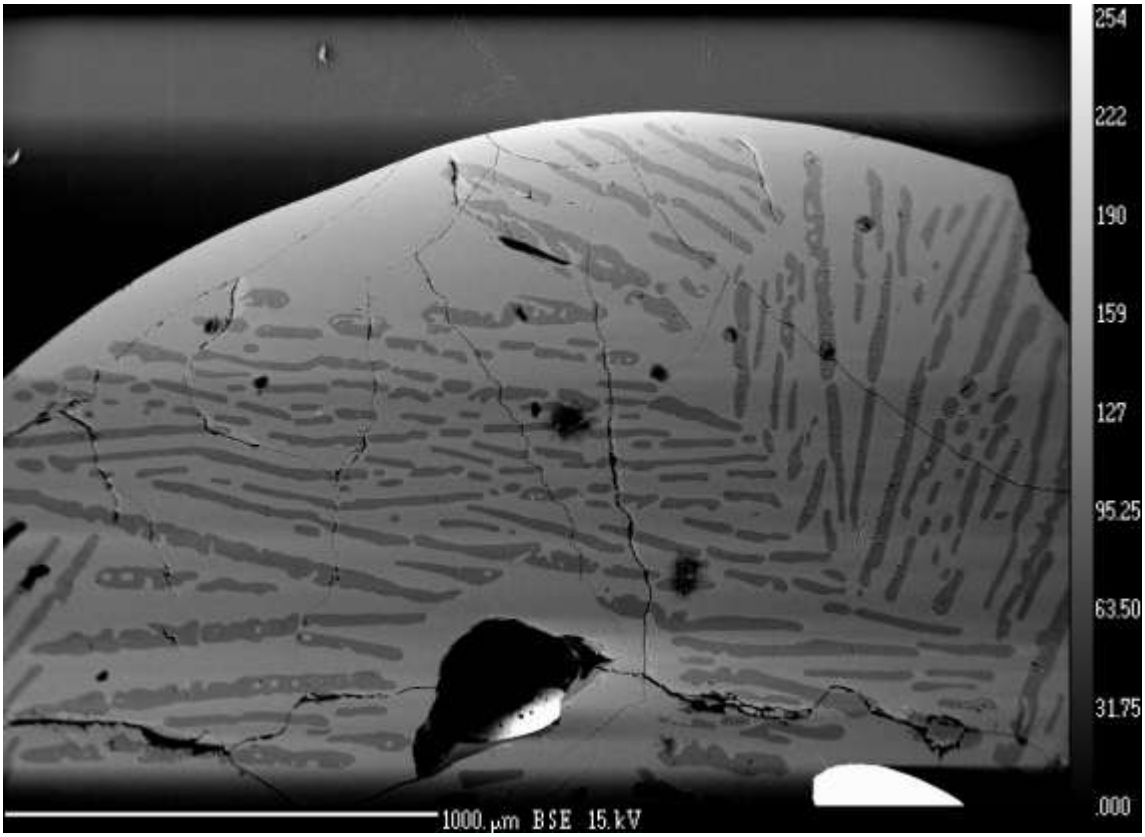

Figure 3-10a: Skeletal olivine (SO) texture replicated in synthetic chondrule BO5-20

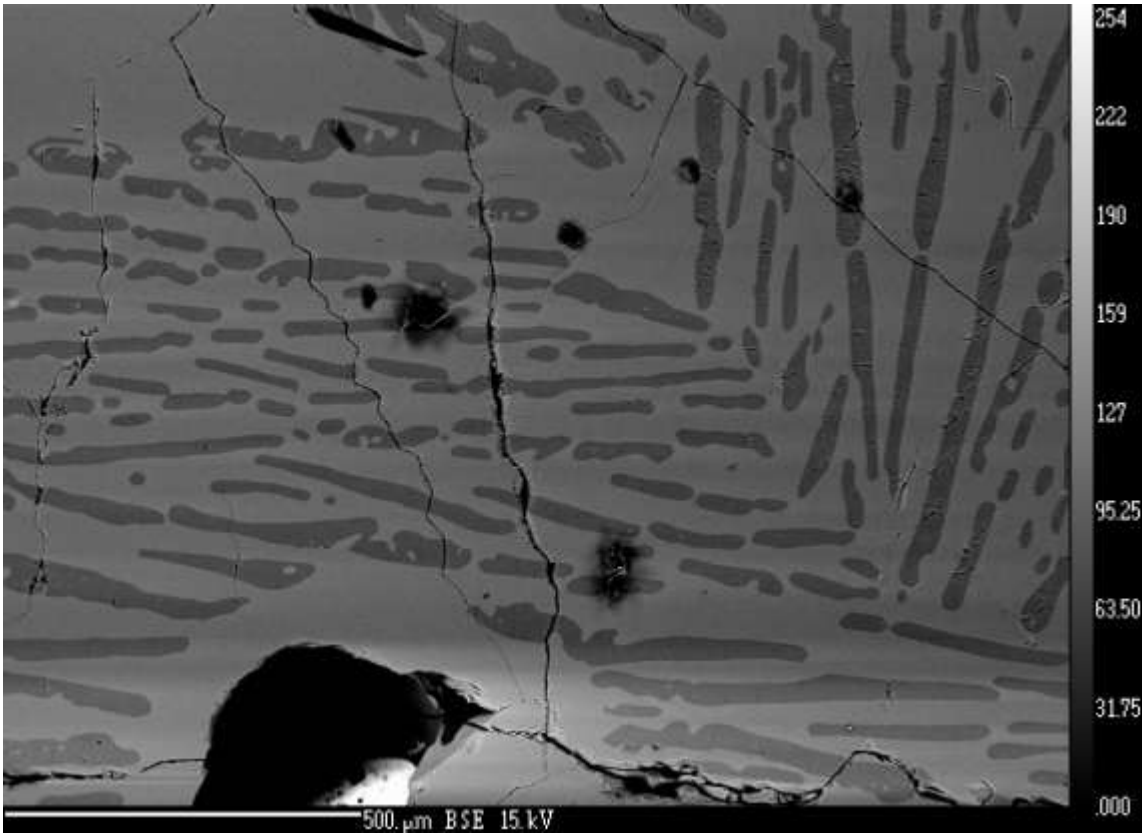

Figure 3-10b: Skeletal olivine (SO) texture replicated in synthetic chondrule BO5-20

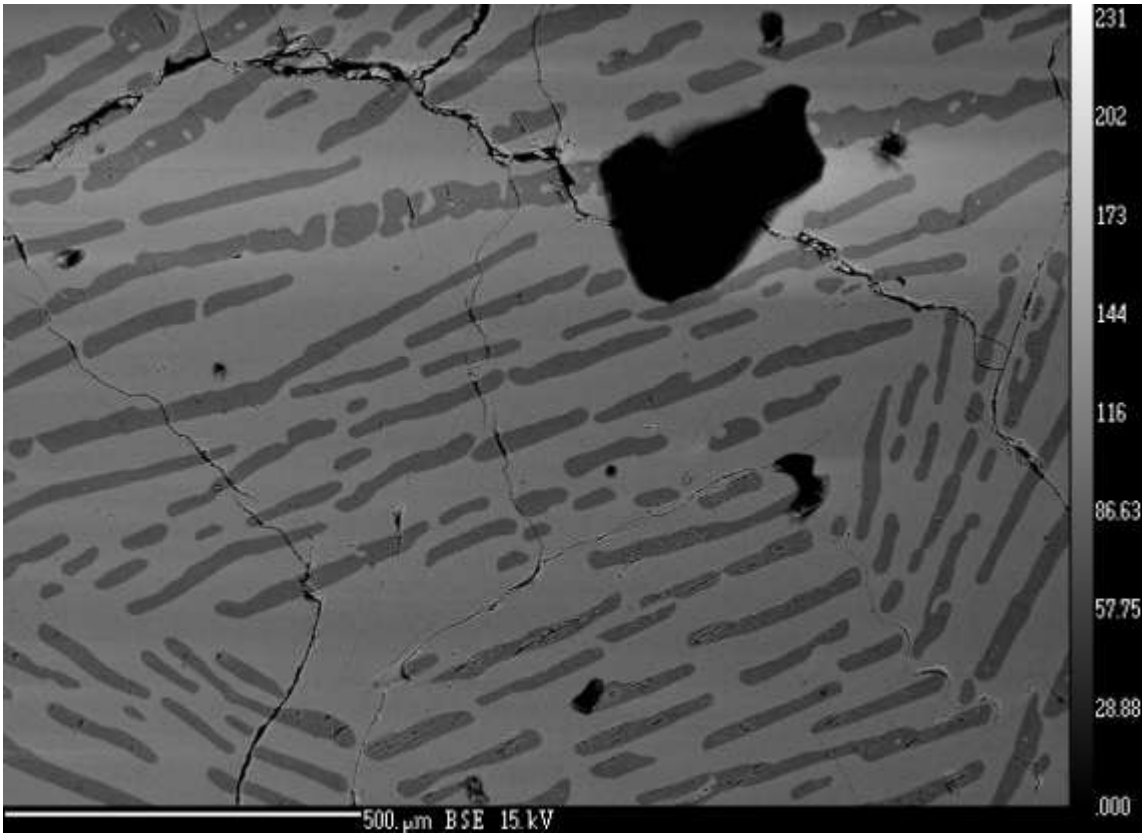

Figure 3-10c: Skeletal olivine (SO) texture replicated in synthetic chondrule BO5-20

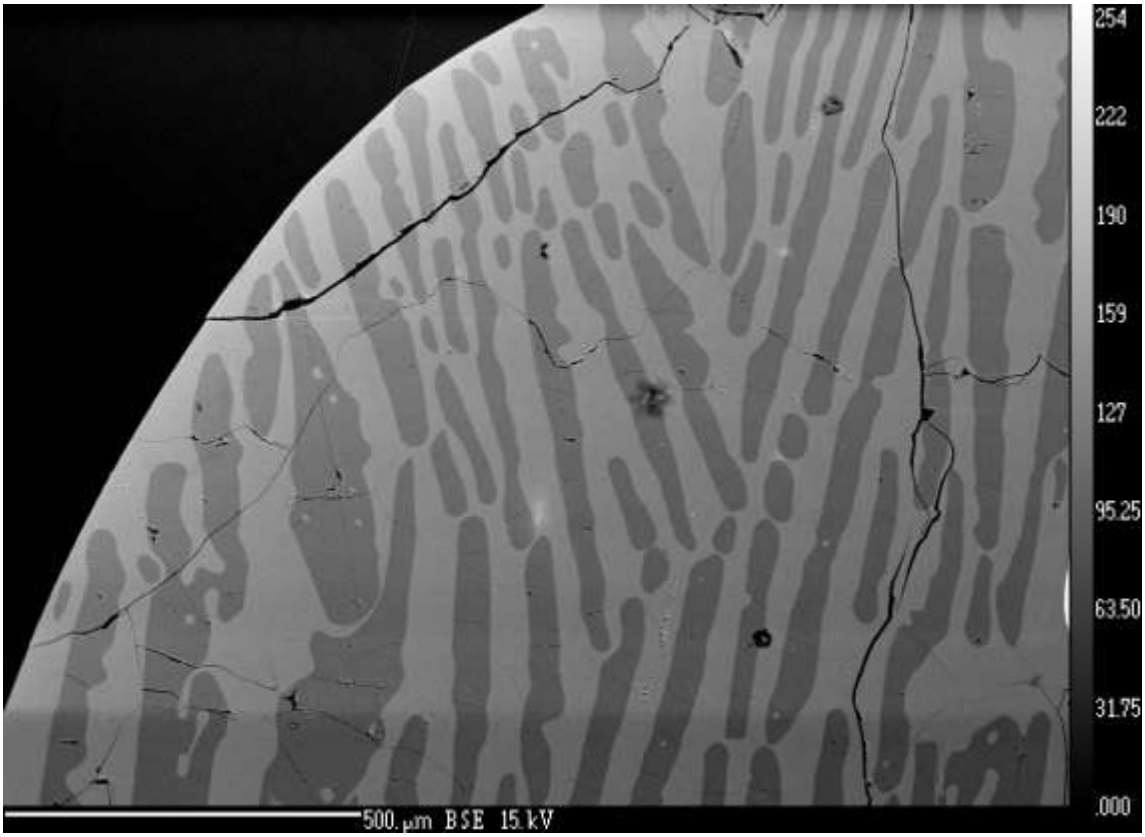

Figure 3-11a: Skeletal olivine (SO) texture replicated in synthetic chondrule BO5-21

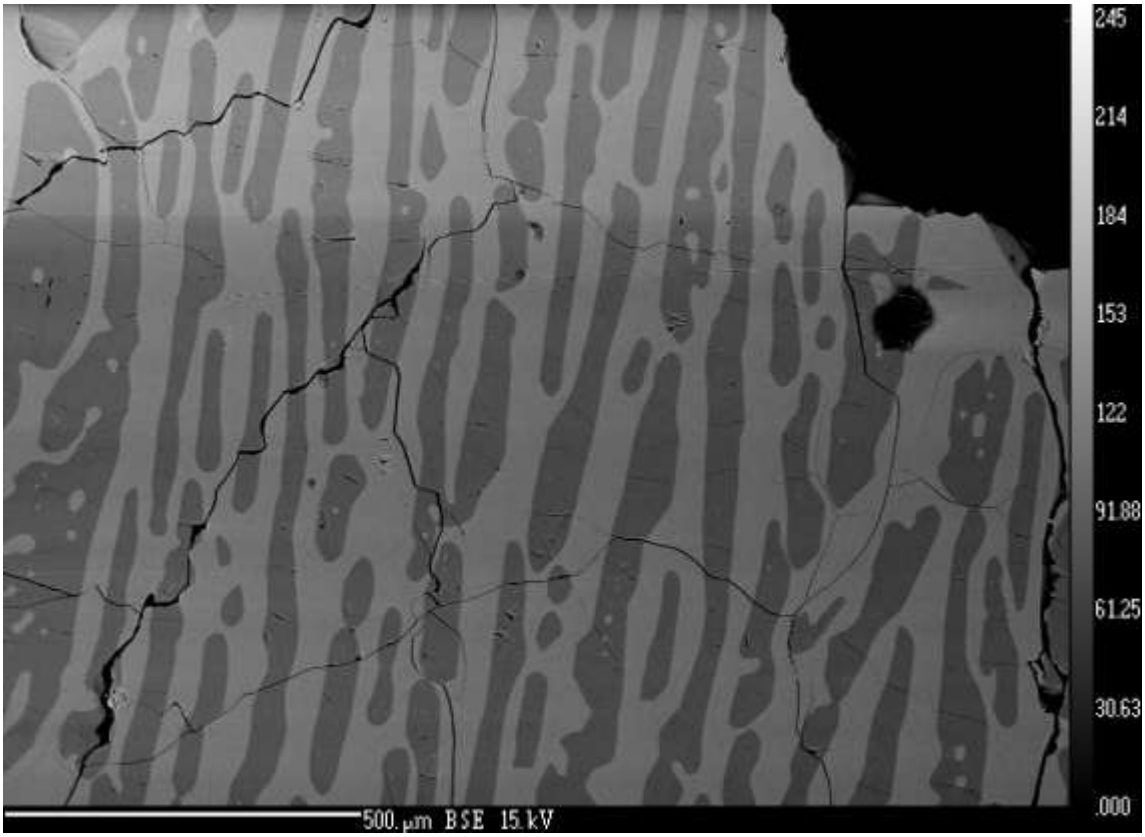

Figure 3-11b: Skeletal olivine (SO) texture replicated in synthetic chondrule BO5-21

Chapter 4: Formation Model

4.1 History of CBb Chondrule Formation Models

Most research suggests that chondrule formation occurred in a nebular setting and in association with metal grains found in the chondrites. My research is not to disprove that some or the majority of chondrules were formed in the nebula but to determine whether chondrules can also form through another mechanism, impact. Much research (Richter et al., 2005; Chambers and Cassen 2002; Desch and Connolly, 2002; Jones et al., 2000; Shu et al., 1996; Grossman 1988; Taylor et al., 1983;) has focused on the solar nebula as the formation region for chondrules while few studies have been done exploring the conditions found in a vapor cloud produced by an impact. I used the data reported for metal grains and chondrules in a nebular setting as a starting point to develop my impact model. Below is a brief synopsis of the published research of the metal grains found in the CR chondrite clan and the clues they give to their region of formation.

4.1.1 History of CB_b Chondrule Formation Models: Clues from Iron Nickel Grains

Grossman and Olsen (1974) and Grossman et al., (1979) suggested that metal grains in the CM Murchison meteorite were pristine high temperature condensates. Their condensation scenario was extended to explain the origin of zoned FeNi metal grains in the CR-clan of chondrites, including CRs, CHs, CB_b, and LEW 85332. These are all characterized by a positive Co versus Ni correlation and a solar Co/Ni ratio (Fig 4.1) (Grossman 1988, Scott 1988, Weisberg 1988). With a moderately low f_{O_2}, metal is stable

and silicates are highly magnesium, and all the Ni and Co enter the metal, which has a near-solar Fe/Ni ratio.

Nickel is a very sensitive indicator of alteration or metamorphism and it is used to distinguish between the most pristine chondrites and chondrites altered by secondary processing. If the metal has nickel concentrations greater than 8wt% it is metastable and the grain will decompose into kamacite and taenite under the slightest secondary processing. Nickel has been used to determine if members of the CR chondrite clan have been processed after their formation. Below are the characteristics of the metal found in theses chondrites suggesting that the members of the CR chondrite clan have not undergone secondary processing.

The majority of metal present in CR chondrites is rounded nodules in chondrules, coarse grained igneous rims surrounding many chondrules, and matrix. It has been suggested that this indicates that the metal was involved in the chondrule forming process (Lee et al., 1992). Weisberg and Prinz (1999) identified large metal grains zoned in Ni which may have escaped chondrule processing or escaped from chondrules forming regions in the matrix of the CR chondrite Renazzo.

In the CB_a Bencubbin, metal is typically observed as large (0.1 - 10mm) compositionally uniform clasts welded together by chondrule silicates or as small amounts of interstitial metal-silicate melt (Newsom and Drake, 1979). Weisberg et al., (1990, 1999, 2000)

reported compositionally zoned FeNi metal grains in the CB_b (Bencubbin-related) chondrites QUE94411 and HH237, which have become the focus of extensive research.

The compositional profiles of Ni, Co, Cr, and Si were taken along transects in smoothly zoned metal grains in two CH chondrites (Meibom, 1999). High Ni concentrations measured in the cores of the grains fell well within the kamacite + taenite field on the Fe-Ni phase diagram. These grains are metastable and would have decomposed into kamacite and taenite upon mild prolonged heating (>300'C) indicating that the smoothly zoned metal grains have not been thermally processed since their formation.

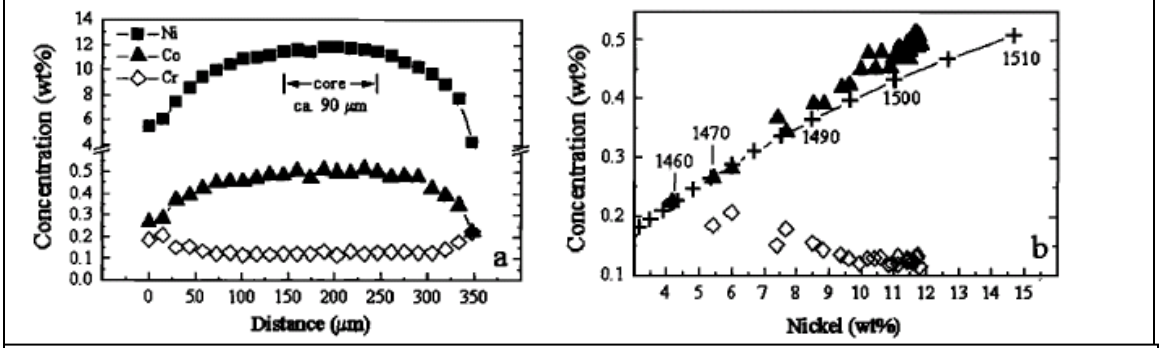

Figure 4.1 a) Electron microprobe traverses across a representative zoned metal grain from QUE 94411 and b) Co and Cr plotted against Ni for the same set of data. There is a strong, positive correlation between Co and Ni (Petaev et al., 2001).

Compositional zoning in the metal grains analyzed by Meibom is consistent with that predicted by thermodynamic calculations of equilibrium condensation from a gas of solar composition (Grossman and Olsen, 1974; Grossman et al., 1979; Kelly and Larimer, 1977). This relationship may indicate that complete equilibrium between the condensing metal and the residual solar nebular gas was not maintained. This may be the result of progressive isolation of metal condensates from the nebula gas or the metal grains

forming as a result of a different mechanism (Meibom et al., 1999). For example, an impact in which the cooling was too rapid for diffusion in the metal to maintain equilibrium or the gas not being solar, but enriched in evaporated dust.

The results of equilibrium calculations in a system of solar composition at total pressure of 10^{-3}, 10^{-4}, and 10^{-5} bar determine that the smoothly zoned metal grains formed at a total pressure of 10^{-4} bars (Meibom et al., 1999). An increase in pressure from 10^{-5} - 10^{-3} bar decreases the maximum Ni content in the metal and increases the condensation temperature of all the phases. The metal, forsterite olivine, Co and Cr in the metal grains do not change with changes in total pressure but Si changes significantly. The equilibrium calculations of Si concentrations in metal are only in agreement with the measured concentrations of Si at 10^{-4} bar (Meibom et al., 1999).

The smooth zoned metal grains grew by gas-solid condensation and cooled fast enough to avoid significant redistribution of Ni, Co, and Cr. Preliminary calculations of the metal grain growth rate from a gas of solar composition at 1400K (1127ºC) at 10^{-4} bar indicate that the metal grains would grow on a timescale of days (Meibom et al., 1999). This timescale is fast enough to avoid homogenization of compositionally zoned metal grains and constrains the cooling rate of the gas ~10K/d in the temperature range of 1370 – 1270K (1097ºC - 997ºC) (Meibom et al., 1999).

The cooling rate obtained by Meibom et al., (1999) (~10K/d) is much lower than typical cooling rates inferred for chondrules (10-1000 K/h), and for a lower temperature range,

but it is much faster than cooling rates expected for the globally heated solar nebula. These authors concluded that FeNi metal condensates described above resulted from localized, brief and highly energetic thermal events in the nebula capable of vaporizing FeNi metal and ferromagnesian silicates (Meibom et al., 1999). The volatility controlled depletion in moderately volatile elements suggests that the cooled metal grains were separated from the hot cooling gas in their formation region before the temperature dropped significantly below 1200K. The mechanism that did this must have been highly efficient and it has been suggested that the X wind may have played an import role if this was a nebular process (Meibom et al., 2001). If the zoned grains formed as a result of a collision their presence could be in response to a rapidly cooling vapor cloud.

Continued research by Meibom et al., (2000) estimated the growth rate of zoned metal grains, obtained a cooling rate for the region of the nebula from which they condensed and discussed a possible astrophysical setting of this event (Meibom et al., 2000). Gas-solid condensation was modeled using spherical metal grains in a cooling gas of solar composition. The total pressure of the gas was 10^{-4} bar (Meibom et al., 1999) and the radius of the grain was ~ 100μm, the typical size of a natural occurring zoned metal grain. The growth time was calculated at 19 days.

Additional work suggested that the zoned iron nickel grains in HaH237 formed by rapid, disequilibrium condensation. The cores in these grains contain up to 12% Ni and the rims and unzoned metal have 6% Ni. The Fe and Ni isotopes were analyzed in these grains and they displayed large mass fractionations and the cores had lighter isotopic

compositions than the rims. The isotope values mirrored values found in condensates relative to gas (Alexander and Hewins, 2004).

More than a hundred zoned metal grains from the NWA 470, HaH 237, and QUE 94411 were analyzed to determine variations in their presumed source region, the nebula, and at least 9 distinct Ni zoning patterns were recognized in the grains studied (Petaev et al., 2007). The zoning patterns are fingerprints of the formation conditions; the patterns indicate conditions more oxidizing than solar during condensation and further suggested these grains had a complex cooling history. As in most papers on zoned metal, the formation region for the zoned grains is suggested to be the nebula; however the complex cooling history and more evidence supporting condensation can be achieved through an impact as well.

4.1.2 History of CB_b Chondrule Formation Models: Clues from PGEs in CB_a Metals

The platinum group elements (PGEs) analyzed in the metal of CB_a chondrites have values of up to 30% higher than values expected from condensation from the solar nebula (Campbell et al., 2001, 2002). It had been initially proposed that that the compositions of CB_a metal formed by condensation in the solar nebula (Newsom and Drake 1979) but the increase in values is unlikely to be caused by higher nebular pressure because such pressures are questionable in the solar nebula (Fig 4.2) (Campbell et al., 2002).

Campbell et al., (2002) used their findings to explore the possibility that these meteorite components condensed from impact ejecta (Wasson and Kallemeyn 1990; Kallemeyn et al., 2001). An impact between two planetesimals would produce a range of pressure and temperature conditions in which an impact generated vapor could have condensed. This behavior can be extended to condensation calculations to determine the effect of variations in the plume on trace elements. The gas was enriched in metal by a factor of 10^7 relative to a solar gas at 10^{-4} bar and the condensation trajectories between the high metal condensation paths and CBa PGE data mimic each other (Fig 4.2) (Campbell et al., 2002). The work was carried over to the moderately volatile siderophiles and this also supported that the metal formed at partial pressures several orders of magnitude higher than what is expected in the solar nebula.

The findings of Campbell et al., (2000, 2001) suggest that all of the metal in the CR chondrite clan was not formed by impact. This previous work indicated that metal in the CB_b chondrites QUE 94111 and HH237 was consistent with a gas that had condensed from a solar composition of 10^{-4} bar (10Pa) total pressure, which had at that time been interpreted as a nebular setting. An impact would produce a range of pressures and temperatures which would change as the impact plume evolved with time. The evolving vapor plume would resolve the calculated condensation pressures for the metal grains found in both the CB_a and the CB_b chondrites. The grains formed as a result of the impact but at different stages or locations in the vapor plume.

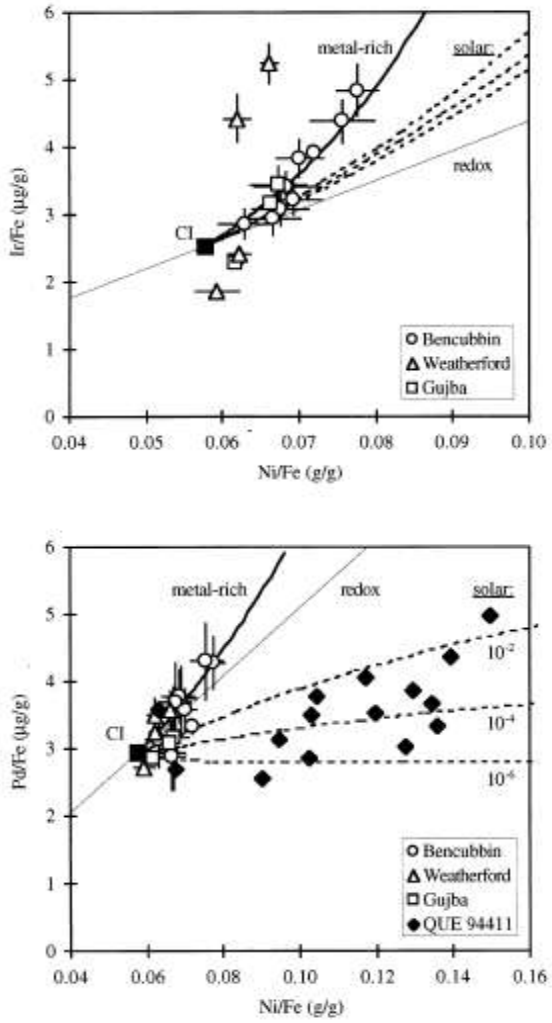

Figure 4.2 Ir/Fe vs Ni/Fe (top) and Pd/Fe vs Ni/Fe (bottom) for metal clasts in Bencubbin (circles), Guijba (squares) and Weatherford (triangles). The chondritic abundances (Anders and Grevesse, 1989) are represented by solid squares. The addition or removal of Fe during redox processing is represented by the thin solid line. Calculated equilibrium condensation trajectories at nebular pressures of 10^{-6} (bottom), 10^{-4} middle, and 10^{-2} (top) bar are indicated by heavy dotted lines. The condensation trajectory of a gas that is metal enriched by a factor of 10^{7}, relative to the nebular conditions, is shown as a heavy solid line. Data from within a single zoned metal grain in QUE 94411 (Campbell et al., 2001a) are shown as solid diamonds; 2σ errors on these points are ~20%. Note that the QUE 94411 data and the Bencubbin data follow different trends in Pd/Fe vs Ni/Fe (Campbell et al., 2002).

4.2 History of the Unique CB_b Chondrule Formation Models

In 2001 Krot et al., suggested that chondrules in HaH 237 and QUE either formed by direct gas liquid condensation or by prolonged heating of the gas solid condensates above their liquidus temperature which would destroy all of their nuclei. Either of these mechanisms would require that formation take place at temperatures higher than 1500°C before metal condenses but inferred enhanced initial dust gas ratios of 1000X favor a gas liquid condensation (Ebel and Grossman, 2000). Krot et al., (2001) observed the continuous range of refractory lithophile element abundances (from ~10 X CI to <.01X CI) and flat element pattern (Fig 4.3) and suggested they were a function of fractional condensation of chondrules or chondrule precursors in a closed system.

In this formation model, the refractory lithophile elements were incorporated into the earliest formed SO chondrules and the CC chondrules formed at lower temperatures when the gas was increasingly depleted in these elements. The depletion of chondrules in moderately volatile elements suggests that they were efficiently isolated from the hot nebular gas before condensation of these elements and then transported to a colder region of the nebula after they formed or they formed in a closed system (Krot et al., 2001).

Chondrules in other chondrite groups formed 4564.7 +/-.6 million years ago (Amelin et al., 2007). Recent radiometric dating using lead isotopes from CB_a (Gujba) and CB_b (HaH 237) carbonaceous chondrite chondrules identify their ages as 4562.7 $\pm$0.5 Myr

and 4562.8 ±0.9 Myr respectively (Krot et al., 2005). In 2005 Krot et al., suggested that the young aged chondrules in CB chondrites formed from a giant impact in the solar

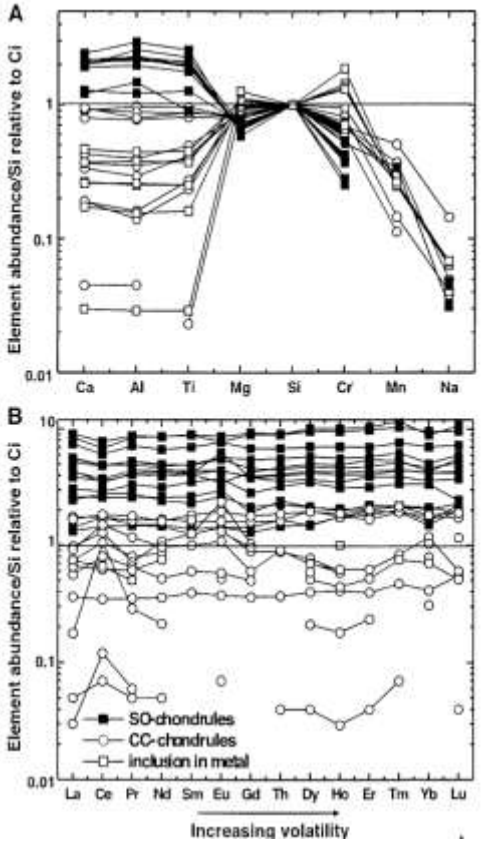

Figure 4.3 a) Bulk concentration of major and minor lithophile elements and b) REEs in SO and CC chondrules normalized to Si and CI chondrite abundances. In both diagrams, the SO chondrules are enriched in refractory lithophile elements (Ca, Al, Ti, REEs), and the CC chondrules are depleted in these elements relative to CI. All chondrules are highly depleted in the moderately volatile elements Mn and Na (Krot 2001).

system. Results from their research established a contemporaneous origin and suggested co-genesis of HaH 237 and Guijba. The ^{207}Pb-^{206}Pb ages of the CB chondrules (Krot et al, 2005) are similar to the ^{182}Hf-^{182}W ages of the metal-silicate fractionation recorded in the CB metal condensates (Kleine et al., 2005); supporting a co-genetic origin for chondrules and metal in the CB meteorites. The very young age of the CB chondrules

and metal grains gave rise to the hypothesis that they were produced by an extremely energetic, single stage formation mechanism (Krot et al, 2005).

In big protoplanetary impacts melting results from shock compression, which is followed by adiabatic decompression; the compression may cause the material to change from solid to liquid or vapor. After shock melting, the expansion would produce and disperse the melt droplets (and there could be some condensation) that are accelerated by the expanding gases (Melosh et al., 2004; Krot et al, 2005). The behavior of olivine has been studied and indicates that the immediate effect of a shock is to transform it to a supercritical fluid at high pressure and temperature. When the velocity is high enough to cause melting the "release path" is typically on the melt side of the critical point which indicates that the expanding hot fluid is essentially behaving like a liquid. If we expand down the arrow nothing happens to the fluid until we cross the solvus and then fluid (now called a liquid) can expand and disperses into droplets (Fig 4.4) (Melosh et al., 2004).

The refractories would be concentrated in partly evaporated residual melts, and evaporated Mg and Si re-condensed into CC. The residual particles would be heated to near or above the calculated SBO liquidus (~1570°C) (Herzberg 1979); as the calculated CC liquidus is higher (> 1646°C) (Herzberg 1979), the droplets would have formed as undercooled liquids (Blander, 1983). In this interpretation, the large skeletal olivine chondrules and metal nodules in Gujba and HaH237 are melts produced by the collision and the smaller cryptocrystalline chondrules and chemically zoned metal grains in

HaH237 are respectively gas-liquid and gas-solid condensates from a vapor phase (Krot et al., 2005).

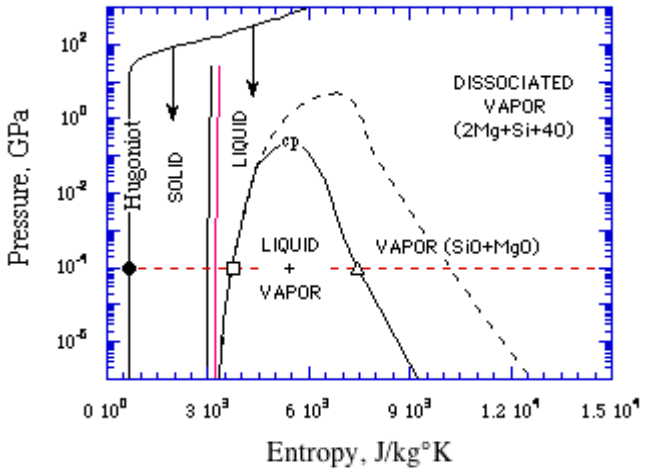

Figure 4.4 The behavior of olivine following impact indicates that the immediate effect of a shock is to transform it to a supercritical fluid at high pressure and temperature. If we expand down the arrow nothing happens to the fluid until we cross the solvus and then fluid (now called a liquid) can boil and disperses into droplets (Melosh et al., 2004).

4.3 Formation Model of Unique CBb Chondrules

A possible genetic relationship between the members of the CR clan has been previously suggested (Weisberg et al., 1995, Krot et al., 2002) which is supported by a unique CR-mixing line of these chondrites' bulk oxygen isotopic compositions (Clayton and Mayeda, 1999; Krot et al,, 2006; Krot et al., 2010). This relationship is the platform that I have used to create a model that displays that the CR clan formed through an impact between and Fe-Ni impactor and a target, Pallas, and not in the solar nebula.

The first step in the development of my model was to determine the parent material or remnants of parent material, that is the target and the impactor that formed the CR chondrite clan unique chondrules. The parent material is from two sources, one being CR, which collided and were processed together in the debris cloud and developed unique compositions while preserving some relatively unaltered CR material.

Spectral analysis is the main tool used to determine the composition of surfaces of asteroids and protoplanets. Through advances in the quality of asteroid spectral data and in the methods used to interpret the data several meteorites have been connected to a parent asteroid through spectral analysis (Gaffey et al., 2002); asteroid 6 Hebe is thought to be the probable parent asteroid of the H Chondrites and the IIE iron meteorites, 4 Vesta is thought to be the probable parent asteroid of howardites, eucrites, and diogenites Through spectral analysis possible parent targets for these chondrules include the A class (289 Nenetta and 446 Aeternitas), the S class (980 Anacostia and 387 Aquitania) (Gaffey et al., 2002), which are all small bodies, or the B class protoplanet Pallas (Schmidt et al., 2009) with the parent impactor being an iron nickel parent body or core.

The protoplanet Pallas was selected as a suitable target. Based on spectroscopic observations (Sato et al., 1997), the primary component of the Pallas surface material is silicate that is low in iron and water and parallels the chemical composition of the CB_b chondrules. . Pallas has most likely remained relatively unchanged since the main asteroid belt first formed. There is a 240 km impact basin (Fig. 4.5a,b) located on the protoplanet's surface suggesting that early in its history it was smashed by a massive

impact that broke off a number of smaller asteroids that share its orbit (Schmidt et al., 2009). Not only does the chemical composition of Pallas make it a suitable candidate as the parent in my model but the recently recognized crater gives tangible evidence that it has been disrupted by a significant impact that caused its surface material to be removed from the parent body. The spectroscopic data indicate that the surface composition of Pallas is similar to that of the Renazzo (CR) carbonaceous chondrite (Sato et al., 1997), which also has a type B spectrum. However, a recent detailed study of B-type asteroids showed that Pallas is more similar spectrally to CV, CO and CK chondrites. Lacking a certain identification of the CR parent, I take Pallas as a proxy because it is the best available match.

A large iron nickel parent body is used in the impact model because it has a greater density which would increase the energy of the impact for a given velocity and volume, increase the amount of ejected material generated and supplies a source for the abundant iron nickel grains characteristic of this unique group of chondrites. Recent theoretical studies *(*Scott et al., 2010, Yang et al., 2010; Yang et al., 2007) have indicated that iron (IVA group) meteorites are debris from protoplanetary collisions, protoplanets were abundant in the asteroid belt, and that parent bodies of iron-rich meteorites were broken up early. At the same time, gravitational interactions with planetary embryos increased impact velocities and caused the planetesimals to break apart when they hit each other (Yang et al., 2007).

Figure 4.5a Hubble Space Telescope images of Pallas with darken terrain indicating probable impact region (Schmidt et al., 2009)

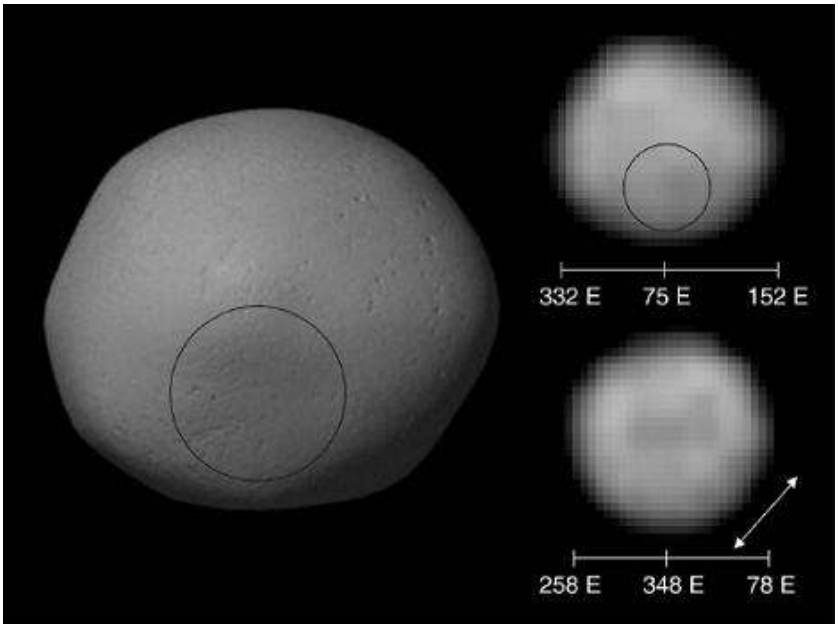

Figure 4.5b The left view is a computer model of Pallas' surface, based on the Hubble Space Telescope imagery at right. The circle indicates a large crater that is likely deeper than the one shown in the model. The imagery was collected in 2007 by the Wide Planetary Camera 2 (WFPC2) that used to be on the Hubble. The protoplanet has several depressions of various sizes, including what appears to be a large crater, 240 km wide. Such craters were likely caused by early impacts that knock loose a family of asteroid fragments link to Pallas (Schmidt et al., 2009).

4.4 Mechanics of Impact

Two impact scenarios would fit my formation model: a direct collision of a projectile onto a target (Pallas) resulting in the formation of a complex crater (Grieve 1987) and extensive vaporization of the impactor; or a hit and run, glancing collision (Asphaug et al., 2006) between the protoplanet Pallas and a large impactor. It has been determined that impacts on small bodies produced much more brecciated rock than melt. Large body impacts produce more melt and also have the ability to separate the melt and clastic fragments because of variations in the escape velocities (Melosh et al., 2004).

4.4.1 Mechanics of Cratering

When an impactor strikes a target its kinetic energy is conserved. The large amount of kinetic energy causes material from both impactor and target to be melted or even vaporized and the impactor may even become completely vaporized by the heat which is produced. The kinetic energy and the momentum will move the material, part of which is driven downward, the rest of which will be ejected from the crater site (Grieve 1987). Crater formation will take place in three stages; compression, excavation, and modification. The most important stage for the impact model for this branch of carbonaceous chondrites is compression and excavation. In the compression stage, the impactor will punch a (relatively) small hole in the target, and a shock wave will pass through the target. The pressure generated by the impact is so great that even solid material can act somewhat fluid, and flow away from the impact site. A limited amount

of material is ejected up and out of the forming crater during this stage, and a plume of impact-generated vapor rapidly expands above the crater (Grieve 1987).

During the excavation stage the shock waves which began in the compression stage continues outwards through the material. The waves spread out from a point below the surface of the target and the wave spreads upwards from the impactor, and sends some of the target material (ejecta) up and out from the impact site. Initially the ejecta forms a plume of hot vapor melt droplets and fine debris. Then a cone-shaped "curtain" of material spreads upwards from the impact site. Some or all of these ejecta will land in the area surrounding the crater, forming an ejecta blanket. In the modification stage loose debris from the impact will tend to slide down the steep crater walls and the morphology of the crater is generated creating a region of central uplift (Grieve 1987).

4.4.2 Mechanics of Cratering: Hit and Run Collisions

The formation of iron meteorites can be understood if hit and run collisions are involved (Asphaug et al., 2006). Previous understanding was that the impacts that formed the iron meteorites smashed the parent body into fragments over billions of years. This process is currently being reevaluated because the ability of an impact being able to strip mantle from the core without destroying the entire object is thought to be less likely (Asphaug et al., 2006).

A new mechanism indicates that iron meteorites (Asphaug et al., 2006) and pallasites (Scott et al., 2010) may have formed by hit and run collisions, glancing, between

protoplanets. In a hit and run collision if the impactor has a mass that is half of the target it will experience loss of the rocky mantle which reaccretes down range and its ratio of metal to silicate will increase. The rocky debris could accrete to form an object with a lower than normal amount of metallic iron. When the impacting protoplanet is small, it is destroyed and a chain of metal rich protoplanets results, possibly leading to the formation of metal rich asteroid (Fig 4.6)

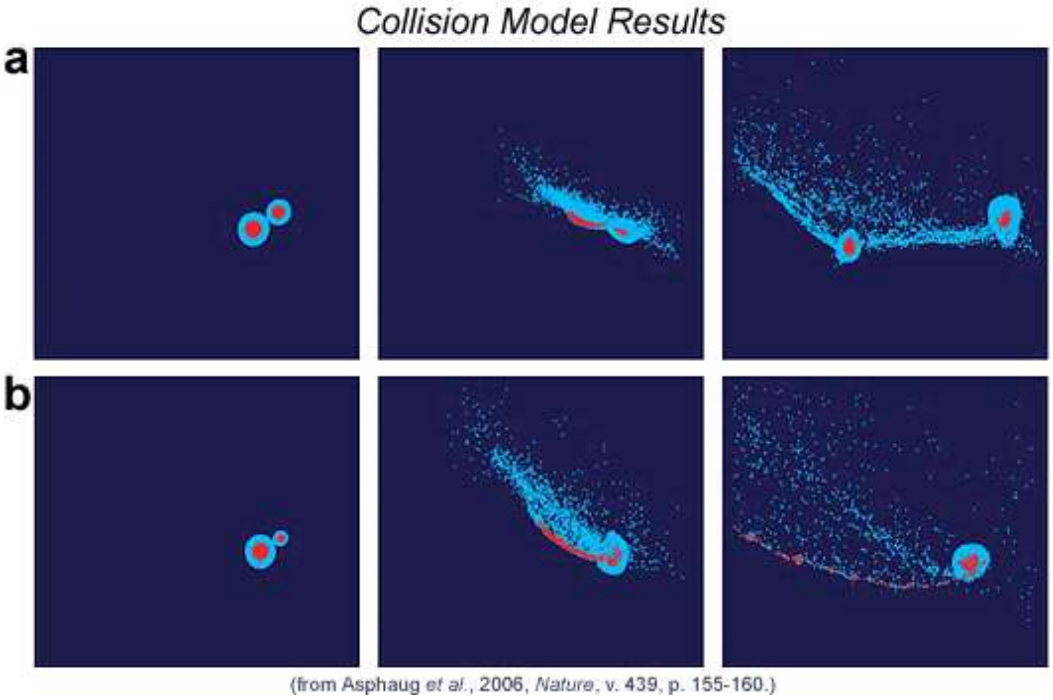

Figure 4.6: Two examples of a non-accretion collision between a protoplanet with the mass of Mars and a smaller protoplanet. In **a** (top sequence), the impactor has a mass equal to half that of the target; in **b** (bottom sequence), the impactor has a mass of only one-tenth that of the target. Red indicates the metallic cores and blue indicates the rocky mantles of the bodies. When the impacting protoplanet is close to the mass of the target protoplanet (top sequence), it experiences loss of rocky mantle, but reaccretes. Its ratio of metal to silicate has increased, however. The rocky debris could accrete to form an object with a smaller than normal amount of metallic iron. When the impacting protoplanet is small (bottom sequence), it is destroyed and a chain of metal-rich protoplanets results, possibly leading to formation of metal-rich asteroids (Asphaug et al., 2006).

Figure 4.7: B.E. Schmidt and S.C Radcliffe, an artist's conception shows an impact event on the protoplanet Pallas. This artwork was created using the three-dimensional shape model (Schmidt et al., 2009)
Credit: Image courtesy of B. E. Schmidt and S. C. Radcliffe

4.5 The Model

The discovery of the crater on Pallas (Schmidt et al., 2009) allows the role of impact as a chondrule forming mechanism to be developed. In the impact model, Pallas is struck by an iron nickel impactor (Fig 4.7). The unique metal-rich composition of CB_b chondrites is a function of the parent materials and the unique chondrule textures are a function of a non-nebular cooling history, which I attribute to the cooling convection cells which were generated following the impact. Convection allows for the transfer of heat in a fluid by the circulation of flow due to temperature differences. The regions of higher temperature, being less dense, rise, while the regions of lower temperature move down to take their place. There is more convection in an expanding impact plume than in gas shock where the event is more continuous with smaller pressure gradients.

The impact between the CR parent, perhaps Pallas, and an iron-nickel impactor explains the relationship between the members of the CR clan. The Pallas parent body material that was ejected from the impact (or remained in the body) and did not undergo any processing is the CR chondrites. The ejected material that did not escape processing was melted or condensed in the impact and became entrained in different convection cells; oscillations and mixing in these cells generated the CB_a, CB_b, and CH chondrites classes. Below is a numbered list of the stages in the impact model that explains the characteristics of the CR chondrite clan.

1. Collision of a metal-rich impactor with the silicate-rich surface of Pallas

The direct impact between Pallas and an iron nickel impactor (Fig 4.8a) would produce melt droplets and a large cloud of gas and dust. In the model the impactor is completely vaporized. The impact causes a vapor cloud to form and transport residual melt droplets by convection. The cryptocrystalline chondrules would form by condensation along with condensate metal in the same reservoir (Krot et al., 2010).

2. Temperature history – oscillations superimposed on a graduate decrease

Some of the target material would be ejected further away from the region of impact and other material in the form of droplets may remain near the remaining portion of the parent material for a limited period of time. The solids and residual melt droplets that remain entrained by gravity near the target would cause this material to be processed making it become homogenized. As this is occurring the gas continues to expand. The material would travel in convection cells that would transport gas, dust, and chondrules in a convective loop. As the gas travels outward to the periphery of the impact vapor cloud, the gas pressures decrease and the gas cools radiatively. When the gas loops back the pressure increases and the gas temperature rises. Regions in the impact cloud will not cool monotonically, but rather have a local oscillating temperature variation superimposed on the overall falling temperature (Blander 1983) which is consistent with the findings of Petaev et al., (2007) and my thermal history for skeletal olivine chondrules.

3. Oscillating temperatures can explain CBb chondrule textures

Blander (1983) suggested the role of convection cells in the solar nebula and his work is used to demonstrate the role of convection cells in an impact. The variation in size composition and texture in the chondrules in the CR chondrite clan is based on the transport of material in these convection cells and the effect they would have on the chondrules' characteristics. The oscillatory temperature of the convection cells in the vapor cloud influences the formation of the chondrules. For example, droplets condensed, crystallized, and accreted to chondrules during the expansive cooling part of the cycle *"going up"* will be reheated during *"coming down"* towards the higher temperature closer to the initial impact. The temperature fluctuations would result in remelting after partial crystallization (Blander 1983). This behavior is made tangible in blebby round edges of the olivine crystals/bars in the SBO chondrules. The formation of the chondrule with the temperature fluctuations expected with turbulence or convection cells had not been previously incorporated into dynamic crystallization experiments and no linear cooling experiments have replicated this blebby texture. It had not been reproduced until my synthetic charges were heated and cooled replicating one of the convection cells which would be produced by an impact.

4. Sorting of chondrules

Chondrules of different size and composition are sorted during the impact; the CB_a chondrules are often centimeter sized and the CB_b are .02-.25mm (Krot el al., 2006) , the CR chondrules are millimeter sized, and the CH chondrules are .02mm *(mixed with normal chondrules)*. Numerous convection cells would form with different ranges of

pressure and temperature in each and this would control the composition and size of the chondrules in each cell. In addition, chondrules would not be contained in a single convection cell. Material from one cell could fall into another cell; this phenomenon would affect the larger material because it would require higher velocities in the cell to remain entrained allowing it to grow to sizes as large as the CB_a barred olivine chondrules. Depending on the nature of the impact, after transport in the cloud, with possible concentration in stagnant zones, chondrules would either fall back to the target (Pallas) or be reaccreted to form a small body down range.

5. Formation of cryptocrystalline chondrules

The cryptocrystalline chondrules (CC) which are smaller cooled quickly around the perimeter of the impact cloud where condensation of supercooled liquids took place. The smaller size of the CC would allow them to remain entrained in the convection cell longer. The CC chondrules are composed of refractory elements and their textures and compositions will not be altered as they are cycling in the convection cells because temperatures will be too low as the cells are losing heat through radiation. The BO and SBO chondrules are residues; they are larger and formed closer to the impact where cooling was slower allowing for more crystal growth and resorbtion; they may have traveled through the loops of different cells affecting their end texture (Figure 4.8b).

6. Formation of barred and skeletally barred olivine

The large residue melt droplets may continue to evaporate on cooling if pressure falls, and they have to nucleate and grow the olivine relatively quickly. They cool quickly

several times, over several hours to days and don't nucleate after the first time. If nucleation took place a typically barred olivine texture would be generated as displayed in the CB_a chondrules. If the chondrules are reheated in the convection cells but temperatures do not exceed their liquidus skeletal barred olivine textures are generated. Evaporation removes magnesium and concentrates the aluminum, and the liquidus temperature will decrease as they evaporate. The droplets become completely molten which destroys the SBO texture and the liquidus temperature decreases because the refractory elements are also incompatible elements.

7. Estimated temperature of the impact cloud

The composition ranges of the two textural types of CB_b chondrules overlap in composition with Al_2O_3/MgO or Al_2O_3/SiO_2 ratios the same at the overlap point as bulk Renazzo (Fig 2.4 in Chapter 2) but with FeO about 3wt% . This suggests the composition of initial droplets after the evaporation of much Fe, but before the loss of significant Si and Mg. The liquidus temperature of this CC-SBO overlap composition is an estimate of the cloud temperature. I calculated liquidus temperatures (Herzberg, 1979) of the representative bulk compositions of the CC and SBO chondrules from QUE 9441 (Krot et al., 2002). The most aluminum-rich chondrules (Al_2O_3 3.7 - 13.8, MgO 38 - 28 wt%) can be considered the most evaporated residues and their liquidus temperature ranges from 1617ºC - 1509ºC, respectively (Table 3.1 in Chapter 3). The CC chondrules are the aluminum-poor condensates from the cloud (Al_2O_3 1.3 - .04, MgO 42 - 45 wt% and their liquidus temperatures range from 1646ºC – 1684ºC, respectively (Table 3.1 in Chapter 3).

The calculated liquidus temperature allows an estimate of the temperature of the impact cloud to be determined by utilizing the temperature for the transition composition between CC and SO. The highest SO calculated liquidus temperature (Herzberg, 1979) is 1617°C (Table 3.1 in Chapter 3). The liquidus temperature of SO decreases with evaporation because aluminum and calcium are being concentrated in the liquid. Because BO textures are associated with peak temperatures close to their liquidus, 1617°C gives a preliminary estimate of the cloud temperature. The lowest calculated liquidus temperature for the CC chondrules is 1646°C. The cryptocrystalline texture of the CC chondrules indicates supercooling, and it is likely that the droplets condense as supercooled liquids, so that their liquidus temperatures are upper limits for the actual temperature. The estimated range of temperatures for the cloud then is between 1617° and 1646°C.

8. The actual temperature estimated above is higher than the liquidus temperature of the residue droplets, which will have no nuclei and develop a BO texture eventually, which will be modified to SO by temperature cycling. Droplets of condensate melt will form below their liquidus and, rather than crystallizing, these viscous SiO_2-rich melts supercool and form nearly glassy chondrules with late nucleated pyroxene fibers. Presumably the barred olivine crystallization and remelting happens before the condensation of cryptocrystalline chondrules which in turn are later in some cases encased in condensing zoned metal. However, there could be temperature gradients in the cloud, as well as remixing of particles from different zones during and after cooling. It is not clear whether there was any recondensation into residue droplets.

9. The perimeter where the CC chondrules condensed continues to cool and nickel and iron begin to condense out producing the zoned grains (12 -44 days for an average sized zoned iron nickel grains to form as it condensed in a large parcel of gas from 1370K – 1270 in a closed system) that are found enveloping some of the CC chondrules (Petaev et al., 2007, Krot 2001, Ebel and Grossman, 2000) The zoned metal grains not undergoing thermal metamorphism indicates that their region of formation cooled rapidly or that the meteorite was not reheated after formation.

9b. The homogenized metal nodules found in CB_a resided in convection currents closer to the impact causing them to be heated for a longer duration resulting in additional processing which homogenized these grains and also made them rounded as they were cyclically reheated and cooled in the convection cell (Figure 4.8c). These metal grains have 30% more PGEs values than what would be found if that had condensed in the solar nebula. The PGEs are refractory and indicates that these would be the first metals to form As the cloud starts to cool the first elements out of the gas will be Al, Ca, and Ti,. The aluminum rich – magnesium poor CC chondrules would be the first to cool from the vapor cloud, assuming nucleation of new droplets.

10. The convection cell materials could form in different cells at different temperature ranges, and materials in a given chondrite are not necessarily formed in a single location. Liquid blobs may tend to split into finer droplets or coalesce depending on relative motion and collisions. Chondrule textures reflect oscillations in the impact cloud

temperature which created the unique SO chondrules. As the impact region continued to cool the material indicative of each of the chondrite groups was brought together or separated and then aerodynamically sorted with its distance from the impact (4.8d) (Table 3.1).

11. Relationship between ejection velocity and meteorite type

Material that remained closer to the impact, larger typical barred olivine chondrules, fewer zoned iron nickel grains, and homogenized larger globular Ni-Fe grains compose the CB_a chondrules. In this region these components continued to be processed because this region cooled more slowly. The chondrules display typical barred olivine textures indicating that they were heated above their liquidus temperatures and cooled by typical linear cooling. As the distance from the impact increases, chondrules with unique SO textures that were entrained in lower temperature convection currents and abundant iron nickel grains found in the CB_b chondrites were formed. These chondrules were never reheated enough to destroy all of their nuclei and create typical barred olivine textures. The temperatures in the perimeter of the vapor plume were lower. At these lower temperatures the zoned grains would initially have condensed and would have escaped homogenization by the higher temperatures found toward the center of the vapor cloud. As the distance from the impact increases, the CH chondrites form. The contact between these two chondrite groups is clearly seen in the CH chondrite Isheyevo showing that they formed in proximity to each other. The contact in Isheyevo is evidence to support the genetic and proximal relationship of these chondrules and Ni-Fe grains. The material that constitutes the CR chondrites is found the furthest from the impact. This material had

initially been ejected from the impact site and had a velocity fast enough to remove prevent it from being reprocessed.

12. Refractory inclusions in CB_b are relict grains; not impact products

The unique CB_b rare refractory inclusions are ^{16}O poor relative to CAIs found in other carbonaceous chondrites. This behavior among the CB_b CAIs may indicate that they formed in a reservoir of nebular gas that was depleted in ^{16}O (Krot et al., 2001, 2002). The CAIs identified in CB_b ($\Delta^{17}O = -7 \pm 3‰$) and some magnesium rich cryptocrystalline CH chondrules ($\Delta^{17}O = -2.3‰ \pm 0.6‰$) were initially reported as also being depleted in ^{16}O (Krot et al., 2009) compared to CAI in typical chondrite groups. However, additional data reported indicates that these CAIs are more enriched in ^{16}O compared to the CC chondrules (Krot et al., 2010). Review of the isotopic data and the age of CAIs found in the chondrites indicate that they are not a byproduct of the impact and that they are relict pre-impact materials that were incorporated into the chondrite body.

	Big metal	Zoned metal	Zoned metal	Normal metal
CR body +impact	10^7 metals??	CC chon	CC+SBO	
	Big BO	SBO	Normal chon	Normal chon
	CB_a	CB_b	CH	CR

Table 4.1: The impact region continued to cool and the material indicative of each of the chondrite groups was brought together or separated and then aerodynamically sorted with its distance from the impact

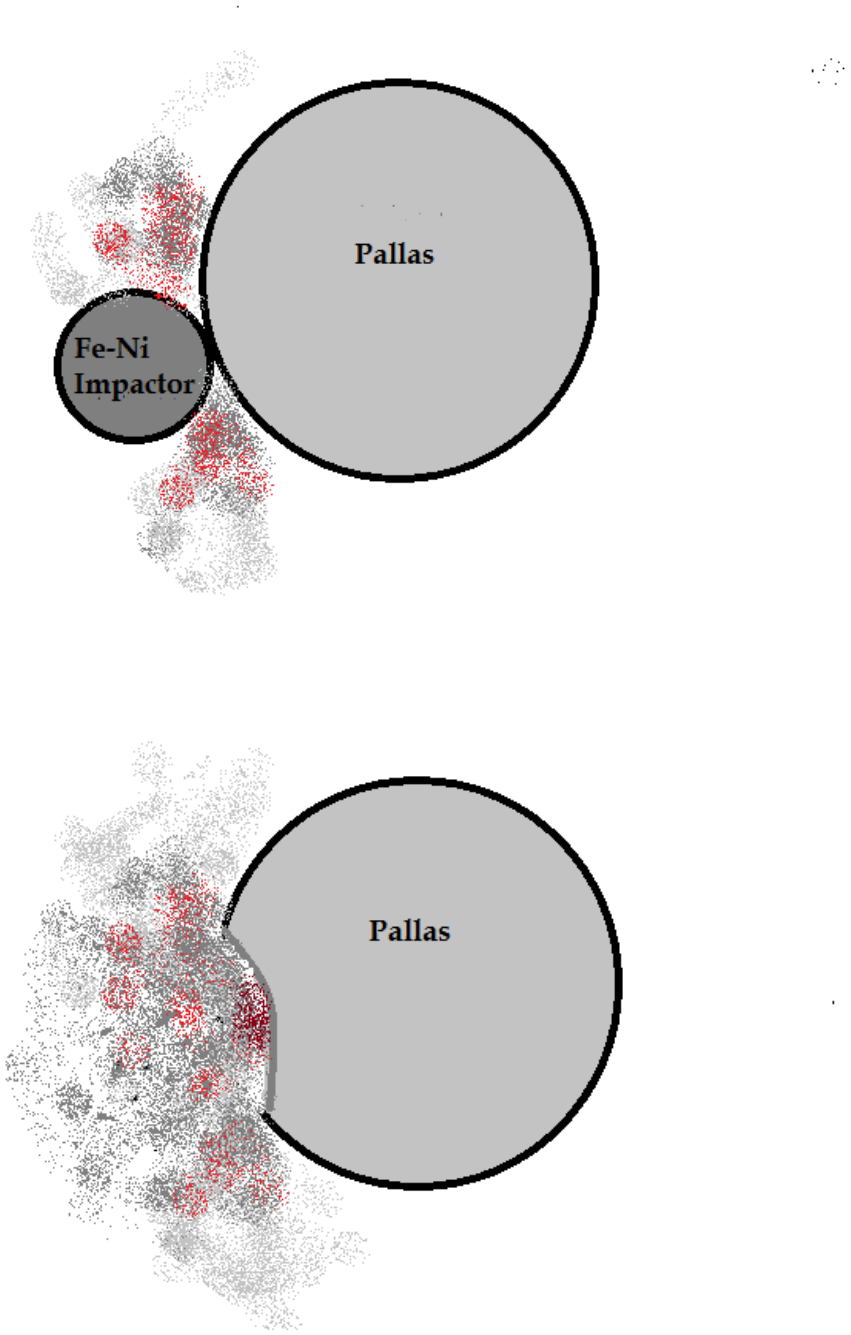

Figure 4.8a: Formation model, initial collision between parent material, Pallas and a Fe-Ni impactor. Very little material is ejected up and out of the forming crater at this time. A plume of impact generated vapor readily expands above the crater. The impactor is completely destroyed.

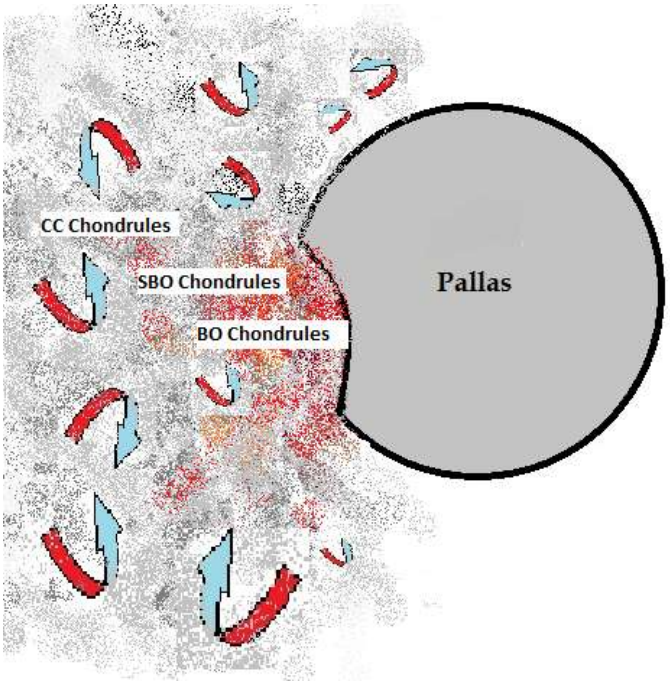

Figure 4.8b: Formation model, development of temporary atmosphere caused by gravitational field of impactor. Some of the target material is ejected from the site. Initially the ejecta form a plume of hot vapor, melt droplets, and fine debris. Then a cone shaped curtain of material is spread up from the site. The first material produced is the CC chondrules. Material entrained in the convection currents produced the unique SBO chondrule textures and material closest to the impact creates typical BO textures.

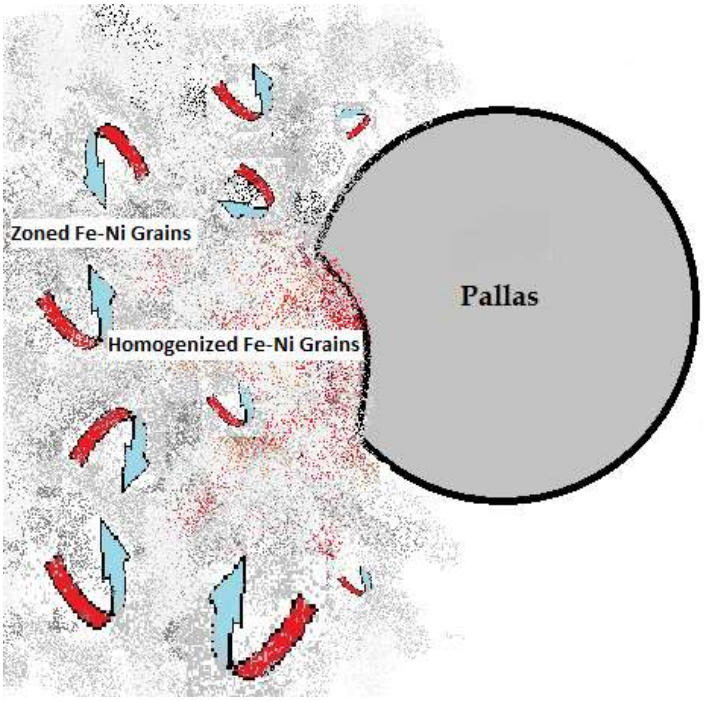

Figure 4.8c : Formation Model, heat loss continues and with falling temperatures Fe and Ni begin to condense out from the condensation cloud. The perimeter of the impact cools most rapidly and the zoned Fe – Ni grains grown at rates calculated between 12-44days. Iron Nickel grains which form closer to the impact become entrained in the convection currents and become homogenized.

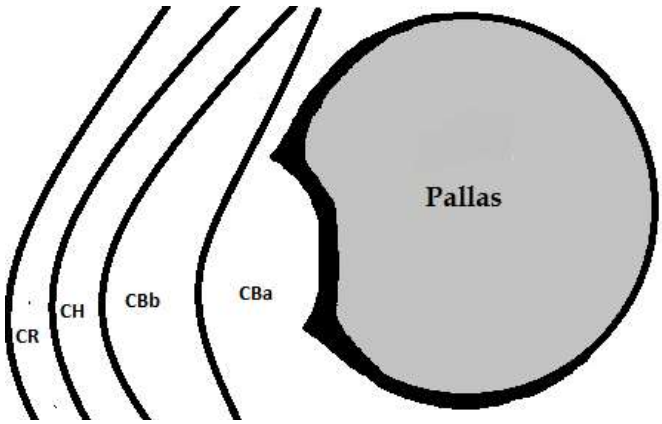

Figure 4.8d Formation of genetically related CR clan following impact. The CR chondrites are impact ejecta from Pallas. The CBa, CBb, and CH chondrites are products of the 'synthesized' parent material which has been modified in convections cells and then aerodynamically sorted into their respective chondrite groups.

Appendix A: Synthetic Olivine Samples BO5 calculated liquidus temperature 1570ºC

Cooling Rate			
	BO5 2 Tmax 1580ºC	Δtmax 15min	Quench 1000ºC
1000ºC/h +ΔT = 10°	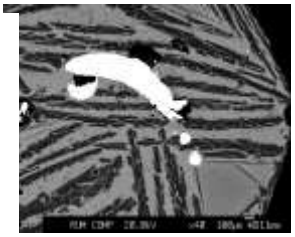	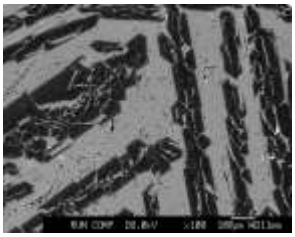	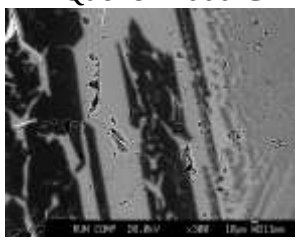
	BO5 3 Tmax 1586ºC	Δtmax 15min	Quench 600ºC
1000ºC/h +ΔT = 16°	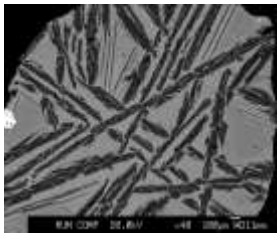	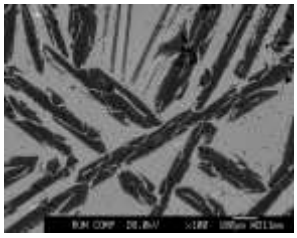	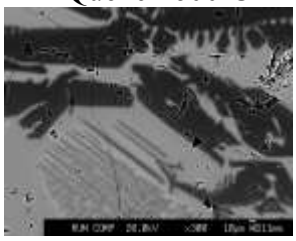
	O5 5Tmax 1593ºC	Δtmax 30 min	Quench 1000ºC
100ºC/h +ΔT = 23°	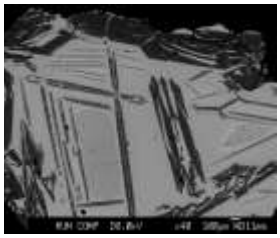	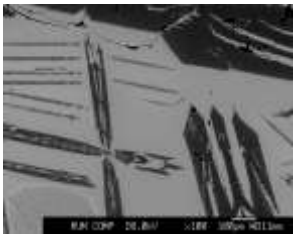	
	O5 1Tmax 1575ºC	Δtmax 30 min	Quench 1000ºC
500ºC/h +ΔT = 5°	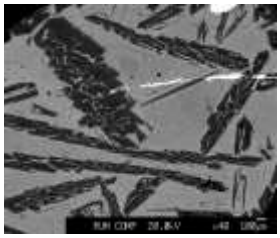	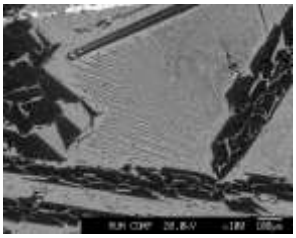	
	O5 6 Tmax 1589ºC	Δtmax 30 min	Quench 600ºC
500ºC/h +ΔT = 19°	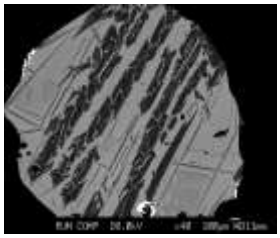	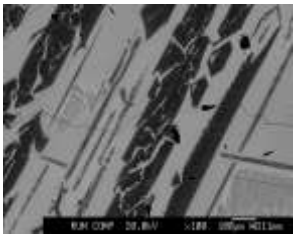	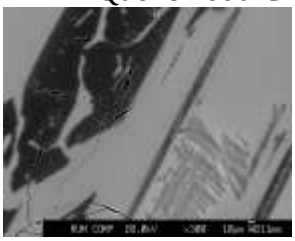
	O5 8 Tmax 1585ºC	Δtmax 30 min	Quench 1000ºC
1000ºC/h +ΔT = 15°	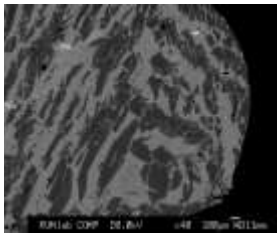	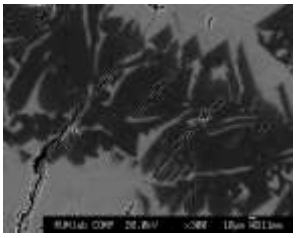	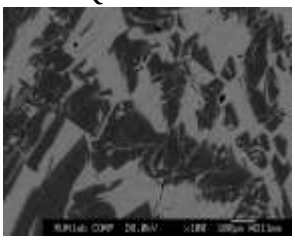

Appendix A: Synthetic Olivine Samples BO5 calculated liquidus temperature 1570ºC

Cooling Rate	BO5 13 Tmax 1603ºC	Δtmax 60 min	Quench 900ºC
10ºC/h +ΔT = 33°	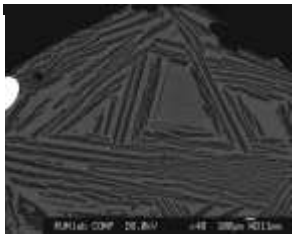	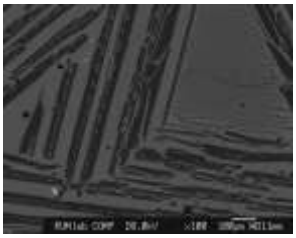	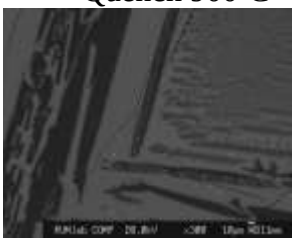
	BO5 11 Tmax 1603ºC	Δtmax 60 min	Quench 1000ºC
50ºC/h +ΔT = 33°	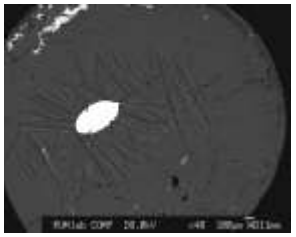	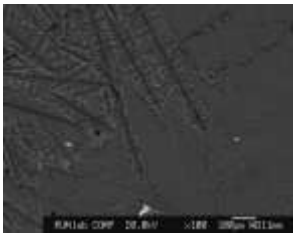	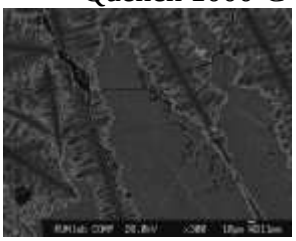
	BO5 9 Tmax 1578ºC	Δtmax 60 min	Quench 1000ºC
500ºC/h +ΔT = 8°	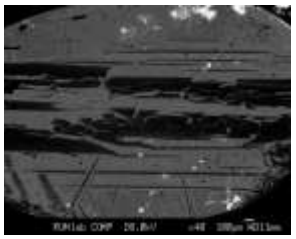	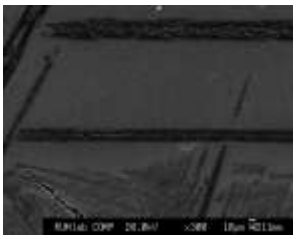	
	BO5 4b Tmax 1594ºC	Δtmax 60 min	Quench 1000ºC
1000ºC/h +ΔT = 24°	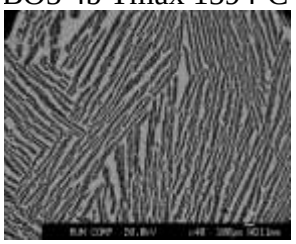	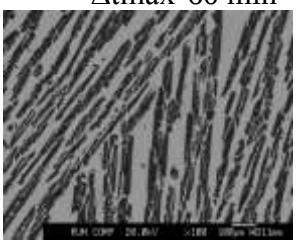	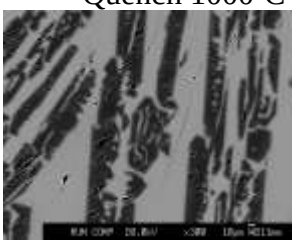
	BO5 10 Tmax 1594ºC	Δtmax 120 min	Quench 1000ºC
1000ºC/h +ΔT = 24°	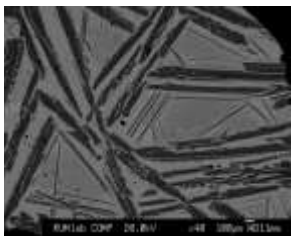	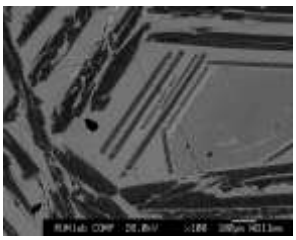	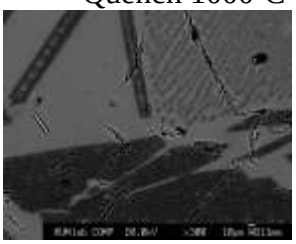
	BO5 12 Tmax 1606ºC	Δtmax 180 min	Quench 1000ºC
1000ºC/h +ΔT = 36°	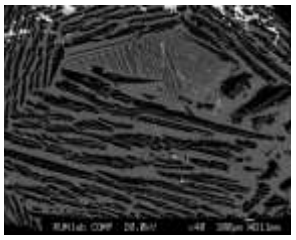	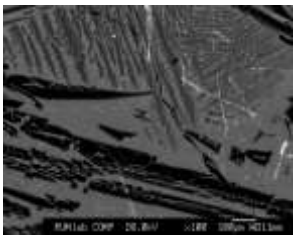	

Appendix A: Synthetic Olivine Samples BO5 calculated liquidus temperature 1570ºC

	BO5 15 Tmax 1606ºC	Δtmax 31hours	Quench 1000ºC
Cooling Rate 1000ºC/h +ΔT = 36°		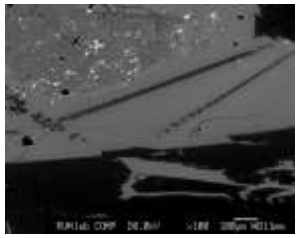	

Appendix B: Synthetic Olivine Samples BO6 calculated liquidus temperature 1509ºC

Cooling Rate

3O6 2 Tmax 1520ºC Δtmax 15 min Quench 1000ºC

1000ºC/h
+ΔT = 11°

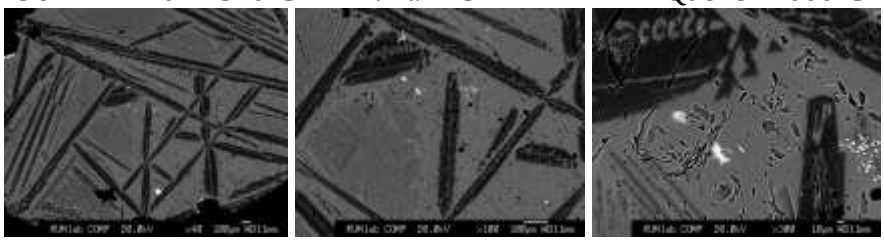

BO6 7b Tmax 1588ºC Δtmax 15 min Quench 1000ºC

1000ºC/h
+ΔT = 79°

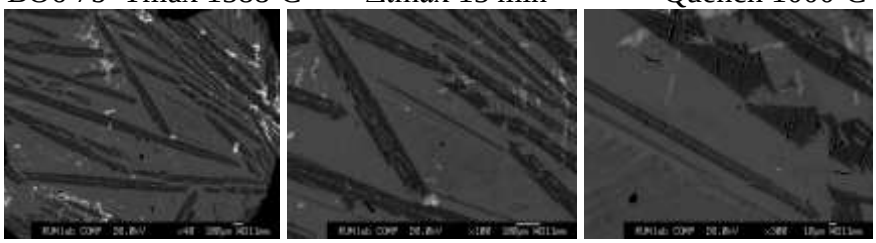

3O6 3 Tmax 1525ºC Δtmax 15 min Quench 600ºC

1000ºC/h
+ΔT = 16°

BO6 7c Tmax 1587ºC Δtmax 15 mins Quench 600ºC

1000ºC/h
+ΔT = 78°

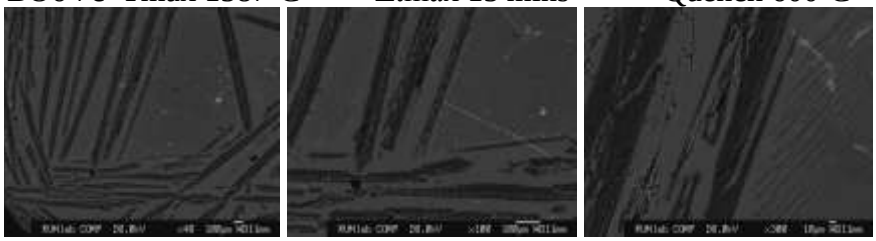

100ºC/h
+ΔT = 25°

3O6 5 Tmax 1534ºC Δtmax 30 min Quench 1000ºC

100ºC/h
+ΔT = 78°

BO6 7e Tmax 1587ºC Δtmax 30mins Quench 1000ºC

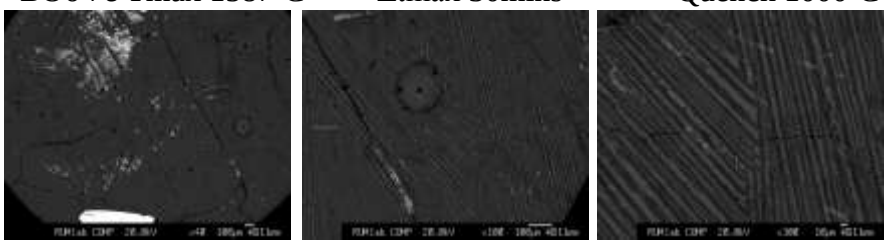

Appendix B: Synthetic Olivine Samples BO6 calculated liquidus temperature 1509ºC

BO6 1 Tmax 1520ºC Δtmax 30 min Quench 1000ºC

Cooling Rate

500ºC/h
+ΔT = 11°

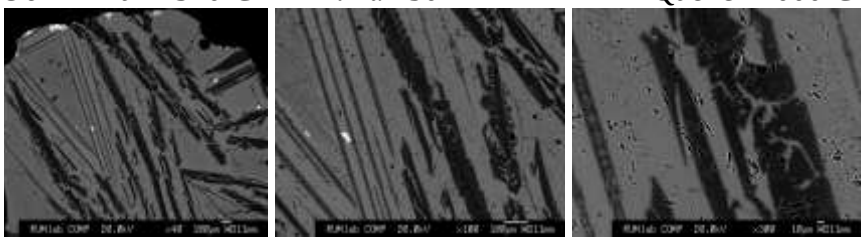

BO6 7a Tmax 1590ºC Δtmax 30 min Quench 1000ºC

500ºC/h
+ΔT = 81°

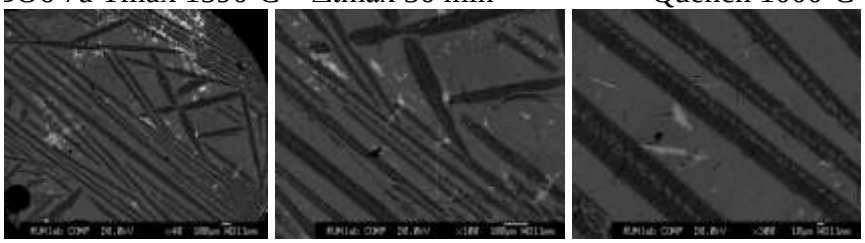

BO6 6 Tmax 1532ºC Δtmax 30 min Quench 600ºC

500ºC/h
+ΔT = 23°

BO6 8 Tmax 1523ºC Δtmax 30 min Quench 1000ºC

1000ºC/h
+ΔT = 23°

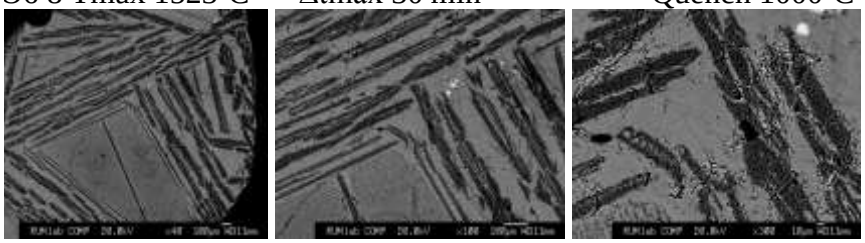

BO6 7n Tmax 1576ºC Δtmax 45 min Quench 1676ºC

Quench
+ΔT = 67°

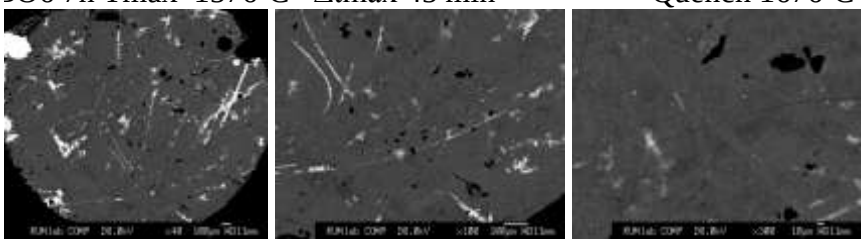

BO6 7m Tmax 1590ºC Δtmax 60min Quench 900ºC

10ºC/h
+ΔT = 81°

Appendix B: Synthetic Olivine Samples BO6 calculated liquidus temperature 1509ºC

Cooling Rate			
	BO6 11 Tmax 1525ºC	Δtmax 60 min	Quench 1000ºC
50ºC/h +ΔT = 16°	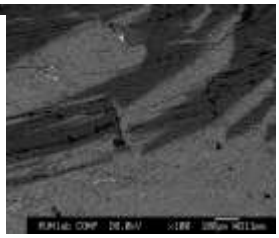	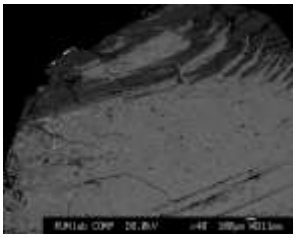	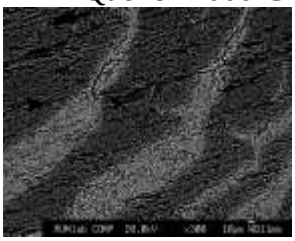
	O6 9 Tmax 1524ºC	Δtmax 60 min	Quench 1000ºC
500ºC/h +ΔT = 15°	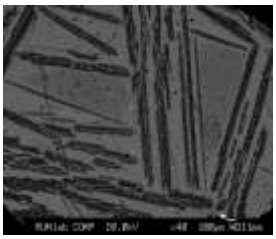	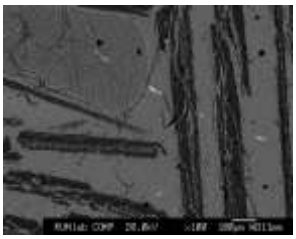	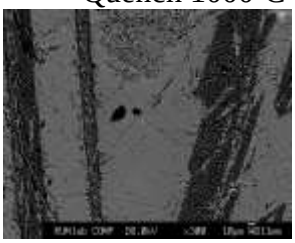
	BO6 7i Tmax 1568ºC	Δtmax 60 min	Quench 1000ºC
500ºC/h +ΔT = 59°	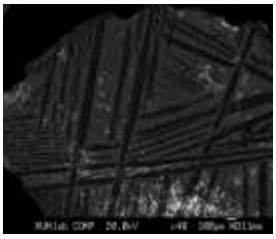	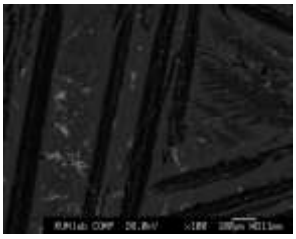	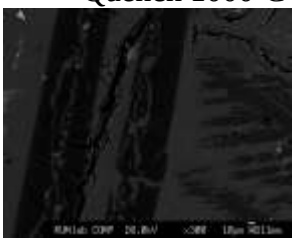
	O6 4 Tmax 1528ºC	Δtmax 60 min	Quench 1000ºC
1000ºC/h +ΔT = 20°	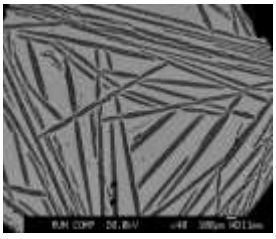	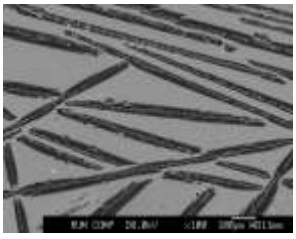	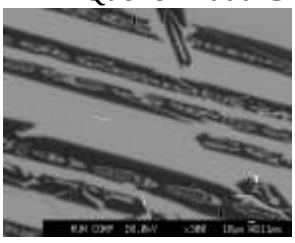
	BO6 7d Tmax 1587ºC	Δtmax 60 min	Quench 1000ºC
1000ºC/h +ΔT = 78°	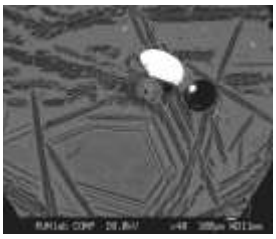	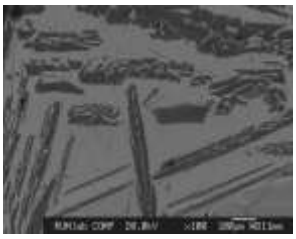	
	O6 10 Tmax 1525°C	Δtmax 120 min	Quench 1000ºC
1000ºC/h +ΔT = 16°	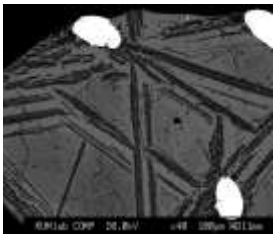	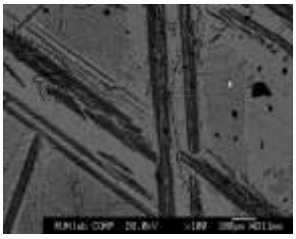	

Appendix B: Synthetic Olivine Samples BO6 calculated liquidus temperature 1509ºC

Cooling Rate	BO6 7j Tmax 1578ºC	Δtmax 120 min	Quench 1000ºC
1000ºC/h +ΔT = 69°	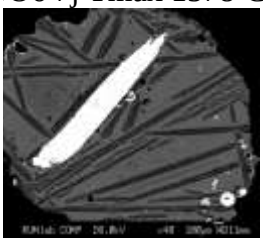	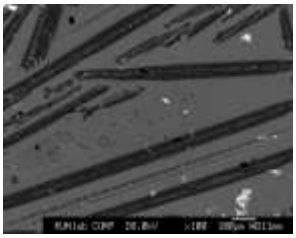	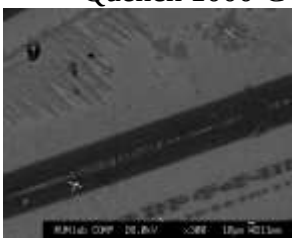
	BO6 12 Tmax 1606ºC	Δtmax 180 min	Quench 1000ºC
1000ºC/h +ΔT = 97°	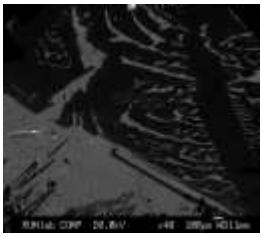	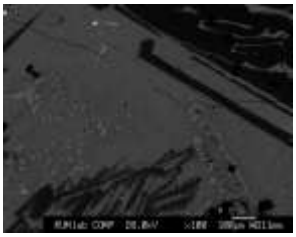	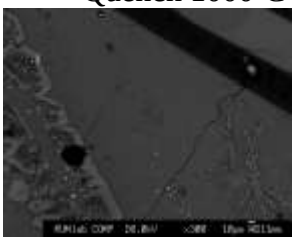
	BO6 15 Tmax 1606ºC	Δtmax 31hrs	Quench 1000ºC
1000ºC/h +ΔT = 97°	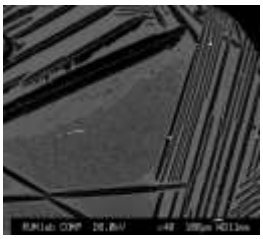	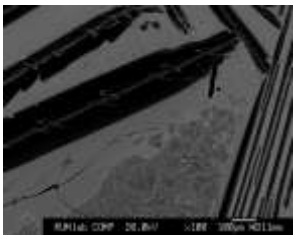	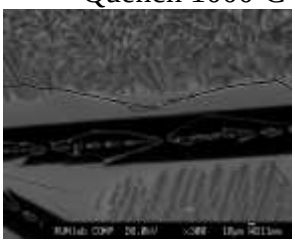

Appendix C: Cryptocrystalline Samples CC2 adjusted calculated liquidus temperature 1493°C

CC2-2 Tmax 1605°C Δt max 15 min +ΔT = 112°
Cooling Rate 1000ºC/h Quench 600°C Quench 1000°C

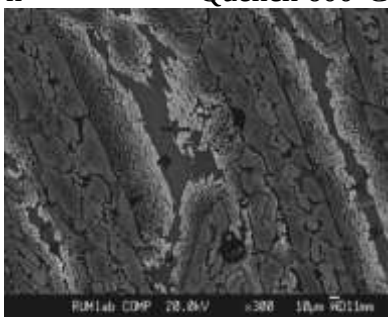
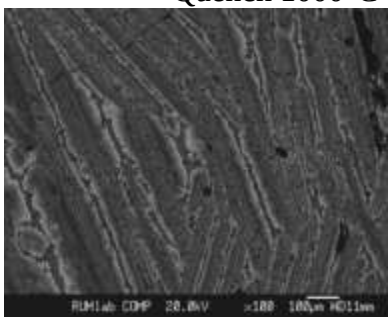

CC2-3 Tmax 1607°C Δt max 15min +ΔT = 114°
Cooling Rate 1000°C/h Quench 600°C Quench 1000°C

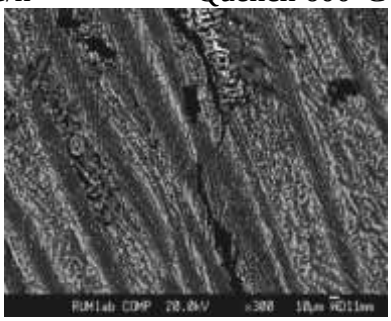
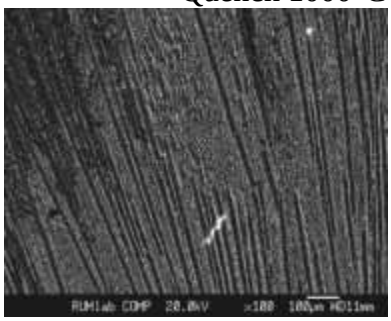

CC2-6 Tmax 1606°C Δt max 30 min +ΔT = 113°
Cooling Rate 500°C/h Quench 600°C Quench 1000°C

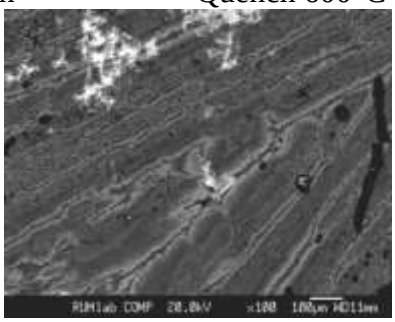
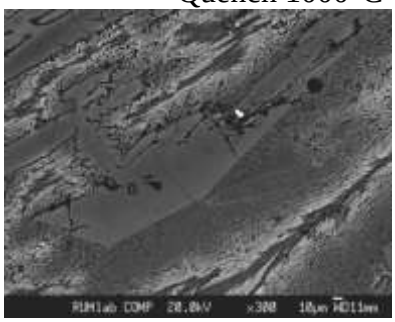

CC2-1 Tmax 1607°C Δt max 30 min +ΔT = 114°
Cooling Rate 500°C/h Quench 600°C Quench 1000°C

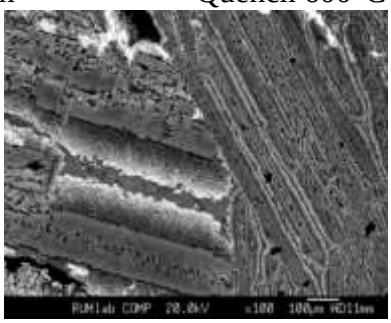
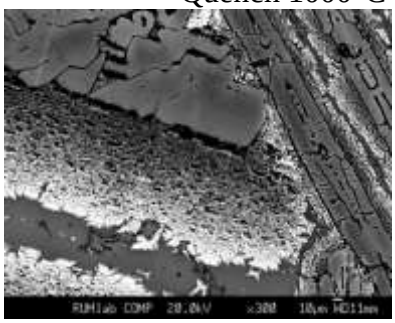

Appendix C: Cryptocrystalline Samples CC2 adjusted calculated liquidus temperature 1493°C

CC2-5 Tmax 1608°C Δt max 30 min +ΔT = 115°
Cooling Rate 100°C/h Quench 1000°C

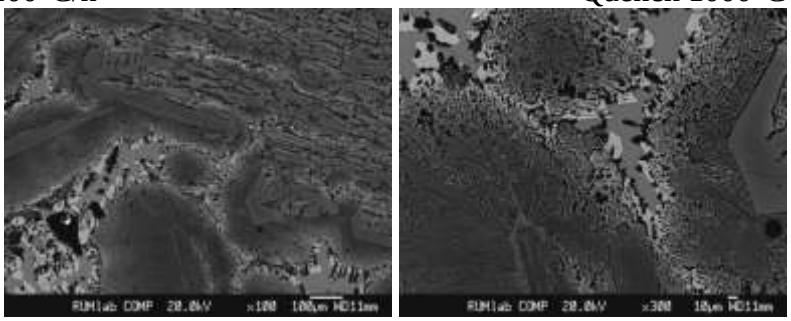

CC2-1 Tmax 1607°C Δt max 30 min +ΔT = 114°
Cooling Rate 500°C/h Quench 1000°C

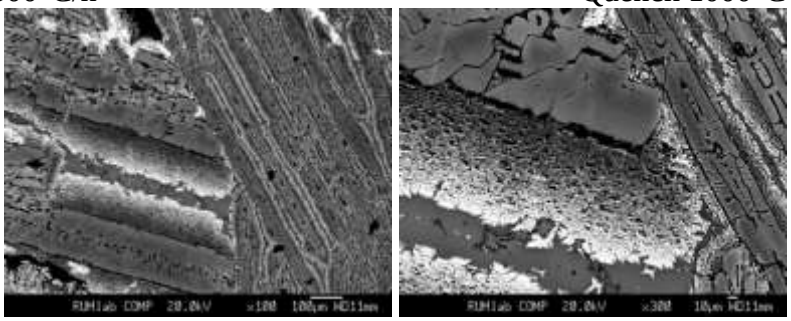

CC2-8 Tmax 1608° C Δt max 30 min +ΔT = 115°
Cooling Rate 1000°C/h Quench 1000°C

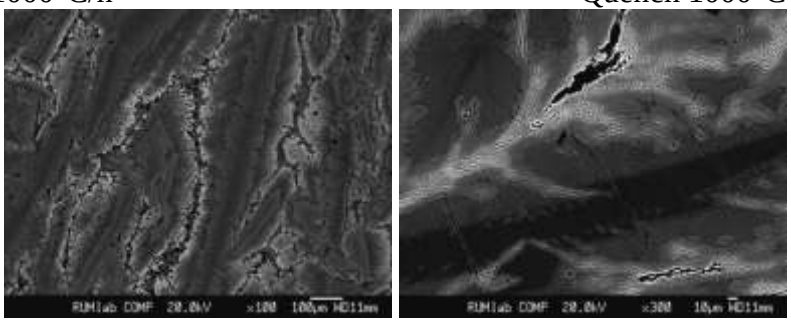

Appendix C: Cryptocrystalline Samples CC2 adjusted calculated liquidus temperature 1493°C

CC2-13 Tmax 1608°C Δt max 60 min +ΔT = 114°
Cooling Rate 10°C/h Quench 1000°C

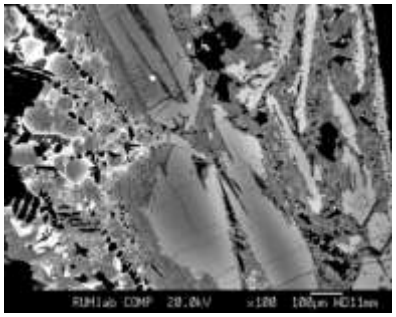
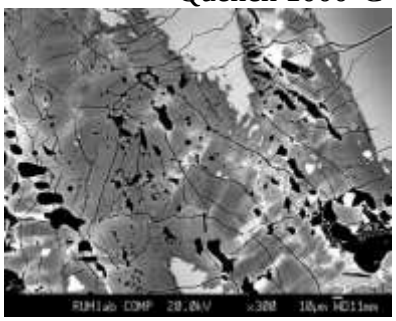

CC2-9 Tmax 1606 °C Δt max 60 min +ΔT =113°
Cooling Rate 500°C/h Quench 1000°C

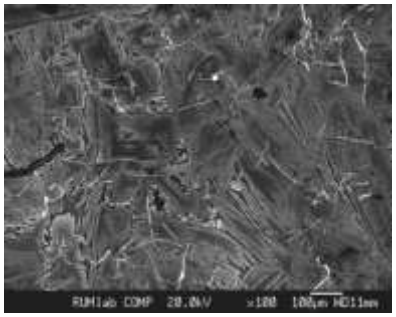
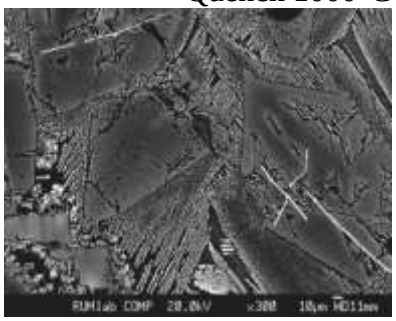

CC2-4 Tmax 1605°C Δt max 60 min +ΔT =112°
Cooling Rate 1000°C/h Quench 1000°C

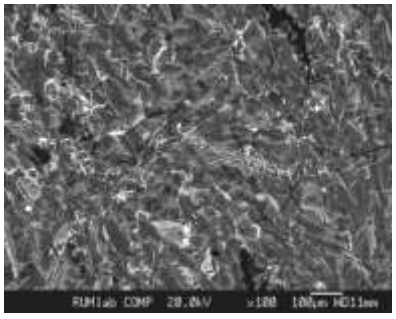
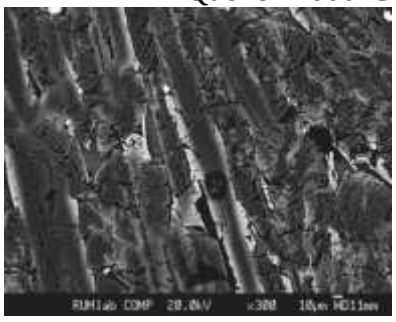

CC2-16 Tmax 1610°C Δt max 60 min +ΔT =117°
Cooling Rate 1000+°C/h Quench 1000°C

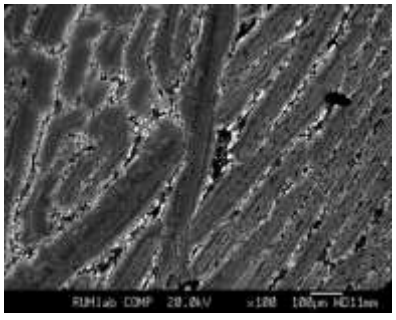
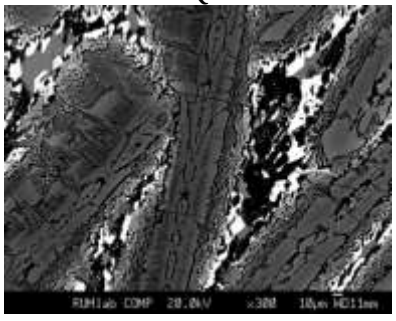

Appendix C: Cryptocrystalline Samples CC2 adjusted calculated liquidus temperature 1493°

CC2-18 Tmax 1610°C Δt max 60 (1hr) +ΔT = 117°
Cooling Rate 1000°C/h to 1400° then 100°C/h to 1000° Quench 1000°C

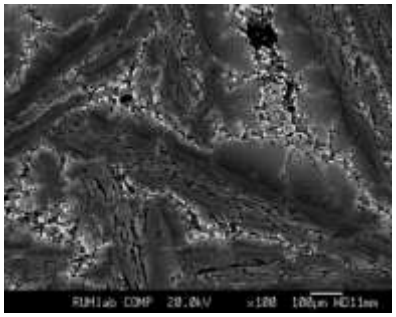
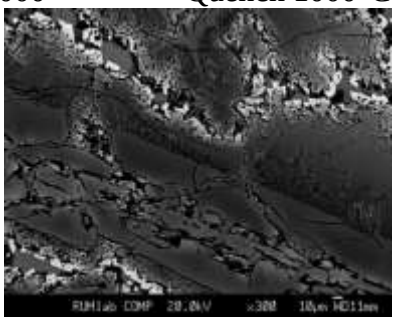

CC2-17 Tmax 1610°C Δt max 120mins (2hrs) +ΔT = 117°
Cooling Rate 1000°C/h to 1400° then 100°C/h to 1000° Quench 1000°C

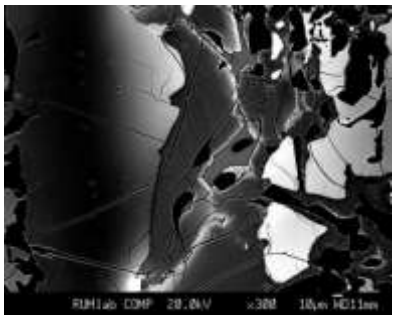
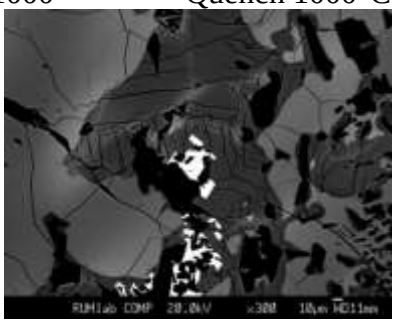

CC2-19 Tmax 1610°C Δt max 4320mins (72hrs) +ΔT = 117°
Cooling Rate 1000°C/h to 1400° then 100°C/h to 1000° Quench 1000°C

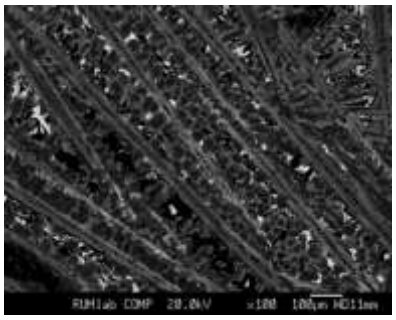
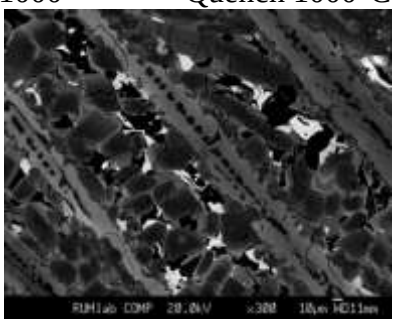

CC2-15 Tmax 1610°C Δt max 240mins (4hrs) +ΔT =117°
Cooling Rate 1000°C/h to 1400° then 500°C/h to 1000° Quench 1000°C

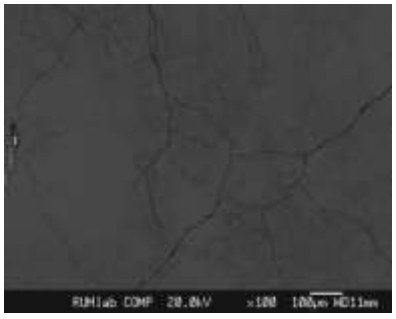
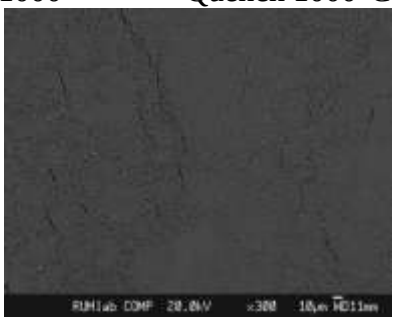

Alexander, C.M.O' D., and Hewins, R. H. (2004). Mass fractionation of Fe and Ni isotopes in metal in Hammadah al Hamrah 237. *Meteorit. Planet. Sci*. 39, A

Alexander , R. (2008). From discs to planetesimals: Evolution of gas and dust discs. *New Astron. Rev*. 52, 60-77.

Amelin, Y., and Krot, A.N. (2007). Pb isotopic age of the Allende chondrules. *Meteorit. Planet. Sci*. 42, 1321-1335.

Amelin, Y., Krot, A.N., Hutcheon, I.D., and Ulyanov, A.A. (2002). Lead isotope ages of chondrules and calcium-aluminum rich inclusions. *Science* 297, 1678-1683.

Amelin, Y., Wadhwa, M., & Lugmair, G. (2006). *37th Lunar Planetary Science Conf*erence, 1970.

Anders, E., and Grevesse, N. (1989). Abundances of the elements: Meteoritic and solar. *Geochim. Cosmochim Acta* 53, 197-214.

Asphaug, E., Jutzi, M., and Movshovitz, N. (2011). Chondrule formation by partial accretion of planetesimals. *42nd Lunar and Planetary Conference*, 1647.

Asphaug, E., Agnor, C. B., and Williams, Q. (2006). Hit-and-run planetary collisions. *Nature* 439, 155-160.

Barucci, M. A., Capria, M. T., Coradini, A., and Fulchignoni, M. (1987).Classification of asteroids using G-mode analysis. *Icarus* 72, 304-324.

Bizzarro, M., Baker J. A., Haack, H. and Lundgaard, K. L. (2005). Rapid timescales for accretion and melting of differentiated planetesimals inferred from ^{26}Al–^{26}Mg chronometry. Astrophys. J. 632, 41–44.

Blander, M. (1983). Condensation of chondrules. In *Chondrules and Their Origins* (eds. E. A. King). Lunar and Planetary Institute, pp. 1-9.

Blander, M., Planner, H. N., Keil, K., Nelson, L. S., and Richardson, N. L. (1976). The origin of chondrules: Experimental investigation of metastable liquid in the system Mg_2SiO_4-SiO_2. *Geochim. Cosmochim. Acta.* 40, 889 -896.

Bottke, W. F. and Martel L. M.V. (2006). Iron meteorites as the Not-so-Distant Cousins of Earth. *Planetary Science Research Discoveries* http://www.psrd.hawaii.edu/July06/asteroidGatecrashers.html

Cameron, A. G.W. (1973). Properties of the Solar Nebula and the Origin of the Moon. *The Moon* 7, 377-383.

Cameron, A. G. W (1995). The first ten million years in the solar nebula. *Meteoritics* 30, 133-61.

Cameron, A. G. W. and Benz, W. (1991). The origin of the Moon and the single hypothesis IV. *Icarus* 92, 204-216.

Campbell, A. J., Humayun, M., and Weisberg, M.K (2002). Siderophile element constraints on the formation of metal in the metal-rich chondrites Bencubbin, Weatheford, and Gujba. *Geochim. Cosmochim. Acta.* 66, 647-660.

Campbell, A. J., Humayun, M., and Weisberg, M.K. (2005). Compositions of unzoned and zoned metal in the CBb chondrites Hammadah al Mamra 237 and Queen Alexandra Range 94627. *Meteoritics and Planetary Science* 40, 1131-1148.

Campbell, A.J., Humayun, M., Meibom, A., Krot, A.N., Keil, K. (2001). Origin of zoned metal grains in QUE94411 chondrite, *Geochim. Cosmochim. Acta* 65, 163-180.

Campbell, A. J., Humayun, M., and Weisberg, M.K. (2000). Siderophile element distributions in zoned metal grains in Hammadah al Hamra 237. *35th Meteorit. Planet. Sci. Conference* 38.

Campbell, A. J., Humayun, M., Meibom, A., Krot, A., N. (1999). Platinum Group Element Distributions in Bencubbinite metal grains. *31st Lunar and Planetary Science Conference*, 1490.pdf.

Canup, R. M., Asphaug, E., Pierazzo, E. and Melosh H. J. (2002). Simulations of Moon-forming impacts. *Lunar Plan. Sci.* 33, 1641-1642.

Carry, B., Dumas, C., Kaasalainen, M., Berthier, J., Merline, W. J., Erard, S., Conrad, A., Drummond, J. D., Hestroffer, D., Fulchignoni, M., and Fusco, T. (2010). Physical properties of (2) Pallas. *Icarus* 205, 460–472.

Cassen, P. (1994) Utilitarian models of the solar nebula. *Icarus*112, 405-429.

Chamberlain, A. (2007) Asteroid Belt Distributions. JPL/Caltech. http://ssd.jpl.nasa.gov/images/ast_histo.ps

Chambers, J.E. and Cassen, P. (2002). The effects of nebula surface density profile and giant planet eccentricities on planetary accretion in the inner Solar System. *Meteoritics Plan. Sci.* 37, 1523-1540.

Chapman, C.R., Morrison, D., Zellner, B. (1975). Surface properties of asteroids – A synthesis of polarimetry, radiometry, and spectrophotometry. *Icarus* 25, 104–130.

Clayton, R. N. and Mayeda, T. K. (1999). Oxygen isotope studies of the carbonaceous chondrites. *Geochim. Cosmochim. Acta* 63, 2089 -2104.

Clayton, R. (1993). Oxygen Isotopes in Meteorites. *Annu. Rev. Earth Planet Sci*. 21, 123.

Cohen B.A. and Hewins R.H. (2000). Evaporation in the young solar nebula as the origin of 'just-right' melting of chondrules. *Nature* 406, 600-602.

Connolly H.C. Jr., Jones B.D., and Hewins R. H. (1998). The flash melting of chondrules: an experimental investigation into the melting history and physical nature of chondrule precursors. *Geochim. Cosmochim. Acta* 62, 2725-2735.

Connolly, H.C. and Hewins, R.H. (1995). Chondrules as products of dust collisions with totally molten droplets within a dust-rich nebular environment: An experimental investigation. *Geochim. Cosmochim. Acta* 59, 3231-3246.

Connelly, J. N., Amelin, Y., Krot, A. N., and Bizzarron, M. (2008). Chronology of the solar system's oldest solids. *The Astrophysical Journal* 675, 121–124.

Connolly, H.C., Radomsky, P. M., and Hewins, R. H. (1988). Chondrule texture: The influence of bulk composition and heating time for uniform thermal conditions. *Lunar Planet. Sci.* 19, 205 – 206.

Cuzzi, J. N., Hogan, R. C. Shariff, K. (2008). Toward planetesimals: Dense chondrule clumps in the protoplanetary nebula. *Astrophys. J.* 687, 1432-1447.

Davis, D. R., Chapman, C. R., Greenberg, R., Weidenschilling, S., and Harris A. W. (1979). Collisional evolution of asteroids: Populations, rotations, and velocities. In *Asteroids* (eds. T. Gehrels). University of Arizona Press, pp. 528-57.

Davis, A.M. and MacPherson, G. J. (1996).Thermal processing in the solar nebula: Constrains from refractory inclusions, in Chondrules and the Protoplanetary Didk, edited by R. E. Hewins, R. H. Jones, and E. R. D. Scott, pp 71-77, Cambridge University Press, New York.

Davis, A. M., Alexander C. M. O'D, Nagahara, H., Richter, F. (2004). Evaporation and condensation during CAI and chondrule formation. *Workshop on Chondrites and Protoplanetary Disk* 9070.

Desch, S. J. and Connolly, H. C. Jr. (2002). A model of the thermal processing of particles in solar nebula shocks: Application to the cooling rates of chondrules. *Meteorit. Planet. Science* 37, 183-207.

Dodd, R. T. (1974). The petrology of chondrules in the Hallingeberg meteorite. *Contrib. Mineral. Petrol.* 47, 91-112.

Dodd R. T. (1971). The petrology of chondrules in the Sharps meteorite. *Contrib. Mineral. Petrol.* 31, 201-227.

Donaldson, C. H. (1976). An experimental investigation of olivine morphology. *Contrib. Mineral. Petrol.* 57, 187-213.

Durba, D. D., and Flynn G. J., (1999). An experimental study of the impact disruption of a porous, inhomogeneous target. *28th Lunar and Planetary Science Conference*, 1298.

Dwyer, F., Nimmo, F., Asphaug, E. (2012). A Physical Model for simultaneous production of CH and CB chondrules during an impact event. *43rd Lunar and Planetary Science Conference*, 2291.

Ebel, D. and Grossman, L. (2000). Condensation in dust-enriched systems. *Geochim. Cosmochim. Acta.* 64, 339 – 366.

Faure, F., Trolliard, G., and Soulestin, B. (2003). TEM investigation of forsterite dendrites. *American Mineralogist* 88, 1241-1250.

Feigelson, E.D., Garmire, G.P., Pravdo, S.H. (2002). Magnetic flaring in the pre-main sequence Sun and implications for the early solar system. *Astrophys. J.* 584, 911 -930.

Flynn, G. J., Moore, L.B., and Klock, W. (1999). Density and porosity of stone meteorites: Implications for the density, porosity, cratering, and collisional disruption of asteroids. *Icarus* 142, 97-105.

Foglia, S., and Masi, G. (1999). New clusters for highly inclined main-belt asteroids. *The Minor Planet Bulletin* 31, 100–102.

Gaffey, M. J., Burbine, T. H., and Binzel, R. P. (1993a). Asteroid spectroscopy: progress and perspective. *Meteoritics* 28, 161-187.

Gaffey M. J., Bell, J. F., Brown, R. H., Burbine, T. H., Platek, J. L., Reed, L. R., and Chaky, D. (1993b). Mineralogical variations within the S-type asteroids class. *Icarus* 106, 573-602.

Gaffey, M.J., E.A. Cloutis, M.S. Kelley and K.L. Reed. (2002). Mineralogy of asteroids. In Asteroids III (eds. W. F. Bottke, A. Cellino, P. Paolicchi and R. P. Binzel,), Univ. of Arizona Press, pp. 183-204.

Giacomuzzo, C., Ferri, F., Bettella, A., Pavarin, D., Francesconi, A., Flamini, E., Angrilli F. (2007). Hypervelocity experiments of impact cratering and catastrophic disruption of targets representative of minor bodies of the Solar System. *Adv. Space Res.* 40, 244–251.

Gibson, R.L. and Reimold, W.U. (2010). Introduction: Impact cratering and planetary studies--a fifty-year perspective. *GSA Special Papers* 465, 7-12.

Gooding, J. L., Keil, K., Fukuoka, T., and Schmitt, R. A. (1980). Elemental abundances in chondrules from unequilibrated chondrites. Evidence for chondrule origin by melting of preexisting materials. *Earth Planet Sci. Lett*. 50, 171-180.

Gooding J. L. and Keil K. (1981). Relative abundances of chondrule primary textural types in ordinary chondrites and their bearing on chondrule formation. *Meteoritics* 16, 17-43.

Gounelle, M. (2011). The Asteroid–Comet Continuum: In Search of Lost Primitively. *Elements* **7**, 29-34.

Gounelle M. et al., (2007) Magnesium isotopic constraints on the origin of CBb chondrites, Earth Plant. Sci. Lett., doi:10,1016/j.epsl.2007.02.007

Gradie, J., and Tedesco, E. (1982). Compositional structure of the asteroid belt. *Science*, 216, 1405-1407.

Grieve, R. A. and Pesonen, L. (1996). Terrestrial impact craters: Their spatial and temporal distribution and impacting bodies. *Earth, Moon, and Planets* 71, 357-376.

Grieve, R. A. F. (1987). Terrestrial Impact Structures. *Ann. Rev. Earth Planetary Science* 15, 245-270.

Grossman, J.N., Rubin A. E., and MacPherson, G. J. (1988). ALH85085; a unique volatile-poor carbonaceous chondrite with possible implications for nebular fractionation process. *Earth Planet Sci. Lett.* 91, 33-54.

Grossman, L. (1972). Condensation in the primitive solar nebula. *Geochim. Cosmochim. Acta.* 36, 597-619.

Grossman L., and Olsen, E. (1974). Origin of the high temperature fraction of C2 chondrites. *Geochim. Cosmochim. Acta.* 38, 173-187.

Grossman L., Olsen, E., and Lattimer, J. M. (1979). Silicon in carbonaceous chondrites metal: Relic of high-temperature condensation. *Science* 206, 449-451.

Grove T. L. (1981). Use of FePt Alloys to Eliminate the Iron Loss Problem in 1 atmosphere gas mixing experiments: Theoretical and Practical Considerations. *Contrib. Mineral Petrology 78, 298-304.*

Heiken, G. (1975). Petrology of lunar soils. *Rev. Geophys.and Space Phys*. 13, 567-587.

Herzberg C. T. (1979). The solubility of olivine in basaltic liquids: an ionic model. *Geochim. Cosmochim. Acta.* 43, 1241-1251.

Hevey, P. J. and Sanders I. S. (2006). A model for planetesimals meltdown by ^{26}Al, and its implications for meteorite parent bodies. *Meteoritics and Planetary Science* 41, 95-106.

Hewins, R. H. and Newsom, H. E. (1988). Igneous Activity in the early solar system. In *Meteorites and the Early Solar System.* (eds. J. F. Kerridge and M .S. Mathews) University of Arizona Press, pp. 73-101.

Hewins, R. H. and Radomsky, P. M. (1990). Temperature and conditions for chondrule formation. *Meteoritics* 25, 309-318.

Hewins, R.H., Connolly, Jr. H.C., Lofgren, G. E., and Libourel G. (2005). Experimental Constraints on Chondrule Formation. *Chondrites and the Protoplanetary Disk ASP Conference Series* 341, 286-315.

Hewins, R.H., and Fox, G. E. (2003). Chondrule texture and precursor grain size; an experimental study. *Geochim. Cosmochim. Acta*. 68, 917-926.

Hewins, R. (1997). Chondrules. *Annu. Rev. Earth Planet. Sci.* 25, 61-83.

Hewins, R.H. (1991) Retention of sodium during chondrule formation. *Geochim. Cosmochim. Acta*. 55, 935-942.

Horz F. and Schaal R. B. (1981). Asteroid agglutinate formation and implications for asteroid surfaces. *Icarus* 46, 337-353.

Horz, F. and Cintal, M. (1997). Impact experiments related to the evolution of planetary regoliths. *Meteorit. Planet. Sci*. 32, 179-209.

Horz, F., Grieve, R., Hieken, G., Spudis, P. and Binder, A. (1991). Lunar surface processes. In Lunar sourcebook. Ed. G. H. Heiken, D. T. Vaniman and B.M. French. Lunar and Planetary Institute, pp. 61-120.

Huang, S., Akridge, G., and Sears, D.W.G (1996). Metal-silicate fractionation in the surface dust layers of accreting planetesimals: Implications for the formation of ordinary chondrites and the nature of asteroid surfaces. *J. Geophys. Res. (Planets)* 101, 29373-29385.

Ivanov, B. A. (2005). Numerical modeling of the largest terrestrial meteorite craters: *Solar System Research* 39, 381–409.

Ivanov, B. A., Melosh, H.J. and Pierazzo, (2010). Basin-forming impacts: Reconnaissance modeling. In *Large meteorite impacts and planetary evolution IV* (eds. R. L. Gibson and W. U. Reimold) The Geological Society of America Inc., Boulder CO.

Ivanova, M, A., Kononkova, N.N., Franchi, I.A., Verchovsky, A.B., Korochantseva, E.V., Trieloff, M., Krot, A.N., and Brandster, F. (2006). Isheyevo meteorite: Genetic Link between CH and CB Chondrites. *37th Lunar and Planetary Science Conference*, 1100.

Johansen, A., Oishi, J.S., Low, M.-M.M., Klahr, H., Henning, T., Youdin, A. (2007). Rapid planetesimal formation in turbulent circumstellar disks. *Nature* 448, 1022–1025.

Jones, R. H., Lee, T., Connolly, H. C. Jr., Love, S. G. and Shang, H. (2000). Formation of Chondrules and CAIs: Theory vs Observation. In *Protostars and Planets IV* (eds. Mannings, A.P. Boss, S.S. Russell), pp. 927-962. Univ Arizona Press, Arizona, USA.

Jones, A. P. (2005). Meteorite Impacts as triggers to large igneous provinces. *Elements* 5, 277-281.

Kallemeyn, G. W. and Wasson, J. T. (1981). The compositional classification of chondrites: I. The carbonaceous chondrite groups. *Geochim. Cosmochim. Acta.* 45, 1217-1230.

Kallemeyn, G. W. and Wasson, J. T. (1982). The compositional classification of chondrites: III. Ungrouped carbonaceous chondrite groups. *Geochim. Cosmochim. Acta.* 46, 2217-1228.

Kallemeyn, G. W. and Wasson, J. T. (1985). The compositional classification of chondrites: IV. Ungrouped chondritic meteorites and clasts. *Geochim. Cosmochim. Acta.* 49, 261-270.

Kallemeyn G. W., Boyton, W. V., Willis, J. and Wasson, J. T. (1978) Formation of the Bencubbin polymict meteoritic breccia. *Geochim. Cosmochim. Acta.* 42, 507-515.

Kallemeyn G. W., Rubin A. E. and Wasson J. T. (1991). The compositional classification of chondrites: V. The Karoonda (CK) group of carbonaceous chondrites. *Geochim. Cosmochim. Acta.* 55, 881-892.

Kallemeyn G. W., Rubin A. E. and Wasson J. T. (1994). The compositional classification of chondrite VI: The CR carbonaceous chondrites. *Geochim. Cosmochim. Acta.* 58, 2873-2888.

Kallemeyn, G. W., Rubin, A. E. and Wasson, J. T. (2001). Compositional studies of Bencubbin dark silicate host and an OC clast: Relationships to other meteorites and implications for their origin. *33rd Lunar and Planetary Science Conference*, 2070.

Kelly, W. R., and Larimer J. W. (1977). Chemical fractionation in meteorites – VIII. Iron meteorites and the cosmochemical history of the metal phase. *Geochim. Cosmochim. Acta.* 41, 93-111.

King, E. A., Jr., Butler, J. C., and Carman, M. F. (1972). Chondrules in Apollo 14 samples and size analyses of Apollo 14 and 15 fines. *Proceedings of the Lunar Science Conference* 2, 673.

Kleine, T., Mezger, K., Palme, H., Scherer, E., and Munker, C. (2005). Early core formation in asteroids and late accretion of chondrite parent bodies: Evidence from 182Hf-182W in CAIs, metal-rich chondrites and iron meteorites. *Geochim. Cosmochim. Acta.* 69, 5805-5818.

Kropf, A., Huss, G. R., Krot, A. N., and Pack, A. (2009). Closed system behavior of alkalis in Type -1 Chondrules – Understanding chondrules as igneous systems. *40th Lunar and Planetary Science Conference*, 2464.

Krot, A. N., Meibom, A., Russell, S. S., O' D. Alexander, C. M., Jeffries T.E., and Keil K. (2001). A New Astrophysical Setting for Chondrule Formation. *Science* 291, 1776-1779.

Krot, A.N., Amelin, Y., Cassen, P., and Meibom, A. (2005). Young chondrules in CB chondrites from a giant impact in the early Solar System. *Nature* 436, 989-991.

Krot, A. N., Ivanova, M., and Ulyanov, A. (2007). Chondrules in the CB/CH-like carbonaceous chondrite Isheyevo: Evidence for various chondrule forming mechanisms and multiple chondrule generations. *Chemie der Erde Geochemistry 67*, 283-300.

Krot, A. N., Nagashima, K., Yoshitake, M., and Yurimoto, H. (2010). Oxygen isotopic compositions of chondrules from the metal-rich chondrites Isheyevo (CH/CB_b), MAC 02675 (CB_b) and QUE 94627 (CB_b). *Geochim. Cosmochim. Acta.* 74, 2190 -2211.

Krot A. N., McKeegan K. D., Meibom A., and Keil K. (2001). Oxygen-Isotope Compositions of Condensate CAIs and Chondrules in the Metal-Rich Chondrites Hammadah Al Hamra 237 and QUE94411. *64th Annual Meteoritical Society Meeting*, 5105.

Krot, A. N., Meibom, A., Weisberg, M. K., and Keil K. (2002). The CR chondrite clan: Implications for early solar system processes. *Meteoritics & Planetary Science* 37, 1451 - 1490.

Krot, A. N. and Keil, K. (2002). Anorthite-rich chondrules in CR and CH carbonaceous chondrites: genetic link between calcium-aluminum-rich inclusions and ferromagnesian chondrules. *Meteoritics & Planetary Science* 37, 91-111.

Krot, A.N., Petaev, M.I., Keil, K., and Russell, S. S. (2001). Anorthite-rich chondrules in carbonaceous chondrites: Significance for understanding the astrophysical setting of CAI and chondrule formation (5109). *64th Annual Meteoritical Society Meeting*.

Krot, A. N. and Nagashima, K. (2009). Oxygen Isotope Compositions of Chondrules from the CH/CB-Like Chondrite Isheyevo and CB Chondrites MAC 02675 and QUE 94627. *40th Lunar and Planetary Science Conference, 1036.*

Krot A. N., Chaussidon M., Yurimoto H., Sakamoto N., Nagashima K., Hutcheon I. D. and MacPherson G. J. (2008). Oxygen isotopic compositions of Allende Type C CAIs: Evidence for isotopic exchange during nebular melting and asteroidal metamorphism. *Geochim. Cosmochim. Acta*. 72, 2534-2555.

Krot, A. N., Yurimoto, H., Hutcheon, I. D., & MacPherson, G. J. (2005). Chronology of the early Solar System from chondrule-bearing calcium-aluminum-rich inclusions. *Nature* 434, 998-1001.

Krot A.N., Yurimoto H., McKeegan K.D., Leshin L., Chaussidon M., Libourel G., Yoshitake M., Huss G.R., Guan Y., Zanda B. (2006). Oxygen isotopic compositions of chondrules: Implications for evolution of oxygen isotopic reservoirs in the inner solar nebula. *Geochemistry* 66, 249-276.

Krot, A. N., Ulyanov, A. A., and Ivanova, M. A., (2006). Refractory inclusions and aluminum rich chondrules in the CB/CH-like carbonaceous chondrite Isheyevo. *37th Lunar and Planetary Science Conference*, 1226

Krot, A. N., and Rubin A. E. (1993). Chromite-rich mafic silicate chondrules in ordinary chondrites: formation by impact melting, *24th Lunar Planetary Science Conference*, 827–828.

Krot, A. N., Meibom, A., Petaev ,M. I., Russell, S. S., Aleon, J., McKeegan, K. D., Amelin, Y., Hezel, D.C., and Keil, K.(2006). On the Origin of Chondrules in the CB (Bencubbin-Like) Carbonaceous Chondrites. Geochim. Cosmochim.

Krot, A.N, Keil, K, Goodrich, C.A., Scott, E.R.D., and Weisberg, M.K. (2005). Classification of meteorites. In Meteorites, Comets, and Planets (Davis, A. M. editor). Treatise on Geochemistry volume 1 (Holland, HD and Turekian, K.K. editors), Elsevier-Pergamon, Oxford, 737 pp., 83-128

Krot A.N. et al 2007. MAPS, 42 (Suppl.), A. 90.

Krot A. N., Fegley B., Lodders K., and Palme H. (2000) Meteoritical and Astrophysical constraints on the oxidation state of the solar nebula. In protostars and Planets IV (2000), V.Mannings, A. P. Boss, and S.S. Russell, Eds. University of Arizona Press.

Lakdawalla, Emily. (2008). The full story of Earth-impacting asteroid 2008 TC http://www.planetary.org/blog/article/00001684/

Lee, M.S., Rubin, A. E., and Wasson, J.T. (1992). Origin of metallic Fe-Ni in Renazzo and related chondrites. *Geochim. Cosmochim. Acta.* 56, 2521-2533.

Lemaitre, A. and Morbidelli, A. (1994). Proper elements for high inclined asteroidal orbits. *Cel. Mech. Dyn. Ast.* 60, 29-56.

Lodders, K. (2003). Solar System abundances and condensation temperatures of the elements. *The Astrophysical Journal* 591, 1220 -1247.

Lofgren, G.E. and Lanier, A.B. (1990). Dynamic crystallization study of barred olivine chondrules. *Geochim. Cosmochim. Acta.* 54, 3537 -3551.

Lofgren, G.E. and Russell, W. J. (1985). Dynamic crystallization experiments on chondrule melts of porphyritic olivine composition. *Lunar and Planet. Sci*. 16, 499 -500.

Lofgren G. E. (1996). A dynamic crystallization model for chondrule melts. In *Chondrules and the Protoplanetary Disk* (eds. R. H. Hewins, R. H. Jones, and E. R. D. Scott), pp. 187–196. Cambridge University Press, Cambridge.

MacPherson, G. J., Simon, S. B., Davis, A. M., Grossman, L., and Krot, A. N. (2005). Calcium-Aluminum-rich Inclusions: Major Unanswered Questions. *Chondrites and the Protoplanetary Disk ASP Conference Series,* 341.

Marvin, U. B., Wood, J. A., and Dicker, J. S. (1970). Ca-Al- rich phases in the Allende meteorite. *Earth Planet. Sci. Lett.* 7, 346-350.

McBride N., Gilmour I., Bland P. A., Moore E. A., Widdowson M., Wright I. (2004). In *An Introduction to the Solar System* (pp. 56). Cambridge University Press. Cambridge, United Kingdom.

Read more: http://www.answers.com/topic/protoplanet#ixzz19YC2GCQI

McCord, T. B., L. A. McFadden, C. T. Russell, C, Sotin, and Thomas, P. C. (2006). Ceres, Vesta, and Pallas: Protoplanets, Not Asteroids. *EOS, Transactions, American Geophysical Union* 87, 105.

McKeegan, K.D., Krot, A. N., Scott, E. R. D. (2001). Variable oxygen isotopic compositions of gaseous reservoirs: Clues to the formation of CAI and chondrules. *64th Annual Meteoritical Society Meeting*, 5381.

McSween H. Y.Jr (1977). On the origin of isolated olivine grains in type 2 carbonaceous chondrites. *Earth Planet. Sci. Lett.* 41, 111-127.

Meibom, A., Desch, S. J., Krot, A. N., Cuzzi, J. N., Petaev, M. I., Wilson, L., and Keil, K. (2000). Large-scale thermal events in the solar nebula: Evidence from Fe, Ni metal grains in primitive meteorites. *Science* 288, 839-841.

Meibom, A., Petaev, M. I., Krot, A.N., Wood, J. A. and Keil, K. (1999). Primitive Fe, Ni metal grains in CH carbonaceous chondrites formed by condensation from a gas of solar composition. *J. Geophys. Res*. 104, 22053-22059.

Meibom, A., Petaev, M. I., Krot, A.N., Keil, K. and Wood, J. A. (2001). Growth mechanism and additional constraints on FeNi metal condensation in the solar nebula. *J. Geophys. Res*. 106, 32797-32,801.

Meibom, A., Desch S. J., Petaev, M. I., Krot, A. N., Cuzzi, J. N., Wood, J. A., and Keil, K. (2000). An astrophysical model for the formation of zoned FeNi metal grains in the Bencubbin/CH-like chondrites QUE 94411 and Hammadah al Hamra 237. *63rd Annual Meteoritical Society Meeting*, 5268.

Meibom, A., Petaev, M. I., Krot, A. N., Keil, K., (2001). Beryllium and Boron Measurements in QUE 94411 Chondrules: Possible Constraints on Formation Temperature. *64th Annual Meteoritical Society Meeting*

Melosh, H.J., Cassen, P., Sears, D., and Lugmair, G. (2004). Role of planetary impacts in thermal processing of chondrite materials. *Workshop on Chondrites and Protoplanetary Disk*, 9119.

Melosh, H.J. (1985). Impact Cratering Mechanics: Relationship between the Shock Wave and Excavation Flow. *Icarus* 62, 339-343.

Melosh, H.J. (1980). Cratering Mechanics - Observational, Experimental, and Theoretical. *The Annual Review of Earth and Planetary Sciences* (book), 8, 626.

Michel P., Benz W., Tanga P., and Richardson D. C. (2001). Collisions and Gravitational Reaccumulation: Forming Asteroid Families and Satellites. *Science* 23, 1696-1700.

Miyamoto, M. and Zolensky, M. E. (1994). Infrared diffuse reflectance spectra of carbonaceous chondrites: amount of hydrous minerals. *Meteoritics* 29, 849–853.

Miyamoto, M. (1992). Infrared diffuse reflectance spectra of several thermally metamorphosed carbonaceous chondrites. *Proc. NIPR Symp. Antarct. Meteorites* 5, 155-164.

Miyamoto, M. and Zolensky M. E. (1992). Absorption bands near 3 um of carbonaceous chondrites and implications for surface material of Ceres and Pallas. *Proc. ISAS Lunar Planet. Symp.* 25th, 32-35.

Morbidelli, A., Bottke, W. F., Nesvorny, D., and Levison, H. F. (2009). Asteroids were born big. *Icarus* 204, 558-573.

Morfill, G.E., Durisen, R.H., and Turner, G.W. (1998). An accretion rim constrain on chondrule formation theories. *Icarus* 134, 180-184.

Morris, M.A. and Desch S. J. (2010). Thermal histories of chondrules in solar nebula shocks. *The Astrophysical Journal* 722, 1474-1494.

Nagahara, H., Mysen, B.O. and Kushiro, I. (1994). Evaporation of olivine – low pressure phase relations of the olivine system and its implication for the origin of chondritic components in the solar nebula. *Geochim. Cosmochim. Acta.* 58, 1951 – 63.

Nagahara, H., Kita, N. T., Ozawa, K., and Morishita Y. (2008). Condensation of major elements during chondrules formation and its implications on the origin of chondrules. *Geochim. Cosmochim. Acta.* 72, 1442-1465.

Nafziger R. H., Ulmer G. C., and Woermann E. (1971). Gaseous buffering for the control of oxygen fugacity at one atmosphere. In *Research Techniques for High Pressure and High Temperature* (ed. G. C. Ulmer), pp. 9–41. Springer-Verlag.

Nakamoto, T. and Nakagawa, Y. (1994). Formation, early evolution, and gravitational stability of protoplanetary disks. *The Astrophysical Journal* 421, 640-650.

Nelson, L. S., Blander, M., Skaggs, S. R., and Keil, K. (1972). Use of CO2 laser to prepare chondrule like spherules from supercooled molten oxide and silicate droplets. *Earth Planet. Sci. Lett.* 14, 338 -334.

Nevorny, D., Voukrouhlicky, D., Morbidelli A., and Bottke, W. F. (2009). Asteroidal source of the L chondrite meteorites. *Icarus* 200, 698-701.

Newsom, H. E. and Drake, M.J. (1979). The origin of metal clasts in the Bencubbin meteoritic breccia. *Geochim. Cosmochim. Acta.* 43, 689-707.

O'Brien, D. P., Morbidelli, A., Levison, H. F. (2006). Terrestrial planet formation with strong dynamical friction. *Icarus* 184, 39–58.

O'Keefe, J.D., and Ahrens, T. J. (1993). Planetary cratering mechanics. *J. Geophys. Res*. 98, 17011-17028.

O'Keefe, J.D. and Ahrens, T. J. (1994). Impact-Induced Melting of Planetary Surfaces. Large Meteorite Impacts and Planetary Evolution (book). *GSA Special Paper* 293, 348.

O'Keefe, J. D. and Ahrens, T.J. (1975). Shock effects from a large impact on the moon. *6th Proc. Luna Science*, 2831 -2844.

O'Keefe, J.D., and Ahrens, T.J. (1977) Impact induced energy partitioning, melting, and vaporization on terrestrial planets, in 8th Lunar Science Conference Proceedings: New York, Pergamon Press, pp. 3357–3374.

O'Hara (1968) Earth-Science Reviews. Vol 4. Pp. 69-133.

Paine, M. (1999) Did Asteroid Induced Firestorm Destroy the Dinosaurs? http://www.space.com/scienceastronomy/astronomy/dinosaurs_fry_991118.html

Paque, J. M.; Toppani, A., Burnett, D. S., Teslich, N., Moberlychan, W., Dai, Z. R., and Bradley, J. P. (2007). TEM/SEM Evidence for Residual Melt Inclusions in Type B1 CAIs. *38th Lunar and Planetary Science Conference*, 1338.

Petaev, M.I., Wood, J. A., Meibom, A. (2003). The ZONMET thermodynamic and kinetic model of metal condensation. *Geochim. Cosmochim. Acta.* 67, 1737-1751.

Petaev, M. I., Meibom, A., Krot, A. N., Wood, J. A., and Keil, K. (2001). The condensation origin of zoned metal grains in Queen Alexandra Range 94411: Implications for the formation of the Bencubbin-Like chondrites. *Meteoritics & Planetary Science* 36, 93-106.

Petaev, M. I. and Wood, J. A. (1998). The Condensation with Partial Isolation (CWPI) Model of Condensation in the Solar Nebula. *Meteorit. Planet. Sci*.33, 1123-1137.

Petaev, M. I., Ivanova, M.A., Krot, A. N., Meibom, A., and Jacobsen, S. B. (2007). Different zoning patterns in metal grains from the CH and CBb Chondrites: Evidence for a complicated cooling history of their nebular source region. *38th Lunar and Planetary Science Conference*, 1641.

Petaev M. I. (2006) Modeling major and trace element chemistry of zoned metal grains from the CH and CB Chondrites. *37th Lunar and Planetary Science Conference*, 1681.

Petaev, M., Krot, A. N., Wood, J. A. and Keil, K. (1999). Primitive Fe, Ni metal grains in CH carbonaceous chondrites formed by condensation from a gas of solar composition. *J. Geophys. Res.* 104, 22053-22059

Pieters, C. M. and McFadden, L. A. (1994). Meteorite and Asteroid reflectance spectroscopy: Clues to early solar system processes. *Annual Review Earth Planetary Science* 22, 457 – 97.

Podosek, F. A. and Cassen, P. (1994). Theoretical, observational, and isotopic estimates of the lifetime of the solar nebula. *Meteoritics* 29, 6-25.

Pohl, J., Stoffler, D., Gall, H., and Ernstoon, K. (1977). The Ries impact crater. In *Impact and Cratering* (eds. D.J. Roddy, R.O Pepin, and R.B. Merrill), pp. 343-404. Pergamon, N.Y.

Pollack, J. B., Hubicky, O., and Bodenheimer, P. (1996). Formation of the Giant Planets by Concurrent Accretion of Solids and Gas. *Icarus* 124, 62-85.

Radomsky P. and Hewins R. (1990). Formation Conditions of pyroxene-olivine and magnesium olivine chondrules. *Geochim. Cosmochim. Acta* 54, 3475-3490.

Richter, F. M., Mendybaev, R.A., and Davis, A.M. (2005). Conditions in the protoplanetary disk as seen by type B CAIS. *Meteoritics and Planetary Science* 41, 83-93.

Righter, K., and O'Brien, D. P. (2011). Terrestrial Planet Formation. *Proceedings of the Natural Academy of Sciences* 108, 19165-19170.

Reimold W. U., Koeberl C., Coney L., Ferrière L., and Gibson R. L. (2007). Results of recent petrographic and geochemical studies of the ICDP drill cores from the interior of the Bosumtwi impact structure, Ghana. *38th Lunar and Planetary Science Conference*, 1137.

Rubin, A. E., Kallemeyn, G. W., Wasson, J. T., Clayton, R. N., Mayeda, T. K., Grady, M., Verchovsky, A. B., Eugster, O., and Lorenzetti, S. (2003). Formation of metal and silicate globules in Gujba: a new Bencubbin-like meteorite fall. *Geochim. Cosmochim. Acta* 67, 3283-3298.

Russell, S. S., Srinivasan, G., Huss, G. R., Wasserburg, G. J. and McPherson, G. J. (1996). Evidence for widespread ^{26}Al in the solar nebula and constraints for nebula time scales. *Science* 273, 757-762.

Russell, S. S., Zhu, X., Gui, Y., Belshaw, N., Gounelle, M., Mullane, E., and Coles B. (2003). Copper isotope systematics in CR, CH-like, and CB meteorites: A preliminary study (abstract). Meteorititcs and Planet. Sci. 38, A124.

Rutkin, Darrel *Galileo, Astrology and the Scientific Revolution: Another Look,* H. Darrel

Rutkin, HPST Colloquia presentation, November 4, 2004, Stanford University: http://www.stanford.edu/dept/HPST/colloquia0405.html

Sanders, I. S. (1996). A chondrule forming scenario involving molted planetesimals. In Chondrules and the Protoplanetary Disk (eds. R. H. Hewins, R. H. Jones and E. R. D. Scott). Cambridge University Press, pp. 327-334.

Sato, K., Miyamoto, M., and Zolensky, M. E. (1997). Absorption bands near 3um in diffuse reflectance spectra of carbonaceous chondrites: Comparison with asteroids. Meteoritics 32, 503–507.

Scheeres, D. J., Durda, D. D, and Geissler, P. E. (2002). The fate of asteroid ejecta. In *Asteroids III* (eds. W. F. Bottke et al. University of Arizona Press) pp. 527 – 44.

Schmidt, B.E, Thomas, P.C., Bauer, J.M., Li, J.-Y., McFadden, L. A., Mutchler, M. J., Radcliffe, S. C., Rivkin, A. S., Russell, C. T., Parker, J. Wm., and Stern S. A. (2009). The shape and Surface Variation of 2 Pallas from the Hubble Space Telescope. *Science* 326, 275-278

Schmidt, B. E., Thomas, P. C., Bauer, J. M., Li, J.-Y., McFadden, L. A., Parker, J. M., Rivkin, A. S., Russell1, C. T., and, Stern, S. A.(2008). Hubble takes a look at Pallas: Shape, size, and surface (abstract # 2502). *39th Lunar and Planetary Science Conference.*

Schmidt, B. E. (2009). Protoplanets frozen in time. Retrieved from http://cosmiclog.msnbc.msn.com/_news/2009/10/08/4350042-protoplanet-frozen-in-time

Scott, E., Yang, J., and Goldstein, J. (2007). When worlds really did collide. *Planetary Science Research Discoveries.* http://www.psrd.hawaii.edu/April07/irons.html

Scott, E., Goldstein, J., and Yang, J. (June, 2010). Formation of stony-iron meteorites in early giant impacts. *Planetary Science Research Discoveries.* http://www.psrd.hawaii.edu/June10/pallasites-origin.html

Scott, E. R. D., Lusby, D, and Keil, K. (1985). Ubiquitous brecciation after metamorphism in equilibrated ordinary chondrites. *Proc. 16th Lunar Planet Science Conference J. Geophys. Res.* 91, 115-23.

Scott, E. R.D. and Krot A. N. (2007). Chondrites and their components (eds. H. D. Holland and K. K. Turekian). Treatise on Geochemistry, Pergamon, Oxford. pp. 1 – 72.

Scott, E.R.D. and Krot, A.N. (2005). Chondritic meteorites and the high-temperature nebular origins of their components. In Chondrules and the Protoplanetary Disk (eds. A. Krot, E. Scott, and B. Reipurth). ASP Conference Series, San Francisco, CA. pp. 15-53.

Scott, E. R. D. (1988). A new kind of primitive chondrite, Allan Hills 85085. *Earth Planet. Sci. Lett.* **91**, 1-18.

Sears D. W. G. (2004) The Origin of Chondrules and Chondrites (eds. F. Bagenal, D. Jewiit, C. Murray, J. Bell, R. Lorenz, F. Nimmo, and S. Russell). Cambridge University Press, Cambridge U.K.

Sears, D. W.G. and Akridge, G. (1998). Nebular or parent body alteration of chondritic material: Neither or both? *Meteorit. Planet. Sci*. 33, 1157-1167.

Sears, D. W. G., Huang, S., Akridge, G., and Benoit, P.H. (1996). Glassy Spherules in suevite from the Ries Crater, Germany, with implications for the formation of meteorite chondrules. *Lunar Planet. Sci*. 27, 1165-1166.

Sears, D. W. G., Shaoxiong, H., and Benoit, P. H. (1995). Chondrule formation, metamorphism, brecciation, an import new primary chondrule group, and the classification of chondrules. *Earth and Planetary Science Letters* 131, 27-39.

Shu, F. H., Shang, H., and Lee, T. (1996). Toward an astrophysical theory of chondrites. *Science* 271, 1545 – 1552.

Shu, F. H., Adams F. C. and Lizano S. (1987) Star Formation in Molecular Clouds: Observation and Theory. Ann. Rev. Astronomy and Astrophysics 25, 23 -81.

Stolper, E.M. and Paque, J.M. (1986). Crystallization sequences of Ca-Al-rich inclusions from Allende: The effects of cooling rate and maximum temperature. *Geochim. Cosmochim. Acta*.50, 1785-1806.

Swindle, T. D., Davies, A. M., Honenberg, c. M., MacPherson, G. J. and Nyquist, l. E. (1996). Formation tines of chondrules and Ca-Al-rich inclusions: Constraints from short-lived radionuclides. In Chondrules and the Protoplanetary Disk (eds. R.H. Hewins, R.H. Jones and E. R. D. Scott) Cambridge University Press, 77-86.

Elkins-Tanton, L.T., Weiss, B.P., and Zuber, M. T. (2011) Chondrites as samples of differentiated planetesimals. Earth and Planetary Science Letters doi: 10.1016/j.epsl.2011.03.010

Taylor, G. J., Scott, E. R. D., and Keil, K. (1983). Cosmic setting for chondrule formation. In *Chondrules and their origins* (eds. E.A. King) pp. 262-278. Houston, TX, Lunar and Planetary Institute.

Teng1, F. - Z., Wadhwa1, M., Janney, P.E., Grossman, L., Simon, S., and Dauphas, N. (2007).Magnesium isotopic systematics of chondrules and CAIs from Allende, Murchison, Murray and Bjurbole. *38th Annual Lunar and Planetary Science*, 1837.

Tsuchiyama, A., Osada, Y., Nakano, T., and Uesugi, K. (2004). Experimental reproduction of classic barred olivine chondrules: Open-system behavior of chondrule formation. *Geochim. Cosmochim. Acta* 68, 653-672.

Tholen, D. J. (1989). Asteroid taxonomic classifications. In *Asteroids II* (eds. R.P. Binzel, T. Gehrels, and M. S. Matthews), pp. 1139-1150. Univ. of Arizona Press, Tucson.

Urey, H.C. and Craig, H. (1953). The composition of the stone meteorites and the origin of the meteorites. *Geochim. Cosmochim. Acta* 4, 36-82.

Wasson, J. T., Krot, A. N., Lee, M.S., Rubin, A.E. (1995). Compound Chondrules. *Geochim. Cosmochim. Acta.* 59, 1847.

Wasson, J. T., and Kallemeyn, G. W. (1990). Allan Hills 85085: A chondritic meteorite of mixed nebular and regolithic heritage. *Earth Planet Sci Lett* 101, 148-161.

Wasson, J. T. (1993). Constraints on chondrule origins. *Meteoritics* 28, 14-28.

Weidenschilling, S. J., Marzari, F., and Hood, L. L. (1998). The origin of chondrules at jovian resonances. *Science* 279, 681-684.

Weisberg, M. K., Prinz, M., Clayton, R.N., Mayeda T.K., Grady, M.M., and Pillinger C. T. (1995). The CR chondrite clan. *Proc. NUPR Symp. Antarct. Meteorites* 8, 11-32.

Weisberg, M. K., Prinz, M., Clayton, R.N., and Mayeda T.K. (1993). The CR (Renazzo-type) carbonaceous chondrite group and its implications. *Geochim. Cosmochim. Acta* 57, 1567-1586.

Weisberg, M. K., Prinz, M., and Nehru, C. E. (1990). The Bencubbin chondrite breccia and its relationship to CR chondrites and the ALH 85085 chondrite. *Meteoritics* 25, 269-279.

Weisberg, M. K., and Huber, H. (2007). The GRO 95577 CR1 chondrite and hydration of the CR parent body. *Meteoritics & Planetary Science 42, 1495-1503.*

Weisberg, M. K. and Kimura, H (2010). Petrology and Raman spectroscopy of high pressure phases in the Guijba CB chondrite and the shock history of the CB parent body. *Meteoritics & Planetary Science 45, 873 -884.*

Weisberg, M. K. (1987). Barred olivine chondrules in ordinary chondrites: Petrologic constraints and implications. *Proc. 17th Lunar. Planet. Sci. Conf.*, E663–678.

Weisberg, M. K., Prinz, M and Nehru, C. E. (1988). Petrology of ALH85085: a chondrite with unique characteristics. *Earth Planet. Sci. Lett.* 91, 19-32.

Weisberg, M. K. and Prinz, M. (1996). Agglomeratic chondrules, chondrule precursors and incomplete melting. In *Chondrules and the Protoplanetary Disk* (ed. R. H. Hewins et al.), pp. 119–127. Cambridge University Press.

Weisberg M. K., Prinz, M., Clayton, R.N., Mayeda T.K., N. Sugiura, N., Zashu S., Ebihara, M., A (2001) A New Metal Rich Grouplet, Meteorit. Planet. Sci. 36, 401-418.

Weisberg, M. K., and Prinz, M. (1999). Zoned metal in the CR clan chondrites. *Proc NIPR Symp. Antarct. Meteorites* 30, 189 – 190.

Weisberg, M. K., Prinz, M., Humayun, M., and Campbell, A. J. (2000). Origin of metl in the CB (Bencubbinite) chondrites. *31st Lunar Planet Sci Conference*, 1466.

Wetherill, G. W. (1986). Accumulation of the terrestrial planets and implications concerning lunar origin. In *Origin of the Moon* (eds. W. K. Hartmann, R.J. Phillips, and G. J. Taylor), pp. 519- 550. Houston, TX: Lunar Planetary Institute.

Weyer S., Anbar A. D., Brey G. P., Mu¨nker C., Mezger K. and Woodland A. B. (2005). Iron isotope fractionation during planetary differentiation. *Earth Planet. Sci. Lett.* 240, 251–264.

Whipple, F. L. (1972a). Accumulation of chondrules on asteroids. In *Physical Studies of Minor Planets*. NASA Special Publication 267, pp. 251-62.

Whipple, F. L. (1972b). On certain aerodynamic processes for asteroids and comets. *In From Plasma to Planet, Nobel Symposium 21* (eds. A. Elvius). John Wiley, pp. 211-32.

Wood, J.A. (1984). On the formation of meteoritic chondrules by aerodynamic drag heating in the solar nebula. *Earth Planet. Sci.* 70, 11-26

Wood, J. A., and Morfill, G. (1988). A review of solar nebular models in J. F. Kerridge and M.S. Mathews (eds.), Meteorties and the Early Solar System, Univ. Arizona Press, pp. 329-347.

Wood, J.A. (1988). Chondritic meteorites and the solar nebula. *Annual Review Earth Planet. Sci.* 16, 53-72.

Wood, J. A. (2000). Pressure and temperature profiles in the solar nebula. *Space Science Reviews* 92, 87-93.

Wunnerman K. and Collins G. S. (2006) The effect of porosity on meteorite impact processes. *Geophysical Research Abstracts*, Vol. 8, 03991

Yang, J., Goldstein J.I., and Scott, E. R. D. (2007). Iron meteorite evidence for early formation and catastrophic disruption of protoplanets. *Nature* 446, 888-891.

Yang, J., Goldstein, J. I., and Scott, E. R. D. (2010). Main-group Pallasites: Thermal history, relationship to IIIAB irons, and origin. *Geochim. Cosmochim. Acta*. 74, 4471-4492.

Zanda B. (2004). Chondrules. *Earth and Planetary Science Letters* 224, 1-17.

Zhang, J., Williams., D. B., and Goldstein, J. I., The microstructure and formation of duplex and black plessite in iron meteorites, *Geochim. Cosmochim. Acta*, 57, 3725-3735, 1993.

Zipfel, J. and Weyer, S. (2007). In situ analyses of Fe isotopes in zoned metal grains of Hammadah al Hamra 237. *38th Lunar and Planetary Science Conference*, 1927.

Zipfel, J. and Weyer, S. (2006). Impact or solar nebula origin of CB chondrites? Evidence from Fe isotopes. *37th Lunar and Planetary Science Conference*, 1902.

Zook, H. A. (1981). On a new model for the generation of chondrules. *Lunar Planet. Sci.* 12, 1242-1244.

Zook, H. A. (1980). A new impact theory for the generation of ordinary chondrites. *Meteorites* 15, 390-391.